Universidad de Valladolid

ESCUELA DE INGENIERÍAS INDUSTRIALES

DEPARTAMENTO DE INGENIERÍA QUÍMICA Y TECNOLOGÍA DEL MEDIO AMBIENTE

TESIS DOCTORAL:

On the Development of Computational Tools for the Modeling and Simulation of SCWO Process Intensified by Hydrothermal Flames.

Presentada por João Paulo Silva Queiroz para optar al grado de
Doctor por la Universidad de Valladolid

Dirigida por:
Doctora María Dolores Bermejo Roda
Profesora Doctora María José Cocero Alonso

Universidad de Valladolid

ESCUELA DE INGENIERÍAS INDUSTRIALES

DEPARTAMENTO DE INGENIERÍA QUÍMICA Y TECNOLOGÍA DEL MEDIO AMBIENTE

TESIS DOCTORAL:

Sobre el Desarrollo de Herramientas Computacionales para el Modelado y Simulación del Proceso OASC Intensificado por Llamas Hidrotermales.

Presentada por João Paulo Silva Queiroz para optar al grado de Doctor por la Universidad de Valladolid

Dirigida por:
Doctora María Dolores Bermejo Roda
Profesora Doctora María José Cocero Alonso

Memoria para optar al grado de Doctor,
con Mención Doctor Internacional,
presentada por el Ingeniero Químico:

João Paulo Silva Queiroz

Siendo los tutores en la Universidad de Valladolid

Dra. María Dolores Bermejo Roda

y

Prof. Dra. Dª María José Cocero Alonso

Y en el Institut für Technische Verbrennung,
University of Stuttgart (Alemania)

Prof. Dr. Andreas Kronenburg

Valladolid, Julio de 2014

Universidad de Valladolid
Escuela de Ingenierías Industriales
Secretaría

La presente tesis doctoral queda registrada en el folio número ____ del correspondiente libro de registro número ____.

Valladolid, a ____ de _____ de 2014

Fdo. El encargado de registro

María Dolores Bermejo Roda
Profesora de Universidad
Departamento de Ingeniería Química y Tecnología del Medio Ambiente
Universidad de Valladolid

y

María José Cocero Alonso
Catedrática de Universidad
Departamento de Ingeniería Química y Tecnología del Medio Ambiente
Universidad de Valladolid

Certifican que:

El ingeniero JOÃO PAULO SILVA QUEIROZ ha realizado en el Departamento de Ingeniería Química y Tecnología del Medio Ambiente de la Escuela de Ingenierías Industriales de la Universidad de Valladolid, bajo nuestra dirección el trabajo: "On the Development of Computational Tools for the Modeling and Simulation of SCWO Process Intensified by Hydrothermal Flames", cuyo título en castellano es "Sobre el Desarrollo de Herramientas Computacionales para el Modelado y Simulación del Proceso OASC Intensificado por Llamas Hidrotermales". Considerando que dicho trabajo reúne los requisitos para ser presentado como Tesis Doctoral expresan su conformidad con dicha presentación.

Valladolid, a _____ de _____ de 2014

Fdo. María Dolores Bermejo Roda Fdo. María José Cocero Alonso

Reunido el tribunal que ha juzgado la Tesis Doctoral titulada "On the Development of Computational Tools for the Modeling and Simulation of SCWO Process Intensified by Hydrothermal Flames" presentada por el Ingeniero Químico João Paulo Silva Queiroz y en cumplimiento con lo establecido en el Real Decreto 1393/2007 de 29 de Octubre ha acordado conceder por _____ la calificación de _____.

Valladolid, a _____ de _____ de 2014

PRESIDENTE SECRETARIO

1er VOCAL 2° VOCAL 3er VOCAL

Dedicado a Maria das Graças
Mainha

In theory, there is no difference between theory and practice.
But in practice, there is.
–Anonymous computer scientist

Abstract

Hydrothermal flames used as internal heat source contribute to overcome many of the challenges present in supercritical water oxidation. The aim of this thesis is to improve the understanding of the hydrothermal flames in the supercritical water oxidation process, developing tools for their modeling and simulation. This knowledge is necessary for the advances on the utilization of SCWO as power generation process.

In the **chapter 1**, the state of the art of the technology, focusing on energy production is reviewed. This revision makes evident the necessities of research in several fields related to the SCWO, besides technical solutions on pumping and pretreatment steps of real biomass feed. Modeling is essential when hydrothermal flames are present, since their behavior can not always be observed directly, and these models require better sub-models on kinetics, turbulence, mixture equations of state and transport properties. Finally, expansion devices appropriate to streams nature and conditions, and efficient enough should be developed and engineered.

In **chapter 2**, the property estimation methods used in this thesis are presented. A simple cubic equation of state shows good accuracy and fast calculation for thermodynamic properties of supercritical mixtures. Densities are calculated with Peng-Robinson EoS with the modification of volume translation, while enthalpies are calculated with the original Peng-Robinson EoS. Transport properties could be predicted with reasonable accuracy at high temperature. However, over the low temperature range (at high densities), the methods have show poor results and mass-weighted mixing laws of tabulated values of pure species are used.

In the third part of the thesis a study of the kinetic description of SCWO at hydrothermal flame regime is made. In **chapter 3**, a method for kinetic determination using easily available experimental data is presented. The method consists of adjusting kinetic parameters in order to match the temperature profiles obtained experimentally. Using this method, a new global reaction rate for the oxidation of isopropyl alcohol in hydrothermal regime is fitted: $r = k_0 \exp\left(-\frac{E_a}{RT}\right) C_{IPA} C_{O_2}$, with $k_0 = (9.308 \pm 3.989) \cdot 10^7 (m^3 \cdot s^{-1} \cdot kmol^{-1})$ and $E_a = 89.441 \pm 2.457 (kJ \cdot mol^{-1})$. The least square error of the fitting is 10.8%. This kinetic model is applied in a parametric analysis of flame formation, and it is used to analyze the behavior of a supercritical water oxidation vessel reactor. The kinetic model is able to describe the behavior of the vessel reactor when working in steady state hydrothermal flame regime at subcritical injection temperatures. The model predicts both flameless and hydrothermal flame regimes. In **chapter 4** the interactions of turbulence with the reactive flow are studied with a turbulent combustion method based on quantifying turbulence fluctuations through probabilities. It has been found that the inclusion of these turbulent fluctuations, even

though affects the flame structure, has no influence on final efficiency on waste elimination or energy generation. This can be explained by the usual oversized volume of reactors, which gives residence times much higher than reaction times.

In **chapter 5** the influence of the internal configuration of vessel reactors for the SCWO process is evaluated by simulation and compared to experimental data. The CFD-model developed provides a good prediction of the experimental results (deviations of 14% for temperature predictions) and can be used for designing reactors working under hydrothermal flame looking at performance and flame stabilization. Residence time distribution curves are obtained providing additional information about non-ideal behavior of the reactor.

The methodologies developed in this work are applied to a new reactor configuration especially designed for energy generation in **chapter 6**. The experimental results obtained are briefly described and model is applied to study the internal behavior of the reactor and how it is affected by the existence of two outlets. Finally the energetic integration is studied, and it is shown that heat integration, generation of high pressure steam and generation of electricity by products expansion, are theoretically feasible in SCWO.

Contents

Índice general

List of Figures

List of Tables

Research goal and objectives

Overall goal: The overall goal of this research is to enhance the understanding of the Supercritical Water Oxidation (SCWO) process at hydrothermal flame regime, through modeling and simulation tools. This should be done by focusing mainly in the energy generation aspect of this technology. The partial objectives needed for a complete description of the process are described below.

Study the methods of property estimation for supercritical pure fluids and aqueous mixtures and their application in simulation tools.

- To study the availability of property calculation methods capable of describing thermal and transport properties of mixtures at supercritical state.
- To build a library of property methods useful for CFD modeling and for simple balance models of hydrothermal flames in the context of SCWO reactors.

Study of kinetics of SCWO in hydrothermal flame.

- To develop a method of determining kinetic parameters from experimental data easily measured, such as temperature changes.
- To fit a kinetic model for the supercritical water oxidation of isopropyl alcohol in hydrothermal flame regime using this method and reduce, in this way, the lack of kinetic parameters at that conditions.
- To validate the kinetic model with different sets of experimental data and different reactor concepts.
- To study how the turbulence interactions affect the hydrothermal flames.

Study how the configuration of the reactor and operational conditions affect the behavior of hydrothermal flame.

- To construct a realistic CFD model for vessel reactors working with an internal hydrothermal flame.
- To validate the model with experimental data of the new cooled wall reactor developed in the University of Valladolid.
- To analyze the effects of the geometry of injector and operational parameters over the behavior of a hydrothermal flame.
- To use the model for obtaining extra information (not accessible experimentally) such as residence time distribution curves.

Apply the CFD model to a new reactor predicting the flow distribution for achieving energy efficiency.

- To study the behavior of new cooled wall reactor with two outlets in order to optimize energy recovery.
- To study the effects of the upper/lower effluent relation on temperature profiles inside the reactor and organic matter elimination in both streams.
- To find the conditions for keeping the maximum heat released by the flame in a clean and high temperature flow leaving the reactor from the upper zone.
- To use CFD results and property methods to perform realistic predictions of SCWO energetic efficiency.

Chapter 1

State of the art

Abstract

Supercritical Water Oxidation (SCWO) has the potential to be considered a clean energy generation process, as the process effluent is a high temperature, high pressure stream with a high enthalpy content that can be converted to heat and shaft work. Even when the state of the art is still far from being ready to build big power station based on this process, as SCWO is a process largely studied as waste elimination technology, the knowledge acquired in that field will allow the rapid development of this technology as a clean energy generation process. Furthermore, when the process is carried out under hydrothermal flame conditions it is intensified by producing higher temperature effluent in extremely compact reactor. In this work, existing proposal of potential heat recovery and power generation using SCWO, both in flame and flameless regime, are reviewed, and the needs on research are remarked. There are two main points in which the technology must be improved to develop energy generation by SCWO. In first place reactors and reaction systems able to process feeds consisting of suspension with high inorganic contents without diluting the effluent reducing its temperature must be developed. On the other hand, the systems of energy recovery must be improved, especially the expanders, in order to recover the pressure work as well as the thermal energy. CFD modeling tools can help in both aspects. But for developing good models a good comprehension of thermal and transport properties of mixtures at supercritical state, as well as oxidation kinetics under that condition are essential data that must be further investigated in order to find energetically efficient processes.

Keywords: Supercritical water oxidation, Kinetics, Hydrothermal flames, CFD modeling, Renewable Energy

1.1 Introduction

Supercritical water oxidation is a process well-known for its environmental applications. Although its industrial development progresses slowly, this year several industrial plants for chemical weapons and sludge treatment are under construction [1]. Due to these development efforts, the limitations and challenges in the implementation of SCWO processes are also well-known, including the control of corrosion and salt precipitation processes [2–4]. Another well-known challenge of SCWO is the energy requirement, which can be high, particularly if simple plug-flow tubular reactors are used, since these designs require preheating of the influent up to supercritical temperatures. However, under appropriate operating conditions, the SCWO process can be energetically self-sufficient or even produce a net excess of energy [5, 6]. The correct use of the energy produced by the oxidation is a crucial step in order to make SCWO processes economically viable.

The main industrial development has been associated to sludge treatment by tubular reactors [1, 7]. Conventional reactors are thin tubes about hundred meters long, with evident plugging problems from solid precipitation. In practice, industrial plants work with two reactors, one under operation and the other undertaking the cleaning of deposited solids. In some applications the change of the reactors takes over 30 minutes. Furthermore, cleaning is a highly energy and time consuming step. Although the reactor effluent energy can be recovered by a Rankine Cycle, the process is still highly demanding. Additionally, oxygen is the most usual oxidant to reduce the energy consumption of the air compressor. The energy associated to the compression could be recovered if the work from effluent depressurization could be retrieved by a turbine.

Another reactor under industrial development is the transpiring wall reactor [8]. The transpiring flow allows a continuous clean water flow that protects the reactor against corrosion and plugging but dilutes the effluent and reduces its temperature, so the heat recovery is reduced.

The cooled wall reactor developed at Valladolid University is the only reactor prototype currently in operation with hydrothermal flame as internal heat source that produces a reduced liquid effluent with dissolved solids and a high-pressure and high-temperature effluent [9, 10]. It has been operated for more than 3 years with liquid feeds. With the appropriate heat integration, the heat recovery from the effluent would allow reach a net energy efficiency of 27%.

Hydrothermal flames were first presented in 1988 by Prof Franck [11]. At that time, they were considered a scientific curiosity due to the extremely high pressure (near 100 MPa) and the high concentration of methane used

in the experiment. These are flames produced in aqueous environments at supercritical conditions [12]. Such flames are formed when fuel and oxidant streams are mixed at conditions that enable autoignition, producing an oxidation process at adequate temperature and rate to produce a luminous flame. The role of the high pressure is to reduce the temperature needed for autoignition, and nowadays the understanding of the phenomenon allows controlling hydrothermal flames at temperatures around 400-500°C. Oxidizing at these temperatures permits reducing the concentration of combustible material in the feed. Besides, the operation under hydrothermal flames allows total oxidation of the wastes within milliseconds residence times, which opens the possibility of developing small combustors to produce high-pressure gas/vapor streams. The application of hydrothermal flames opens a wide field for the production of energy from wastes.

Research is still needed to improve the reactors development in order to operate with waste suspensions for energy production and reducing the reactor cost. It is also necessary to progress in the effluent energy recovery, not only the thermal energy but also the work. The improvement of this energy recovery will open the opportunity to operate with air as an oxidant and in small scale plants. The knowledge and experience obtained from SCWO environmental applications can foster the development of SCWO energy generation processes. The main differences are the operation with higher organics concentration (fuel) that needs to be taken into account along with the physical properties of the mixture. Also, the hydrothermal flame kinetic studies and modeling are essential to improve the understanding of the process.

In this manuscript a review of the research in the use of SCWO for energy production to date is presented as well as the research needs for the future development of this process.

1.2 Supercritical water as reaction media

1.2.1 Properties

Supercritical water (SCW) acts as a non-polar dense gas and its solvation properties resemble those of a low-polarity organic solvent. SCW shows complete miscibility with "permanent" gases, such as nitrogen, oxygen, and carbon dioxide, while inorganic salts are almost insoluble in it [13]. It presents also high diffusivities and low viscosities. Concerning the modeling of industrial SCWO processes working with high organic material concentrations, interest is focused on knowing the properties of aqueous mixtures.

When energy balances are necessary, a good estimation of the thermo-

physical properties is required, and when Computational Fluid Dynamics (CFD) modeling is performed a good knowledge of the transport properties is also needed. With the scaling up of processes and the interest in their heat integration, models taking into account mass and energy balances were developed [5, 6, 14, 15]. To obtain accurate results from this kind of models, precise values of densities, enthalpies, and heat capacities are needed, for both water and aqueous mixtures. Calculating the properties of aqueous systems in the surroundings of the critical point of water is a difficult task. Conventional cubic equations of state (EoS) are not very accurate in this region, although the Peng-Robinson EoS with the volume translation correction (VTPR EoS) [16, 17] is able to reproduce densities of the water-air system quite accurately and to reproduce the behavior of real SCWO reactors (eg. [18, 19]). Anikeev et al. [20] also used a cubic EoS, the Redlich-Kwong-Soave (RKS) [21], to describe the dehydration of 2-propanol in supercritical water. Kutney et al. [22, 23] developed a hard-sphere volume-translated van der Waals EoS able to calculate thermodynamic properties of several substances involved in the SCWO and their mixtures in conditions up to 40 MPa and 500°C. Densities and residual properties can be predicted with average errors of 5 and 7%, respectively. The presence of salts in the mixture modifies the liquid-vapor equilibrium and more complicated EoS are necessary. Anderko et al. [24] summarized several EoS developed for modeling high-temperature and supercritical electrolyte-aqueous systems, including the Anderko-Pitzer EoS [25]. It is a comprehensive EoS for representing liquid-vapor and solid-liquid equilibria as well as volumetric properties. In the Anderko-Pitzer model, the EoS parameters were fitted to an extensive amount of experimental data of the water-NaCl system in the temperature range from 573 to 773 K and to a more limited amount of data above 773 K and pressures up to 500 MPa. In both temperature regions, the EoS reproduces the liquid-vapor equilibrium, volumetric properties, and solubility of solid NaCl within experimental uncertainty. An extensive list of salt-water systems correctly described by extensions of the Anderko-Pitzer EoS can be found in Bermejo and Cocero [7]. Even though there are several models for thermodynamic properties calculation, most of the works available in literature estimate mixture properties using cubic EoS or averaging tabulated reference properties of the pure components, as shown in table 1.1.

The development of more complex reactor designs, such as the reverse flow reactor vessel or the transpiring wall reactor, and the awareness of the importance of the reagents mixing [40] have opened the way to more complicated models using CFD tools [18, 33, 39] to accurately describe the flow pattern inside the reactor. With this objective, the momentum balance must be solved and accurate values of the transport properties are needed.

Table 1.1: Thermodynamic models used for calculations of density and heat capacity in SCWO mixtures.

Work	Density	Cp
Anikeev et al. [20]	RKS	-
Bermejo et al. [26]	VTPR	IM (NIST)[a]
Chen et al. [27]	Pure Water	Pure Water
Donatini et al. [15]	PSRK	-
Dutournié et al. [28]	Pure Water	Pure Water
Lavric et al. [6]	PR	PR
Leybros et al. [29]	IM (VTPR)[a]	IM (VTPR)[a]
Lieball [18]	IM (VTPR)[a]	IM (VTPR)[a]
Moussière et al. [30]	Ideal Mixing	Ideal Mixing
Moussière et al. [31]	IM (NIST)[a]	IM (NIST)[a]
Narayanan et al. [32]	IM (VTPR)[a]	IM (VTPR)[a]
Oh et al. [33]	IM (SR-Polar, NIST)[ab]	IM (SR-Polar, NIST)[ab]
Queiroz et al. [34]	VTPR	PR
Queiroz et al. [35]	VTPR	PR
Sierra-Pallares et al. [36]	VTPR	VTPR
Vielcazals et al. [37]	Pure Water	Pure Water
Zhou et al. [38]	IM (NIST)[a]	IM (NIST)[a]
Zhou et al. [39]	SUPER-TRAPP	SUPER-TRAPP

[a] IM stands for ideal mixture. The property of each pure component is calculated by the method inside parenthesis.
[b] NIST for water; SR-Polar for other species.

Viscosity. The prediction equation described by Huber et al. [41] is recommended by the International Association for Properties of Water and Steam (IAPWS) [42] for calculating water viscosity. This equation computes viscosity as a function of reduced temperature and density and can be applied for pressures up to 1000 MPa and temperatures up to 900°C in some conditions, with uncertainty of 3%. Poling et al. [43] discuss three methods of viscosity estimation for gas mixtures at high pressures: Lucas [44], Chung et al. [45] and TRAPP method [46, 47]. The three methods yield similar results, but TRAPP procedure can be extended to liquid region.
Thermal Conductivity. The formulation recommended by IAPWS for the calculation of the thermal conductivity of water as a function of temperature and density is presented by Huber et al. [48]. The range of application is up to 1000 MPa and up to 900°C, and the uncertainties at the usual conditions of SCWO are between 4 and 6% [49]. Poling et al. [43] presented also three methods to estimate thermal conductivity of high-pressure gas mixtures (Stiel and Thodos [50], Chung et al. [45] and TRAPP [46, 47]), all of them with errors averaging about 5 to 7%. However, the database used for testing is small and does not contain polar fluid mixtures.
Diffusion Coefficient. Most of the research work done in the field of diffusion coefficients in supercritical fluids is focused on extraction processes and chromatography. Hence, the experimental data and correlations available for diffusivities come mainly from non-aqueous systems, where the solvent is an organic (e.g. ethylene, propane, hexane) or CO_2 [51, 52]. For aqueous systems, diffusivity data near the critical point are much more limited. Kutney [51] studied a large list of methods for the prediction of self-diffusion coefficients for the system acetone-water and recommended two methods: the method of Mathur and Thodos [53], based on Kinetic Theory; and the modified method called Tracer Liu-Silva-Macedo [54], based on Hard-Sphere Theory. Poling et al. [43] recommend the simple correlation of He and Yu [55] for binary diffusion coefficients, while Svishchev and Plugatyr [56] used Molecular Dynamics simulation for modeling the SCWO of o-dichlorobenzene. In practice, the industrial and pilot SCWO plants work with flow rates that lead to turbulent flow regime, where the diffusive transport is negligible if compared to the "turbulent diffusion" result of fluctuations in the advective transport. Thus, detailed models for the laminar diffusion coefficient are not necessary.

Table 1.2 shows the approaches used in some works concerning CFD simulation of SCWO reactors.

Table 1.2: Methods of estimation of transport properties used in CFD models of SCWO.

Work	Viscosity	Thermal Cond.	Diffusivity
Bermejo et al. [26]	IM (NIST)[a]	IM (NIST)[a]	-
Chen et al. [27]	Pure Water	Pure Water	Pure Water
Dutournié et al. [28]	Pure Water	Pure Water	-
Leybros et al. [29]	Ideal Mixing	Ideal Mixing	-
Lieball [18]	IM (Chung et al.)[a]	IM (Chung et al.)[a]	Liu & Macedo, He [c]
Moussière et al. [30]	Ideal Mixing	Ideal Mixing	-
Moussière et al. [31]	IM (NIST)[a]	IM (NIST)[a]	-
Narayanan et al. [32]	IM (Chung et al.)[a]	IM (Chung et al.)[a]	He
Oh et al. [33]	IM (SR-Polar, NIST)[ab]	IM (SR-Polar, NIST)[ab]	-
Queiroz et al. [35]	IM (NIST)[a]	TRAPP	-
Sierra-Pallares et al. [36]	Lucas et al.	Lucas et al.	Mathur & Thodos
Zhou et al. [38]	IM (NIST)[a]	IM (NIST)[a]	-
Zhou et al. [39]	SUPER-TRAPP	SUPER-TRAPP	-

[a] IM stands for ideal mixing. The property of pure component is calculated by the method inside parenthesis.
[b] NIST for water; SR-Polar for other species.
[c] Liu & Macedo for water; He for other species.

1.2.2 Kinetics

The development on the SCWO process as waste elimination technology has impulsed the quantitative understanding of the SCWO reaction rates of different types of organic species at the lower temperatures of 450-500°C [57]. The focus of these kinetic studies has typically been on model compounds rather than on actual waste. These compounds have been chosen because they contain key functional groups of importance and/or represent the rate limiting step in the breakdown of a range of complex waste species [58]. Considering only homogeneous reactions without catalysts, extensive data on SCWO kinetics have been reported for a number of model compounds [57–62].

In the field of complex chemistry, Webley and Tester [63] did the pioneering work by adapting a gas-phase combustion mechanism with 56 reversible elementary reactions to SCWO conditions. They found that the model predicts methanol oxidation to be much more faster than it was observed experimentally, and this mismatch led them, and others, to speculate on how SCW might be influencing the kinetics. More recent work in the field, however, which consistently finds good agreement between experimental and predicted kinetics, suggests that the chief reason for this earlier discrepancy was the authors' use of a value for the rate constant for the reaction $H_2O_2 \leftrightarrow OH + OH$ that was about two orders of magnitude too high. This high value appeared to result from Webley and Tester erroneously extrapolating the low-pressure limit rate constant to the high-pressure encountered in SCWO [64]. Dagaut et al. [65] used a mechanism derived from that published for the atmospheric combustion of natural gas. The pressure dependencies, relevant for the SCWO conditions were included as well as the collision efficiency of water, when appropriate, using literature values. Troe's formalism [66] was used to derive the modified Arrhenius expressions used at high pressure. Alkam et al. [67] investigated oxidation kinetics of methanol and hydrogen in a supercritical water medium. They suggested that kinetic models developed for low-pressure applications, even the models that contain pressure-dependent reaction rates, should be corrected to account for high-pressure encountered in SCWO conditions. According this work, the decomposition of H_2O_2 into $OH\cdot$ radical is the dominant reaction controlling the destruction of methanol at high pressures, and the reaction rate is twenty times higher than at atmospheric pressure.

Most kinetics found in literature were obtained in flameless conditions and are not able to describe flame regime, predicting slower reaction rates [68]. What is more, these models are not always consistent with each others in the same range of conditions [57, 69]. To the best of our knowledge,

the only kinetic model adjusted in hydrothermal flame regime is reported by Queiroz et al. [34], developed by adjusting temperature increments in time in order to detect the sharp composition change associated to these temperature changes. Kinetic models could be improved by knowing the concentration of key compounds at different points of reactors especially in hydrothermal flame regime where the reaction rates are faster. Concentration profiles in SCWO reactors are very difficult to obtain due to fast reaction rates and usually only global conversions are reported, except when optical devices are used [70–72]. The lack of reliable kinetic models is one of the reasons why most of the modeling of hydrothermal flames is based on mixing controlled reactions [32, 73]. This approach is valid for non-premixed flames at high temperatures since it assumes that chemical reaction is fast compared to the transport processes involved in the flow.

1.3 Hydrothermal flames

Hydrothermal flames are defined as flames produced in aqueous environments at conditions above the critical point of water (P $>$ 22.1 MPa and T $>$ 374°C)[12]. Usually a flame is defined as the visible part of the combustion reaction and consists of a surface where reaction occurs. This surface separates the oxidant from the fuel, in the case of diffusion (non-premixed) flames; or it separates the reagents from the reaction products, in case of premixed flames [74]. In premixed flames, that surface is moving towards the reagents with a flame front velocity. If this velocity is the same as the fluid velocity, the flame will remain stationary. If flow velocity is higher or lower than flame front velocity, the flame is blown away from the tube or it will move against the flow, resulting in backfire, respectively [74].

The term "hydrothermal combustion" was first used by Franck to describe oxidation processes taking place in dense aqueous environments [11]. The presence of a flame in a SCWO should enhance the elimination efficiency of the SCW medium [75]. However, only a few works about hydrothermal flames have been published [12]. In general, flames ignited spontaneously beyond a certain temperature, normally between 400 and 500°C [76]. This auto ignition temperature was decreased for higher pressures and fuel concentrations.

The first reactor probably working with a premixed hydrothermal flame inside was the MODAR reactor [33]. Serikawa et al. [77] developed a continuous refrigerated facility for observing hydrothermal flames oxidizing isopropyl alcohol. The ETH Zurich has been developing different continuous hydrothermal burners working with non premixed flames [78, 79]. They used the hy-

drothermal flame as an internal heat source in a transpiring wall reactor. The direct injection of the waste into a hydrothermal flame was developed as a solution to avoid the external preheating of the feed up to supercritical conditions [78–80]. Sobhy et al. [81] designed a semi-batch visual flame cell, working with methanol-air flames. In the reactors used in the University of Valladolid, operational conditions were above the ignition conditions of IPA according to Serikawa et al. [77], thus they can be described as working at hydrothermal flame regime with a premixed flame [68, 82, 83]. These reactors present the advantage that the cold feed can be directly injected in the flame without preheating.

SCWO with a hydrothermal flame has a number of advantages over the flameless process. Some of these advantages permit overcoming the traditional challenges that make the successful and profitable commercialization of SCWO technology difficult [12]:

- It allows the destruction of the organics in residence times of a few milliseconds, which permits the construction of smaller reactors.

- Higher operation temperatures improve the energy recovery.

- It is possible to initiate the reaction with feed injection near to room temperature, avoiding problems such as plugging and corrosion in a preheating system, and having an advantage from the operational and energy integration perspective.

Compared to typical reaction temperatures of 450-600°C in conventional SCWO reactors, hydrothermal flames can reach temperatures above 1000°C, although temperatures between 600 and 700°C are normally used. Higher temperatures enable a higher thermodynamic efficiency in the energy recovery, but extraction of hot fluid directly from the hydrothermal flame has significant technical challenges, including corrosion problems. Most reactor designs working in hydrothermal flame regime rely on the injection of coolant streams in order to protect reactor walls from damage caused by the oxidation conditions at such high temperatures [78, 80, 84]. Such coolant streams dilute the reactor effluent and reduce its thermal quality.

Recently, our research group patented a new cooled wall reactor working with a hydrothermal flame as a heat source that presents the additional advantage that part of the products can be extracted of the reactor by its upper part, without mixing with the cold water, allowing better energy integration because an effluent at temperatures between 600 and 700°C can be obtained [10].

1.4 Reactors for SCWO

The design of SCWO reactors has evolved on the direction of solving the main problems of the process, as a waste elimination technology without paying attention to the energy integration of the process: corrosion and salt deposition. Thus, besides the largely used tubular reactors, the main developments have been centered on transpiring wall (TWR) and cooled wall reactors (CWR) [85]. These reactors minimize the corrosion by reducing the wall temperature. The cooling effect is provided by a flow of water transpiring through a porous wall (TWR) or by a film of cool water (CWR). In any case, temperature of water is usually subcritical, to dissolve the salts, and as a consequence the hot products of oxidation are cooled and diluted, so the outlet temperature of the products is not high enough for a good heat recovery [7]. Due to this, among the many reactors and process modifications developed so far, only a few of them are susceptible to be used if energy production is the main objective of the SCWO facility.

Tubular Reactor. The tubular reactor is the simplest design and the most used one. Most big and industrial plants constructed so far use this kind of reactor [1]. It has been demonstrated that it is able to sustain hydrothermal flame and complete the reaction in residence times lower than 1 s [68, 86], providing a simple and compact device for energy production if "clean" feeds, free of inorganic substances, are used. When dealing with feeds containing inorganic compounds or solids suspension this device presents a series of limitations. Its main disadvantage is the easy plugging of the reactor itself due to precipitation of salts during the oxidation process. To avoid this, the diameters of tubular reactors should be small enough for obtaining a high speed of the circulating fluid in order to reduce the deposition of salts and even then, the precipitated salts can stick to the reactor walls. This lead to another associated problem. Hydrothermal flame presents low flame front propagation velocities, and high flow velocities would make the flame to be blown out of the reactor [83]. Thus, ignition must be produced in every element of the fluid, by preheating feed up to the autoignition temperature of the reaction mixture, which in most cases is around 400°C. This would lead to serious plugging and corrosion problems also in the preheating system.

Another disadvantage, is the high temperature that the walls of the tube should support (600-700°C). The whole reactor must be constructed in materials resisting such high temperatures like Ni-Alloys. As in this kind of reactors the wall is supporting also the pressure, thick walls of this special materials must be used increasing the cost of reactors. In addition it is possible to suffer the formation of hot spots when oxidation reactions run out of control. A control system discussed in several patents [4] consists

of carefully dosing feed, oxidant and/or quenching water through multiple-injection schemes. This method is a good solution if feed is injected to control the temperature of the reactor as it also allows heating the feeds introduced through the lateral inlets by direct contact with the reaction products, avoiding feed preheating, improving energy integration and avoiding salt precipitation problems during preheating. On the other hand, quench water injection would highly disfavor energy balance of the facility.

Furthermore, the strategy to periodically wash the equipment with room-temperature water to clean salt deposits, even when having more than one reactor connected in parallel (while one reactor is cleaned the remaining reactors could stay operational) would disfavor tremendously the energy balances. A lot of energy is lost in cooling this heavy thick wall reactors for cleaning and preheating them again for operation.

Reverse Flow Tank Reactor with a Brine Pool (MODAR Reactor). This reactor presents a very appropriate design for energy generation and working in hydrothermal flame regime. It consists of an elongated cylinder which constitutes the inner reaction chamber. Inside it there are two different zones: an upper zone at supercritical temperature (near 600°C), and a lower region at subcritical temperature ($\sim$ 300°C). The oxidation reaction takes place in the upper zone in which supercritical conditions are achieved. Inorganic salts or other dense material introduced with the feed or formed by chemical reactions are insoluble in supercritical fluids, thus, they precipitate and pass to the subcritical zone where they are dissolved in the brine pool. Furthermore, to avoid the deposition of these substances inside the wall reactor, it has a water film which covers the wall [33]. The upper effluent, free of salts, is available at high temperature, while the salts are retired dissolved in the secondary effluent (brine at subcritical conditions).

Cooled Wall Reactor. The cooled wall reactor has a design that separates the effects of temperature and pressure in the SCWO. The external wall, which holds the pressure, is maintained at about 400°C by the action of a cooling water flow pumped downward between the external and internal walls. This external pressure vessel can be constructed of stainless steel because it is not exposed to oxidizing atmosphere nor temperatures higher than 400°C. The internal wall is where the reactants are mixed and the reaction takes place. It is built with a special material capable of resist the oxidizing atmosphere at temperatures up to 800°C [7]. A new cooled wall reactor working with a hydrothermal flame as a heat source was patented in 2009 [10]. The main difference compared to previous designs is that aqueous feed and air can be injected cold in the reactor over the hydrothermal flame, while the stream circulating between the pressure vessel and the reaction chamber is simply cold pressurized water. This water stream is entering in

the reaction chamber by its lower part, accumulating as a subcritical water "pool" that dissolves the salt precipitated in the upper area of the reactor. It has been tested successfully with salty feeds and with sewage sludge [83, 87]. This reactor presents the additional advantage that part of the products can be extracted by its upper part, without mixing with the cold water, allowing better energy integration since an effluent at temperatures between 600-700°C can be obtained.

1.5 SCWO for energy production

The importance of energy recovery (and/or power generation) for successful SCWO commercialization is already highlighted by the interest of SCWO companies in optimizing the energy integration of this processes. SuperWater Solutions claim that their process for sewage sludge oxidation is as efficient generating steam and converting it to electricity as a coal power plant [88]. SuperCritical Fluids International offers as benefit of AquaCritox®process for sludge treatment, the generation of renewable energy by replacing the boiler in a standard steam loop [89].

Basic theoretical calculations indicate that feeds with an energy content of 930 kJ/kg (roughly equivalent to an aqueous solution with 2% ww of hexane) can supply enough energy to preheat the feed from room temperature up to 400°C, and to generate electric power equivalent to that consumed by the high-pressure pump and the air compressor [5]. In practice, higher energy contents are required to achieve an energetically self-sustaining process, due to inefficiencies in the conversion and use of energy.

Vadillo et al. [90] compared some studies, in which technical constraints limit the energy recovery of the process when the outlet temperature of reactors is below 400°C. In that case, the energy can be recovered by low pressure steam generation or by heating municipal water. They conclude that, from the point of view of power generation, higher temperatures of effluents of SCWO reactor are needed to increase the efficiency of a feasible Rankine cycle. High temperatures at the outlet can only be achieved if the reactor is designed attending this purpose. The potential of this application is mentioned in some patents [91, 92].

One of the key parameters that must be considered for the design of a SCWO system for energy production is the choice of the oxidant. From the reaction point of view, using air or oxygen shows no influence on the conversion of the feed oxidized [40]. Thus, the election of the oxidant is a question of safety and economy, depending on the size of the facility, the energy source available or the working hours. Air is the cheapest material, but

it contains a large amount of nitrogen that has to be pressurized, and that acts as a diluent that reduces the temperature of effluents and, therefore, its thermal quality. On the other hand, cryogenic liquid oxygen carries no diluents, and air compressors could be replaced by low consumption cryogenic pumps. Furthermore, pure oxygen does not need to be preheated up to feed injection temperature. However, the cost and energy consumption of producing pure oxygen could affect the viability of the process. For example, Cabeza [9], studied the energy production by SCWO of urban sludge, assuming that the products of reaction could be expanded in a turbine. It was found that, if oxygen is produced in situ by air distillation, the net electricity produced would be positive if the consumption in the distillation process is below 0.99 kWh/kg-O_2. As reference value, Kansha et al. [93] gives an energetic consumption of 0.40 kWh/kg-O_2, for a conventional cryogenic plant. An intermediate option is the use of oxygen-enriched air. It is commercially available at different proportions with an oxygen content as high as 95%. Using rich-air with 40% of oxygen, the higher cost of equipment, including compressors and selective membranes for air enrichment, are compensated by moderate electrical cost, since the air flow is nearly half of the corresponding flow of atmospheric air.

Several studies of the production of electrical energy from SCWO has been proposed. Some of them are commented here as function of the global energy production efficiency defined as the electrical energy produced minus the energy consumed divided by the heat content of the waste, as shown in eq. (1.1).

$$\text{Global efficiency} = \frac{\text{Produced Power} - \text{Consumed Power}}{\text{Heat of Reaction}} \tag{1.1}$$

Smith Jr. et al. [14] used exergy analysis to study the partial and total oxidations of methane in supercritical water for a heat-integrated supercritical water reactor and electrical energy production system. They assume a direct expansion of products (at 400°C) in a turbine, followed by heat recovery of the expanded stream. It was found that the process could be energy self-sufficient and optimum flow rates were calculated in order to minimize reactor heat requirements or maximize net electrical work.

Lavric et al. [6] studied theoretically the energy integration of a SCWO process to treat dilute organic waste at a temperature of 650°C. Firstly the thermal self-sufficiency is ensured by preheating the feed in a heat exchanger using the hot products. The power self-sufficiency is studied for three possible solutions:

1. Supercritical water expansion in a turbine.

2. Closed Brayton Cycle.

3. Organic Rankine cycle.

Using a small supercritical turbine, the effluent stream at 650°C is split and 27.5% of the flow is expanded to produce electricity, the remainder being used to preheat the feed. They report a production of 154 kW, enough to cover the consumptions of pump and compressor, with efficiency in producing electricity of 12%. They found that Closed Brayton Cycle with helium or carbon dioxide as working fluids could not even achieve a sufficient production of energy to cover consumption in the process, unless unrealistic efficiencies were assumed for compressors and turbines. In the application of an Organic Rankine Cycle the authors proposed to use the effluent of the reactor at 650°C to preheat the feed, and using the cooled effluent at 250°C as a heat source of the Brayton cycle. They found several organic solvents that can be used in the Organic Rankine Cycle covering the power requirements of the plant. The best efficiencies were achieved using R123 as working fluid, and ammonia and isopentane also were suitable choices. The global efficiencies obtained were between 0.15 and 2.6% considering the heat released in the reactor. The results obtained showed that a small scale SCWO plant can be energetically self-sufficient using either a small supercritical turbine or an Organic Rankine Cycle.

Bermejo et al. [94] performed a theoretical study of power generation plant from oxidation of coal by SCWO using a transpiring wall reactor. Two versions of SCWO power plant were proposed. In the first one, the effluent at 650°C and 30 MPa is expanded in a steam turbine until atmospheric pressure, with an efficiency of 37%. The second alternative of SCWO power plant considers an intermediate reheating for partially expanded steam to get a higher efficiency (40%). It is observed that much higher amount of energy is obtained in this last work than in the work performed by Lavric et al. [6]. In one hand, the objectives of both works are different: in one case it is important to make self-sufficient a small facility, while in the other the viability of a full scale power plant is investigated, thus the solutions adopted in each case are different. In addition, in the second work they make use of an additional fuel to make the preheating of the feed. Even when the calorific power of the additional fuel was taken into account for calculating the global energy efficiency, it is much favorable from the energetic point of view to use this external fuel to preheat the feed than using the effluent. This can be explained because the effluent has a certain amount of energy due to the high pressure that it is lost if the heat content of this stream is used by heat transmission instead of using by expanding in a turbine.

Donatini et al. [15] also discuss the SCWO of coal in power plants with low CO_2 emissions. The power generation system is constituted by a conventional reheat Rankine cycle, using the reactor as boiler (around 600°C), and an efficiency of 27.9% was found. An innovative application is the use of rotary separator turbines (RST) at depressurization (instead of valves) for recovering part of the pressure work. The RST has the ability to generate power using a two-phase, liquid-vapor stream, while simultaneously separating and pressurizing the liquid in preparation for reinjection. Some conventional applications of RST are geothermal energy systems [95] and refrigeration cycles [96]. However, to the best of our knowledge, practical applications of RST at supercritical pressures are still not reported.

Another analysis was made by Cabeza et al. [87]. In this work, a theoretical analysis of the feasibility of producing energy from the SCWO of sludge was performed. Optimal conditions for the reaction were temperature of 600°C and pressure of 23 MPa, thus this was considered as the conditions of the effluent. In this work the energy production was considered taking into account different options: direct expansion of the effluent in a supercritical turbine, or generation of steam for a Rankine cycle at 4.6 MPa and 400°C. Direct expansion gives an efficiency of 9% with feed at room temperature and preheating the feed with an external heat source improves the process efficiency. Steam generation does not cover the plant demand. However, direct expansion is hampered by higher equipment and operation costs due to harsh operational conditions in the turbine. Another design consideration made in this work is whether reactor feed preheating is carried out by heat exchange with the effluent, or if an external heating system is used. It was found that using an external heat source for feed preheating is more efficient than spending part of effluent energy on it. This result is valid assuming air as oxidant, but have small influence when oxygen is used.

In general, the option of directly expanding the SCWO effluent is, by far, the most energetically efficient. However, it will not be applicable in the short term, mainly due to the fact that the composition of the effluent (50-80% mole of water, carbon dioxide and nitrogen if air is used as oxidant) makes it not suitable for expansion in a conventional turbine, being the effluent an intermediate between the pure water used in steam turbine and the flue gases, products of combustion used in gas turbines. Thus, technical issues prevent the effective implementation of direct expansion in the short term and that is why research is needed in order to develop this energetically more favorable alternative of energy recovery [97].

1.6 Modeling of SCWO

To enhance the development of SCWO processes for industrial-scale applications, including power generation, it is necessary to understand the reactor performance and develop reliable simulation models. Bermejo et al. [98] gave a classification of these models in three main categories. The simplest kind of models assumes some level of conversion (without kinetic modeling) and solves mass and energy balances, like in the works of Cocero et al. [5] and Lavric et al. [99]. This kind of model is useful for analysis of energy efficiency in SCWO, and it just needs accurate values of enthalpies and heat capacities. Increasing complexity, models that include simple flow patterns (plug flow or perfect mixing) can give more information about the behavior of particular reactors (e.g. [19, 27, 100–102]). Models like those need a kinetic model for the reaction and also good predictions of densities. Due their simplicity they can easily solve non-stationary reactors and can be used in control systems that demands fast responses [102, 103]. To overcome the problems of corrosion and salt deposition, and to improve the energy recovery efficiency, several reactors with complex designs have been developed. These reactors can present flow patterns quite different from plug flow or perfectly mixed. Models for these new reactors are also more complicated and usually use CFD tools [18, 26, 31, 32, 39]. Thus, this family of models solves conservation equations, the applicable constitutive equations, and dynamically calculates transport properties at different conditions as needed. CFD models can describe temperatures and conversions, show recirculation areas, and predict how the salt deposition occurs. These models are very important when a hydrothermal flame is present or when multiple outlets reactors are used.

When dealing with hydrothermal flames, the turbulence-chemistry interactions become important given the time scale of the processes. The chemical time scale (related to reaction rate) and the mixing time scale (related to turbulence) must be known in order to choose the correct model [104]. In a flameless oxidation, the mixing of reagents is usually faster than the reaction, hence the process is limited by chemistry and an accurate kinetic model is necessary. On the other hand, in presence of a flame, the high temperatures make the reaction rate much higher than the mixing rate, leading to the concept of "mixed is burnt", where the mixing controls the combustion and a correct mixing model is needed [104]. For non-premixed flames, the mixing refers to fuel and oxidant, while for premixed flames, it is related to mixing cold reagents and hot products. In most of CFD works (see table 1.2), both characteristic times are calculated and the slowest process is assumed as dominant. Using this approach, Oh et al. [105] identified the zones of their

reactor where the reaction is chemistry or mixed controlled. They affirm that the mixing zone downstream of the nozzle where the fluids are mixed is chemical-kinetics limited, and outside of this mixing zone the reaction is diffusion limited. Sierra-Pallares et al. [36] used a mixing model developed for liquid phase, and found better results than the traditional model for gas phase.

Given the importance of turbulence for hydrothermal flames, more developments in turbulence models must be done. Turbulence models are important not only for the mixing description, but also for the heat transfer calculation. The flow in vertical reactors is affected by buoyancy and the heat transfer coefficients can be deteriorated or enhanced, depending on buoyancy forces [106]. Even though there are some studies about the performance of turbulence models for supercritical fluids ([73, 106–108]), there is still not a common opinion about the choice of the turbulence model.

1.7 Research needs and challenges

Oxidation under hydrothermal flame can intensify the supercritical water oxidation process in order to develop micro combustors to produce high pressure and temperature steam from wastes. To develop this process research should be addressed to study the hydrothermal flame oxidation conditions and kinetics of key chemical compounds and wastes. In such applications, feed can be directly introduced in the flame avoiding the highly corrosive preheating step.

Biomass could be also an interesting feed material to produce energy by SCWO with hydrothermal flame as internal heat source. The study of the conditions to produce hydrothermal flame from biomass is a challenge to develop decentralized biorefineries. In addition technical solutions for injecting biomass in a hydrothermal flame combustor must be developed. For example continuously pumping highly concentrated biomass suspensions up to supercritical pressures and its reactor injection is still a challenge.

Different waste and fuels with high concentration in inorganics and heteroatoms, problematic to be burnt with the conventional atmospheric combustion, are potential fuels to be used in SCWO for energy production because, with this technology, clean combustion can be obtained. Nevertheless, inorganics are not soluble in SCW and are susceptible to cause plugging problems in the reactor. What is more, the introduction of these inert materials in the reactor cause significant energy inefficiency. Research needs to develop SCW pretreatment steps that avoid the introduction of these solids in the SCWO reactor.

Currently, there are a number of reactor designs susceptible to work under hydrothermal flame regime with the main objective of producing energy efficiently such as tubular reactors, reverse flow reactors or cooling wall reactors. Nevertheless their performance in these conditions must be thoroughly investigated and their design and construction materials optimized in order to accomplish this new challenge.

Existing literature on SCWO process focusing on clean energy production has been reviewed. Most of the practical (including commercial) development is based on recovering the heat released by waste oxidation and generating steam. Many theoretical works point that the process would be much more efficient if the compression energy could be recovered as work.

Considering its high temperature and pressure conditions power/shaft work and high grade thermal energy can be potentially recovered from SCWO reactors outlet streams rendering these processes net producers of energy. But those severe conditions, as well as the non-conventional – in the energy-production processes field – composition of streams pose challenges that need to be addressed in order to develop this aspect of the technology. Expansion devices appropriate to streams nature and conditions, and efficient enough should be developed and engineered. This is a major undertaking mainly due to the difficulties related to aero/hydrodynamic, structural and mechanical design concerns. Those will certainly be accompanied by operational issues concerning the handling and mixing of streams at very different pressures and temperatures in common flowpaths, corrosion issues due to particles present in expanding streams, special conditions thermal transfer between streams and dynamic behavior of the energy producing SCWO unit in relation to the plant as a whole in case of tight energy integration.

Modeling is an essential tool to reduce experimental work and to study the scale-up of processes. It becomes even more important when hydrothermal flames are present, since their behavior can not always be observed directly. The improvement of models will require coupling experimental studies with CFD simulations of the reaction process. These models will need better sub-models, especially kinetic, turbulent, and mixture equations of state and transport models. For example, there is still need for transport property methods capable of predicting aqueous mixtures properties in both regions, liquid and supercritical. Also, turbulence models must be validated when applied to supercritical fluids, where strong variations on thermal and transport properties are expected. Abundant information can be extracted from the supercritical water oxidation previous studies, but there is still space for much more work.

Nomenclature

P	pressure (MPa)
T	temperature (K)
c_p	constant pressure heat capacity ($J\,kg^{-1}K^{-1}$)

Abbreviations

CFD	computational fluid dynamics
EoS	equation of state
PR	Peng-Robinson equation of state
IPA	isopropyl alcohol
NIST	National Institute of Standards and Technology
PSRK	Predictive Soave-Redlich-Kwong EoS
RKS	Redlich-Kwong-Soave EoS
SCW	supercritical water
SCWO	supercritical water oxidation
SR-Polar	Schwartzentruber-Renon EoS
TOC	total organic carbon
TWR	transpiring wall reactor
VTPR	volume translated Peng-Robinson EoS

Acknowledgments

The authors thank the Spanish Ministry of Science and Innovation for the Projects CTQ2011-23293 (subprogram PPQ) and ENE2012-33613. J. P. S. Queiroz thanks the Spanish Ministry of Education's FPU program (AP2009-0399) for his PhD grant.

Bibliography

[1] P. A. Marrone, Supercritical water oxidation - current status of full-scale commercial activity for waste destruction, The Journal of Supercritical Fluids 79 (2013) 283–288.

[2] P. Kritzer, Corrosion in high-temperature and supercritical water and aqueous solutions: a review, The Journal of Supercritical Fluids 29 (2004) 1–29.

[3] P. Marrone, G. Hong, Corrosion control methods in supercritical water oxidation and gasification processes, Journal of Supercritical Fluids 51 (2009) 83–103.

[4] A. Martin, M. D. Bermejo, M. J. Cocero, Recent developments of supercritical water oxidation: A patents review, Recent Patents on Chemical Engineeringe 4 (2011) 219–230.

[5] M. J. Cocero, E. Alonso, M. T. Sanz, F. Fdz-Polanco, Supercritical water oxidation process under energetically self-sufficient operation, The Journal of Supercritical Fluids 24 (2002) 37–46.

[6] E. D. Lavric, H. Weyten, J. De Ruyck, V. Pleşu, V. Lavric, Delocalized organic pollutant destruction through a self-sustaining supercritical water oxidation process, Energy Conversion and Management 46 (2005) 1345–1364.

[7] M. D. Bermejo, M. J. Cocero, Supercritical water oxidation: A technical review, AIChE Journal 52 (2006) 3933–3951.

[8] D. Xu, S. Wang, C. Huang, X. Tang, Y. Guo, Transpiring wall reactor in supercritical water oxidation, Chemical Engineering Research and Design (2014). In Press, available online 4 March 2014. doi: 10.1016/j.cherd.2014.02.028.

[9] P. Cabeza, Studies in the development of SCWO vessel reactors with hydrothermal flame as an internal heat source, PhD thesis, Universidad de Valladolid, Valladolid, 2012.

[10] M. D. Bermejo, P. Cabeza, J. P. S. Queiroz, C. Jimenez, M. J. Cocero, Aparato y pocedimiento para la generación de llamas hidrotermales autotérmicas, ES2381345 A1, 2012.

[11] W. Schilling, E. Franck, Combustion and diffusion flames at high-pressures to 2000 bar, Berichte Der Bunsen-Gesellschaft-Physical Chemistry Chemical Physics 92 (1988) 631–636.

[12] C. Augustine, J. Tester, Hydrothermal flames: From phenomenological experimental demonstrations to quantitative understanding, Journal of Supercritical Fluids 47 (2009) 415–430.

[13] P. A. Marrone, G. T. Hong, Supercritical water oxidation, in: M. Kutz (Ed.), Environmentally Conscious Materials and Chemicals Processing, John Wiley & Sons, Inc., 2007, pp. 385–453.

[14] R. L. Smith Jr., T. Adschiri, K. Arai, Energy integration of methane's partial-oxidation in supercritical water and exergy analysis, Applied Energy 71 (2002) 205–214.

[15] F. Donatini, G. Gigliucci, J. Riccardi, M. Schiavetti, R. Gabbrielli, S. Briola, Supercritical water oxidation of coal in power plants with low CO2 emissions, Energy 34 (2009) 2144–2150.

[16] D.-Y. Peng, D. B. Robinson, A new two-constant equation of state, Industrial & Engineering Chemistry Fundamentals 15 (1976) 59–64.

[17] A. Peneloux, E. Rauzy, R. Freze, A consistent correction for redlich-kwong-soave volumes, Fluid Phase Equilibria 8 (1982) 7–23.

[18] K. S. Lieball, Numerical Investigations on a Transpiring Wall Reactor for Supercritical Water Oxidation, Doctor of technical sciences, Swiss Federal Institute of Technology Zurich, Zurich, 2003.

[19] M. D. Bermejo, F. Fernandez-Polanco, M. J. Cocero, Modeling of a transpiring wall reactor for the supercritical water oxidation using simple flow patterns: Comparison to experimental results, Industrial & Engineering Chemistry Research 44 (2005) 3835–3845.

[20] V. I. Anikeev, A. Yermakova, J. Manion, R. Huie, Kinetics and thermodynamics of 2-propanol dehydration in supercritical water, The Journal of Supercritical Fluids 32 (2004) 123–135.

[21] G. Soave, Equilibrium constants from a modified redlich-kwong equation of state, Chemical Engineering Science 27 (1972) 1197–1203.

[22] M. C. Kutney, V. S. Dodd, K. A. Smith, H. J. Herzog, J. W. Tester, A hard-sphere volume-translated van der waals equation of state for supercritical process modeling 1. pure components, Fluid Phase Equilibria 128 (1997) 149–171.

[23] M. C. Kutney, V. S. Dodd, K. A. Smith, H. J. Herzog, J. W. Tester, Equations of State for Supercritical Process Modeling, Laboratory Report MIT EL 94-003MIT, Energy Laboratory and Department of Chemical Engineering, Massachusetts Institute of Technology, Cambridge, MA, 1996.

[24] A. Anderko, P. Wang, M. Rafal, Electrolyte solutions: from thermodynamic and transport property models to the simulation of industrial processes, Fluid Phase Equilibria 194–197 (2002) 123–142.

[25] A. Anderko, K. S. Pitzer, Equation-of-state representation of phase equilibria and volumetric properties of the system NaCl-H2O above 573 k, Geochimica et Cosmochimica Acta 57 (1993) 1657–1680.

[26] M. D. Bermejo, A. Martin, J. P. S. Queiroz, I. Bielsa, V. Rios, M. J. Cocero, Computational fluid dynamics simulation of a transpiring wall reactor for supercritical water oxidation, Chemical Engineering Journal 158 (2010) 431–440.

[27] P. Chen, L. Li, E. Gloyna, Simulation of a concentric tube reactor for supercritical water oxidation, in: Innovations in supercritical fluids, number 608 in ACS Symposium Series, Americal Chemical Society, Washington, DC, 1995, pp. 348–363.

[28] P. Dutournié, J. Mercadier, D. Matéos, F. Cansell, Hydrothermal oxidation treatment reactor: Experimental and simulated study of a non-anticipated phenomenon at the reactor inlet, The Journal of Supercritical Fluids 42 (2007) 234–240.

[29] A. Leybros, A. Roubaud, P. Guichardon, O. Boutin, Supercritical water oxidation of ion exchange resins in a stirred reactor: Numerical modelling, Chemical Engineering Science 69 (2012) 170–180.

[30] S. Moussière, C. Joussot-Dubien, P. Guichardon, O. Boutin, H.-A. Turc, A. Roubaud, B. Fournel, Modelling of heat transfer and hydrodynamic with two kinetics approaches during supercritical water oxidation process, The Journal of Supercritical Fluids 43 (2007) 324–332.

[31] S. Moussière, A. Roubaud, O. Boutin, P. Guichardon, B. Fournel, C. Joussot-Dubien, 2D and 3D CFD modelling of a reactive turbulent flow in a double shell supercritical water oxidation reactor, The Journal of Supercritical Fluids 65 (2012) 25–31.

[32] C. Narayanan, C. Frouzakis, K. Boulouchos, K. Príkopský, B. Wellig, P. Rudolf von Rohr, Numerical modelling of a supercritical water oxidation reactor containing a hydrothermal flame, Journal of Supercritical Fluids 46 (2008) 149–155.

[33] C. Oh, R. Kochan, T. Charlton, A. Bourhis, Thermal-hydraulic modeling of supercritical water oxidation of ethanol, Energy & Fuels 10 (1996) 326–332.

[34] J. Queiroz, M. Bermejo, M. Cocero, Kinetic model for isopropanol oxidation in supercritical water in hydrothermal flame regime and analysis, The Journal of Supercritical Fluids 76 (2013) 41–47.

[35] J. P. S. Queiroz, M. D. Bermejo, M. J. Cocero, Numerical study of the influence of geometrical and operational parameters in the behavior of a hydrothermal flame in vessel reactors, Chemical Engineering Science 112 (2014) 47–55.

[36] J. Sierra-Pallares, M. Parra-Santos, J. Garcia-Serna, F. Castro, M. Cocero, Numerical modelling of hydrothermal flames. micromixing effects over turbulent reaction rates, Journal of Supercritical Fluids 50 (2009) 146–154.

[37] S. Vielcazals, J. Mercadier, F. Marias, D. Matéos, M. Bottreau, F. Cansell, C. Marraud, Modeling and simulation of hydrothermal oxidation of organic compounds, AIChE Journal 52 (2006) 818–825.

[38] L. Zhou, S. Wang, H. Ma, Y. Gong, D. Xu, Oxidation of cu(II)-EDTA in supercritical water—Experimental results and modeling, Chemical Engineering Research and Design 91 (2013) 286–295.

[39] N. Zhou, A. Krishnan, F. Vogel, W. A. Peters, A computational model for supercritical water oxidation of organic toxic wastes, Advances in Environmental Research 4 (2000) 75–90.

[40] B. D. Phenix, J. L. DiNaro, J. W. Tester, J. B. Howard, K. A. Smith, The effects of mixing and oxidant choice on laboratory-scale measurements of supercritical water oxidation kinetics, Industrial & Engineering Chemistry Research 41 (2002) 624–631.

[41] M. L. Huber, R. A. Perkins, A. Laesecke, D. G. Friend, J. V. Sengers, M. J. Assael, I. N. Metaxa, E. Vogel, R. Mareš, K. Miyagawa, New international formulation for the viscosity of H2O, Journal of Physical and Chemical Reference Data 38 (2009) 101–125.

[42] IAPWS, IAPWS 2008 formulation for viscosity of ordinary water, 2012. Http://www.iapws.org/relguide/viscosity.html.

[43] B. E. Poling, J. M. Prausnitz, J. P. O'Connell, The Properties of Gases and Liquids, McGraw-Hill, New York, 5 th edition, 2007.

[44] K. Lucas, Die druckabhängigkeit der viskosität von flüssigkeiten – eine einfache abschätzung, Chemie Ingenieur Technik 53 (1981) 959–960.

[45] T. H. Chung, M. Ajlan, L. L. Lee, K. E. Starling, Generalized multiparameter correlation for nonpolar and polar fluid transport properties, Industrial & Engineering Chemistry Research 27 (1988) 671–679.

[46] J. F. Ely, H. J. M. Hanley, A computer program for the prediction of viscosity and thermal conductivity in hydrocarbon mixtures, number 1039 in NBS Technical Note, National Bureau of Standards (U.S.), 1981.

[47] M. L. Huber, H. J. M. Hanley, Chapter 12 the corresponding-states principle: Dense fluids, in: J. Millat, J. H. Dymond, C. A. N. d. Castro (Eds.), Transport properties of fluids: their correlation, prediction, and estimation, IUPAC/Cambridge University Press, Cambridge, 1996, p. 283.

[48] M. L. Huber, R. A. Perkins, D. G. Friend, J. V. Sengers, M. J. Assael, I. N. Metaxa, K. Miyagawa, R. Hellmann, E. Vogel, New international formulation for the thermal conductivity of H2O, Journal of Physical and Chemical Reference Data 41 (2012) 033102.

[49] IAPWS, IAPWS 2011 formulation for thermal conductivity of ordinary water, 2012. http://www.iapws.org/relguide/ThCond.html.

[50] L. I. Stiel, G. Thodos, The thermal conductivity of nonpolar substances in the dense gaseous and liquid regions, AIChE Journal 10 (1964) 26–30.

[51] M. C. Kutney, Thermodynamic and transport property modeling in super critical water, Thesis, Massachusetts Institute of Technology, 2005. Thesis (Sc. D.)–Massachusetts Institute of Technology, Dept. of Chemical Engineering, 2005.

[52] I. Medina, Determination of diffusion coefficients for supercritical fluids, Journal of Chromatography A 1250 (2012) 124–140.

[53] G. P. Mathur, G. Thodos, The self-diffusivity of substances in the gaseous and liquid states, AIChE Journal 11 (1965) 613–616.

[54] H. Liu, C. M. Silva, E. A. Macedo, Unified approach to the self-diffusion coefficients of dense fluids over wide ranges of temperature and pressure—hard-sphere, square-well, Lennard–Jones and real substances, Chemical Engineering Science 53 (1998) 2403–2422.

[55] C.-H. He, Y.-S. Yu, New equation for infinite-dilution diffusion coefficients in supercritical and high-temperature liquid solvents, Industrial & Engineering Chemistry Research 37 (1998) 3793–3798.

[56] I. M. Svishchev, A. Plugatyr, Supercritical water oxidation of o-dichlorobenzene: degradation studies and simulation insights, The Journal of Supercritical Fluids 37 (2006) 94–101.

[57] F. Vogel, J. Blanchard, P. Marrone, S. Rice, P. Webley, W. Peters, K. Smith, J. Tester, Critical review of kinetic data for the oxidation of methanol in supercritical water, Journal of Supercritical Fluids 34 (2005) 249–286.

[58] L. Li, P. Chen, E. Gloyna, Kinetic-model for wet oxidation of organic-compounds in subcritical and supercritical water, Supercritical Fluid Engineering Science - Fundamentals and Applications 514 (1993) 305–313.

[59] R. K. Helling, J. W. Tester, Oxidation of simple compounds and mixtures in supercritical water: carbon monoxide, ammonia and ethanol, Environmental Science & Technology 22 (1988) 1319–1324.

[60] J. Ploeger, P. Bielenberg, J. Dinaro-Blanchard, R. Lachance, J. Taylor, W. Green, J. Tester, Modeling oxidation and hydrolysis reactions in supercritical water-free radical elementary reaction networks and their applications, Combustion Science and Technology 178 (2006) 363–398.

[61] P. Webley, J. Tester, H. Holgate, Oxidation-kinetics of ammonia and ammonia-methanol mixtures in supercritical water in the temperature-range 530-degrees-c 700-degrees-c at 246 bar, Industrial & Engineering Chemistry Research 30 (1991) 1745–1754.

[62] J. Abelleira, J. Sánchez-Oneto, J. R. Portela, E. J. Martínez de la Ossa, Kinetics of supercritical water oxidation of isopropanol as an auxiliary fuel and co-fuel, Fuel 111 (2013) 574–583.

[63] P. A. Webley, J. W. Tester, Fundamental kinetics of methanol oxidation in supercritical water, in: Supercritical Fluid Science and Technology, number 406 in ACS Symposium Series, American Chemical Society, 1989, pp. 259–275.

[64] E. E. Brock, P. E. Savage, J. R. Barker, A reduced mechanism for methanol oxidation in supercritical water, Chemical Engineering Science 53 (1998) 857–867.

[65] P. Dagaut, M. Cathonnet, J.-C. Boettner, Chemical kinetic modeling of the supercritical-water oxidation of methanol, The Journal of Supercritical Fluids 9 (1996) 33–42.

[66] J. Troe, Predictive possibilities of unimolecular rate theory, The Journal of Physical Chemistry 83 (1979) 114–126.

[67] M. K. Alkam, V. M. Pai, P. B. Butler, W. J. Pitz, Methanol and hydrogen oxidation kinetics in water at supercritical states, Combustion and Flame 106 (1996) 110–130.

[68] M. D. Bermejo, P. Cabeza, M. Bahr, R. Fernandez, V. Rios, C. Jimenez, M. J. Cocero, Experimental study of hydrothermal flames initiation using different static mixer configurations, Journal of Supercritical Fluids 50 (2009) 240–249.

[69] M. D. Bermejo, F. Cantero, M. J. Cocero, Supercritical water oxidation of feeds with high ammonia concentrations pilot plant experimental results and modeling, Chemical Engineering Journal 137 (2008) 542–549.

[70] T. Hunter, S. Rice, R. Hanush, Raman spectroscopic measurement of oxidation in supercritical water .2. conversion of isopropyl alcohol to acetone, Industrial & Engineering Chemistry Research 35 (1996) 3984–3990.

[71] S. P. Maharrey, D. R. Miller, A direct sampling mass spectrometer investigation of oxidation mechanisms for acetic acid in supercritical water, The Journal of Physical Chemistry A 105 (2001) 5860–5867.

[72] S. Rice, T. Hunter, A. Ryden, R. Hanush, Raman spectroscopic measurement of oxidation in supercritical water .1. conversion of methanol to formaldehyde, Industrial & Engineering Chemistry Research 35 (1996) 2161–2171.

[73] J. Sierra-Pallares, M. Parra-Santos, J. Garcia-Serna, F. Castro, M. Cocero, Numerical analysis of high-pressure fluid jets: Application to RTD prediction in supercritical reactors, Journal of Supercritical Fluids 49 (2009) 249–255.

[74] J. Warnatz, U. Maas, R. W. Dibble, Combustion: Physical and Chemical Fundamentals, Modeling and Simulation, Experiments, Pollutant Formation, Springer, Berlin ; New York, 4th edition edition, 2006.

[75] G. M. Pohsner, E. U. Franck, Spectra and temperatures of diffusion flames at high pressures to 1000 bar, Berichte der Bunsengesellschaft für physikalische Chemie 98 (1994) 1082–1090.

[76] T. Hirth, E. U. Franck, Oxidation and hydrothermolysis of hydrocarbons in supercritical water at high pressures, Berichte der Bunsengesellschaft für physikalische Chemie 97 (1993) 1091–1097.

[77] R. M. Serikawa, T. Usui, T. Nishimura, H. Sato, S. Hamada, H. Sekino, Hydrothermal flames in supercritical water oxidation: investigation in a pilot scale continuous reactor, Fuel 81 (2002) 1147–1159.

[78] B. Wellig, K. Lieball, P. von Rohr, Operating characteristics of a transpiring-wall SCWO reactor with a hydrothermal flame as internal heat source, Journal of Supercritical Fluids 34 (2005) 35–50.

[79] K. Príkopský, B. Wellig, P. R. von Rohr, SCWO of salt containing artificial wastewater using a transpiring-wall reactor: Experimental results, The Journal of Supercritical Fluids 40 (2007) 246–257.

[80] B. Wellig, M. Weber, K. Lieball, K. Prikopsky, P. von Rohr, Hydrothermal methanol diffusion flame as internal heat source in a SCWO reactor, Journal of Supercritical Fluids 49 (2009) 59–70.

[81] A. Sobhy, I. S. Butler, J. A. Kozinski, Selected profiles of high-pressure methanol–air flames in supercritical water, Proceedings of the Combustion Institute 31 (2007) 3369–3376.

[82] M. D. Bermejo, I. Bielsa, M. J. Cocero, Experimental and theoretical study of the influence of pressure on SCWO, AIChE Journal 52 (2006) 3958–3966.

[83] M. D. Bermejo, C. Jimenez, P. Cabeza, A. Matias-Gago, M. J. Cocero, Experimental study of hydrothermal flames formation using a tubular injector in a refrigerated reaction chamber. influence of the operational and geometrical parameters, Journal of Supercritical Fluids 59 (2011) 140–148.

[84] M. D. Bermejo, P. Cabeza, J. P. S. Queiroz, C. Jimenez, M. J. Cocero, Analysis of the scale up of a transpiring wall reactor with a hydrothermal flame as a heat source for the supercritical water oxidation, Journal of Supercritical Fluids 56 (2011) 21–32.

[85] H. Schmieder, J. Abeln, Supercritical water oxidation: State of the art, Chemical Engineering & Technology 22 (1999) 903–908.

[86] P. Cabeza, M. D. Bermejo, C. Jimenez, M. J. Cocero, Experimental study of the supercritical water oxidation of recalcitrant compounds under hydrothermal flames using tubular reactors, Water Research 45 (2011) 2485–2495.

[87] P. Cabeza, J. P. S. Queiroz, S. Arca, C. Jiménez, A. Gutiérrez, M. D. Bermejo, M. J. Cocero, Sludge destruction by means of a hydrothermal flame. optimization of ammonia destruction conditions, Chemical Engineering Journal 232 (2013) 1–9.

[88] The SuperWater process, 2014. SuperWater Solutions. http://www.superwatersolutions.com/technology.html.

[89] Sludge treatment | SCFI - smarter environmental technology, 2014. Http://www.scfi.eu/products/sludge-treatment-3/.

[90] V. Vadillo, J. Sánchez-Oneto, J. R. Portela, E. J. Martínez de la Ossa, Chapter 9 - supercritical water oxidation for wastewater destruction with energy recovery, in: V. Anikeev, M. Fan (Eds.), Supercritical Fluid Technology for Energy and Environmental Applications, Elsevier, Boston, 2014, pp. 181–190.

[91] M. Modell, Processing methods for the oxidation of organics in supercritical water, WO1981003169 A1, 1981.

[92] C. J. Molnar, System and method for generating electricity from super critical water oxidation process, US7703285 B2, 2010.

[93] Y. Kansha, A. Kishimoto, T. Nakagawa, A. Tsutsumi, A novel cryogenic air separation process based on self-heat recuperation, Separation and Purification Technology 77 (2011) 389–396.

[94] M. D. Bermejo, M. J. Cocero, F. Fernandez-Polanco, A process for generating power from the oxidation of coal in supercritical water, Fuel 83 (2004) 195–204.

[95] R. DiPippo, Chapter 9 - advanced geothermal energy conversion systems, in: R. DiPippo (Ed.), Geothermal Power Plants (Third Edition), Butterworth-Heinemann, Boston, 2012, pp. 183–221.

[96] J. J. Brasz, Two phase flow turbine, US 5467613 A, 1995.

[97] M. D. Bermejo, Á. Martín, J. P. S. Queiroz, P. Cabeza, F. Mato, M. J. Cocero, Chapter 15 supercritical water oxidation (SCWO) of solid, liquid and gaseous fuels for energy generation, in: Z. Fang, C. C. Xu (Eds.), Near-critical and Supercritical Water and Their Applications for Biorefineries, number 2 in Biofuels and Biorefineries, Springer Verlag, 2014.

[98] M. D. Bermejo, D. Rincón, V. Vazquez, M. J. Cocero, Supercritical water oxidation: Fundamentals and reactor modeling, Chemical Industry and Chemical Engineering Quarterly 13 (2007) 79–87.

[99] E. D. Lavric, H. Weyten, J. De Ruyck, V. Pleşu, V. Lavric, Supercritical water oxidation improvements through chemical reactors energy integration, Applied Thermal Engineering 26 (2006) 1385–1392.

[100] A. Ermakova, V. I. Anikeev, Modeling of the oxidation of organic compounds in supercritical water, Theoretical Foundations of Chemical Engineering 38 (2004) 333–340.

[101] E. Fauvel, C. Joussot-Dubien, E. Pomier, P. Guichardon, G. Charbit, F. Charbit, S. Sarrade, Modeling of a porous reactor for supercritical water oxidation by a residence time distribution study, Industrial & Engineering Chemistry Research 42 (2003) 2122–2130.

[102] K. R. Muske, J. D. Littell, P. C. Dell'Orco, L. A. Le, R. L. Flesner, Hydrothermal treatment of C-N-O-H wastes: Model-based reactor effluent control, Industrial & Engineering Chemistry Research 40 (2001) 1397–1405.

[103] P. Dutournié, J. Mercadier, Unsteady behaviour of hydrothermal oxidation reactors: theoretical and numerical studies near the critical point, The Journal of Supercritical Fluids 35 (2005) 247–253.

[104] T. Poinsot, D. Veynante, Theoretical and Numerical Combustion, Second Edition, R.T. Edwards, Inc., Philadelphia, 2 edition, 2005.

[105] C. H. Oh, R. J. Kochan, J. M. Beller, Numerical analysis and data comparison of a supercritical water oxidation reactor, AIChE Journal 43 (1997) 1627–1636.

[106] M. Bazargan, M. Mohseni, Algebraic zero-equation versus complex two-equation turbulence modeling in supercritical fluid flows, Computers & Fluids 60 (2012) 49–57.

[107] S. He, W. S. Kim, J. H. Bae, Assessment of performance of turbulence models in predicting supercritical pressure heat transfer in a vertical tube, International Journal of Heat and Mass Transfer 51 (2008) 4659–4675.

[108] M. Mohseni, M. Bazargan, The effect of the low reynolds number k-e turbulence models on simulation of the enhanced and deteriorated convective heat transfer to the supercritical fluid flows, Heat and Mass Transfer 47 (2011) 609–619.

Chapter 2

Property methods for SCWO modeling

Abstract

The methods for estimation of properties of mixtures at supercritical state are presented. Density is calculated by Peng-Robinson equation of state, with constant volume translation. Enthalpy is calculated by original Peng-Robinson EoS. The mean deviations on predicting density and excess enthalpy for the system H_2O + N_2 are 3.9% and 5.6%, respectively. Viscosity and thermal conductivity are calculated using mass-weighted mixing laws and reference values of pure components. TRAPP method for thermal conductivity can be used if the mixture is well above its critical point on the entire domain.

2.1 Introduction

For the numerical flow description (CFD) it is important that the property models used are as accurate as possible yet not computationally costly. In the cases studied in this work, the temperature range extents from room temperature (where water is in liquid state) to high temperatures in the flame (where all species are at supercritical state). In order to estimate properties of mixtures, there are 2 main approaches: calculating the mixture properties by weighting the pure properties according to their mass or molar fraction; or weighting the parameters for entering the correlations as one fluid.

The methods described bellow have been used in this work through routines implemented in MATLAB and ANSYS FLUENT.

2.2 Thermodynamic Properties

2.2.1 Density

The density of the supercritical mixture ρ is calculated by Peng-Robinson equation of state with constant volume translation (VTPR-EoS) [1].

$$P = \frac{RT}{v + vt - b} - \frac{a(T)}{(v + vt)(v + vt + b) + b(v + vt - b)} \tag{2.1}$$

The parameters for pure components are calculated by equations (2.2) to (2.4).

$$a_k = 0.45724 \frac{R^2 T_{c,k}^2}{P_c} \alpha_k(T) \tag{2.2}$$

$$b_k = 0.07780 \frac{RT_{c,k}}{P_{c,k}} \tag{2.3}$$

$$\alpha_k(T) = \left[1 + m_k(1 - \sqrt{T_r})\right]^2 \tag{2.4}$$

For the parameter m_k, function of acentric factor, it is used the definition given by Magoulas and Tassios [2].

$$m_k = 0.384401 + 1.52276\omega_k - 0.213808\omega_k^2 + 0.034616\omega_k^3 - 0.001976\omega_k^4 \tag{2.5}$$

The volume translation vt was fitted for each component that constitute the system (H_2O, O_2, N_2, CO_2 and isopropyl-alcohol – IPA), at the operation pressure. Figure 2.1 shows the fitting of the densities of pure compounds by VTPR-EoS. The continuous line corresponds to NIST data [3] as a function of temperature at 23 MPa, and the dotted line corresponds to the predicted

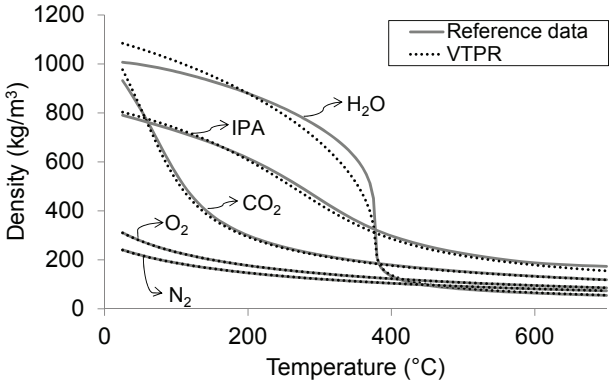

Figure 2.1: Densities of pure components as function of temperature at 23 MPa.

densities. The volume correction was estimated for each substance in order to minimize the differences between the reference data and the predicted values (see table 2.1). For isopropyl-alcohol, density data are not available on the NIST database, so the reference data were obtained by SR-Polar-EoS [4] calculations in Aspen Plus.

Table 2.1: Volume Translation at 23 MPa for application in VTPR-EoS.

	$vt(cm^3/mol)$
H_2O	4.291073
O_2	-2.545861
N_2	-3.743775
CO_2	1.284445
IPA	3.721115

The density of the mixture is computed replacing the pure-component parameters a, b and vt, in equation (2.1), by the mixture parameters a_m, b_m and vt_m, with the following composition dependent mixing rules:

$$a_m = \sum_{k=1}^{n} \sum_{l=1}^{n} y_k y_l a_{kl} \tag{2.6}$$

$$b_m = \sum_{k=1}^{n} \sum_{l=1}^{n} y_k y_l b_{kl} \tag{2.7}$$

$$vt_m = \sum_{k=1}^{n} y_k vt_k \tag{2.8}$$

Table 2.2: Binary interaction parameters for PR-EoS.

	H_2O	O_2	N_2	CO_2	IPA
H_2O	0	-0.7575008	0.4788	0.12	0
O_2	-0.7575008	0	-0.0119	-0.10458767	0
N_2	0.4788	-0.0119	0	0	0
CO_2	0.12	-0.10458767	0	0	0
IPA	0	0	0	0	0

And the appropriate combination rules:

$$a_{kl} = \sqrt{a_k a_l}\,(1 - k_{kl}) \tag{2.9}$$

$$b_{kl} = \frac{b_k + b_l}{2} \tag{2.10}$$

The binary interaction parameters k_{kl} for the five species considered are shown in table 2.2. Figure 2.2 shows the performance of VTPR-EoS on predicting the density of the binary mixture water-nitrogen for different compositions at 390°C. The experimental points presented are taken from Abdulagatov et al. [5]. The mean error over the entire pressure range is 3.9%, and a very good agreement is found around the operating pressure, 23 MPa.

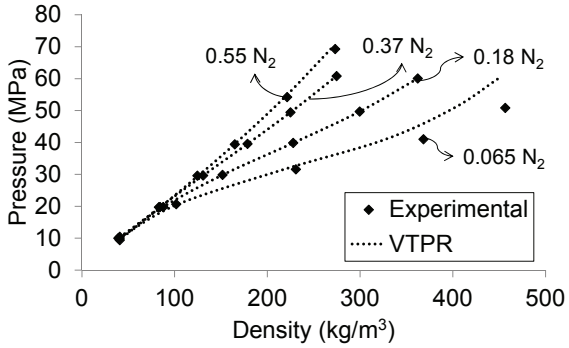

Figure 2.2: P-ρ curves at constant composition for water + nitrogen at $T =$ 390°C. Experimental data from Abdulagatov et al. [5].

Once the density of the mixture is obtained, it is addressed to the solver through the macro `DEFINE_PROPERTY` [6].

2.2.2 Enthalpy

The enthalpy of a real gas (or mixture) can be divided into an ideal gas term (ig) and a residual term (res):

$$h = h^{ig} - h^{res} \tag{2.11}$$

With the application of the appropriate departure function [7] and using Peng-Robinson EoS (PREoS), we obtain equation (2.12) for the residual component of enthalpy.

$$\frac{h^{res}}{RT} = 1 - Z + \frac{a_m}{2\sqrt{2}b_m RT}\left(1 - \frac{T\frac{da_m}{dT}}{a_m}\right)\ln\left(\frac{Z + \left(1+\sqrt{2}\right)B}{Z + \left(1-\sqrt{2}\right)B}\right) \tag{2.12}$$

Where $B = b_m \frac{P}{RT}$, and

$$T\frac{da_m}{dT} = -\sum_k^n \sum_l^n y_k y_l m_k (1 - k_{kl})\sqrt{a_k a_l}\sqrt{\frac{T_{rk}}{\alpha_k}} \tag{2.13}$$

Enthalpy calculations were checked against experimental data for the system water-nitrogen. Figure 2.3 shows the excess enthalpy as function of composition at three different conditions. Experimental points are given by Wormald and Colling [8], and the average error found is 5.6%. Here, the

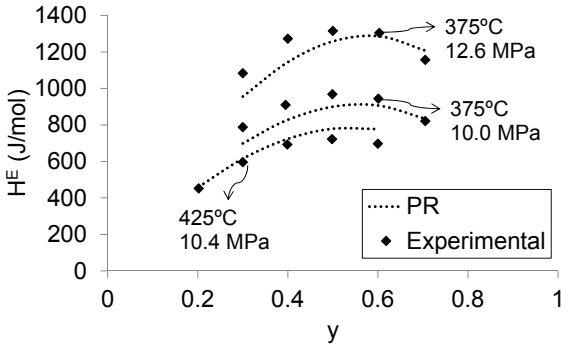

Figure 2.3: Excess enthalpy H^E of $(yH_2O + (1-y)N_2)$. Experimental data from Wormald and Colling [8].

original PREoS is used, since the constant volume translation used in section 2.2.1 does not improve enthalpy calculation. The heat capacity of the mixture is obtained by numerical derivative of enthalpy and both, c_p and h, are addressed to the solver through the macro `DEFINE_SPECIFIC_HEAT` [6].

2.3 Transport Properties

2.3.1 Viscosity

Due to the difficulty of finding a method for mixture viscosity calculation valid for liquid and supercritical regions, a linear mixing law is assumed.

$$\mu_m = \sum_k^n y_k \mu_k \tag{2.14}$$

Viscosities of pure components are obtained from NIST database [3] at 23 MPa as function of temperature.

2.3.2 Thermal Conductivity

Two approaches were used for estimation of thermal conductivity of a supercritical mixture. Firstly TRAPP method was implemented [9] assuming the one-fluid approach. In this method, the thermal conductivity of the mixture at high pressure is related to its value at low pressure and to the excess thermal conductivity of a reference fluid (propane) [7]:

$$\lambda_m - \lambda_m^o = F_{\lambda m} X_{\lambda m} \left[\lambda^R - \lambda^{Ro}\right] \tag{2.15}$$

The method is acceptable at high temperatures but shows poor results at predicting pure conductivities in the low temperature region, as shown in figure 2.4. The continuous line corresponds to NIST data [3] as function of temperature at 23 MPa, and the dotted line corresponds to the predicted conductivity. The deviation at subcritical temperatures indicates that the method is not suitable for polar substances. Thus, for the simulations of cold

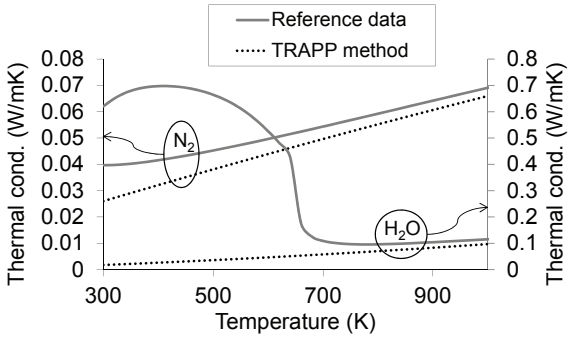

Figure 2.4: Thermal conductivity of water and nitrogen as function of temperature at 23 MPa.

injection of feed, a linear mixing law was used instead.

$$\lambda_m = \sum_k^n y_k \lambda_k \tag{2.16}$$

Thermal conductivities of pure components are obtained from NIST database [3] at 23 MPa as function of temperature.

2.3.3 Diffusivity

The self-diffusion coefficient is calculated using the Mathur & Thodos equation [10], as recommended by Kutney [11]. The coefficient is calculated depending on the reduced density, and the method can be extended to the liquid region.

$$D_{aa} = \begin{cases} \frac{10.7 \cdot 10^{-5} T_r}{\rho_r \beta} & \rho_r \leq 1.5 \\ \frac{3.67 \cdot 10^{-5} T_r^{3.5}}{P_r^{0.1} \beta} & \rho_r > 1.5 \end{cases} \tag{2.17}$$

In equation (2.17), D_{aa} is given in $cm^2 s^{-1}$, and β is calculated as in equation (2.18).

$$\beta = \frac{\sqrt{M_m} P_{cm}^{1/3}}{T_{cm}^{5/6}} \tag{2.18}$$

with pressure in atm. The reduced parameters are computed using the following mixing rules for the critical properties:

$$T_{cm} = \sum_k^n y_k T_{ck} \tag{2.19}$$

$$V_{cm} = \sum_k^n y_k V_{ck} \tag{2.20}$$

$$Z_{cm} = \sum_k^n y_k \frac{P_{ck} V_{ck}}{R T_{ck}} \tag{2.21}$$

$$P_{cm} = \frac{Z_{cm} R T_{cm}}{V_{cm}} \tag{2.22}$$

The value of diffusion coefficient is passed to the CFD solver through the macro `DEFINE_DIFFUSIVITY` [6].

Bibliography

[1] A. Peneloux, E. Rauzy, R. Freze, A consistent correction for redlich-kwong-soave volumes, Fluid Phase Equilibria 8 (1982) 7–23.

[2] K. Magoulas, D. Tassios, Thermophysical properties of normal-alkanes from c1 to c20 and their prediction for higher ones, Fluid Phase Equilibria 56 (1990) 119–140.

[3] E. W. Lemmon, M. O. McLinden, D. G. Friend, Thermophysical properties of fluid systems, in: P. J. Linstrom, W. G. Mallard (Eds.), NIST Chemistry WebBook, NIST Standard Reference Database, 69, National Institute of Standards and Technology, Gaithersburg MD, 20899, 2011. Last access: 05/24/2013.

[4] J. Schwartzentruber, H. Renon, S. Watanasiri, Development of a new cubic equation of state for phase equilibrium calculations, Fluid Phase Equilibria 52 (1989) 127–134.

[5] I. M. Abdulagatov, A. R. Bazaev, A. E. Ramazanova, P-v-t-x measurements of aqueous mixtures at supercritical conditions, International Journal of Thermophysics 14 (1993) 231–250.

[6] ANSYS, ANSYS FLUENT UDF manual release 12, 2009.

[7] B. E. Poling, J. M. Prausnitz, J. P. O'Connell, The Properties of Gases and Liquids, McGraw-Hill, New York, 5 th edition, 2007.

[8] C. J. Wormald, C. N. Colling, Excess enthalpies for (water + nitrogen)(g) up to 698.2 k and 12.6 MPa, The Journal of Chemical Thermodynamics 15 (1983) 725–737.

[9] J. F. Ely, H. J. M. Hanley, A computer program for the prediction of viscosity and thermal conductivity in hydrocarbon mixtures, number 1039 in NBS Technical Note, National Bureau of Standards (U.S.), 1981.

[10] G. P. Mathur, G. Thodos, The self-diffusivity of substances in the gaseous and liquid states, AIChE Journal 11 (1965) 613–616.

[11] M. C. Kutney, Thermodynamic and transport property modeling in super critical water, Thesis, Massachusetts Institute of Technology, 2005. Thesis (Sc. D.)–Massachusetts Institute of Technology, Dept. of Chemical Engineering, 2005.

Chapter 3

Kinetic model for isopropanol oxidation in supercritical water in hydrothermal flame regime and analysis

Abstract

Supercritical water oxidation (SCWO) in hydrothermal flame regime has advantages over the oxidation in flameless regime. The main advantage is that the feed can be injected into the reactor at low temperatures, avoiding plugging and corrosion problems in a preheating system. However, there is a lack of kinetic data capable of properly describing the flame regime oxidation. In this study, new global reaction rate parameters for the oxidation of isopropyl alcohol in hydrothermal regime were adjusted from temperature profiles of our group's previous experimental data. The kinetics obey first order rate with regard to the fuel and the oxidant, and follows the Arrhenius law. The parameters are $k_0 = (9.308 \pm 3.989) \cdot 10^7 (m^3 \cdot s^{-1} \cdot kmol^{-1})$ and $E_a = 89.441 \pm 2.457 (kJ \cdot mol^{-1})$, and the least square error of the fitting was 10.8%. This kinetic model was applied in a parametric analysis of flame formation, and it was used to analyze the behavior of a supercritical water oxidation vessel reactors. The kinetic model is able to describe the behavior of the vessel reactor when working in steady state hydrothermal flame regime at subcritical injection temperatures (246°C). The model predicts both flameless and hydrothermal flame regimes.

Keywords: Kinetics, parameter identification, hydrothermal flames, CFD

The Journal of Supercritical Fluids 76 (2013), 41-47

modeling, Supercritical water oxidation, Mathematical modeling

3.1 Introduction

Supercritical water oxidation (SCWO) in hydrothermal flame regime is a promising technology for the total destruction of waste because overcomes the challenges that have delayed the successful and profitable commercialization of this technology: corrosion, salt deposition and high energy demand [1, 2]. Working with residence times below 1 s, the process can be performed in microreactors. When the temperature of the mixture becomes greater than the ignition temperature a flame is produced, and in this kind of dense aqueous environment it is known as hydrothermal flame [3]. Hydrothermal flames were referred to for first time by Franck and coworkers [4]. Several research groups have developed reactors working with a hydrothermal flame as heat source [5, 6], since SCWO reactors using a hydrothermal flame have a number of advantages [3]:

- Pollutants can be destroyed in residence times of a few milliseconds.
- The higher operation temperatures improve energy recovery.
- It is possible to initiate the reaction with feed injection temperatures near to room temperature [7].

This last point presumes an advantage from the operational and energetic integration points of view, as it avoids problems of plugging and corrosion in a preheating system.

The High Pressure Process Group (HPPG) of the University of Valladolid (UVa) (Spain) recently demonstrated the formation of hydrothermal flames in tubular reactors [8]. Using this simple device, the extinction temperatures of the flame could not be reduced to less than 370°C. Vessel reactors have shown to be more successful in maintaining steady stable hydrothermal flames with injection temperatures near to room temperature [5, 6, 9]. The flame stability is related to the injection temperature and flow velocity, and vessel reactors provide flow velocities that are compatible with hydrothermal flame front velocities [10]. It is thought that vessel reactors provide a space for recirculation in which the cold reagents are preheated to the ignition temperature and are brought into contact with the radicals already formed, making it possible for the flame to be formed. CFD simulations of these reactors show the existence of a flame front where most of the reaction takes place [11].

This development on the SCWO process has been possible, in part, as a result of the increase in the quantitative understanding of the SCWO reaction initiation rates of different types of organic species at the lower temperatures

of 450-500°C [12]. The focus of these kinetic studies has typically been on model compounds rather than on actual waste. These compounds have been chosen because they contain key functional groups of importance and/or represent the rate limiting step in the breakdown of a range of complex waste species. Considering only homogeneous reactions without catalysts, extensive data on SCWO kinetics have been reported for a number of model compounds [12–16]. However, these kinetic data from literature are not able to describe flame regime oxidation [8]. Concentration profiles in the SCWO reactor are very difficult to obtain due to fast reaction rates and usually only global conversions are reported, except when optical devices are used [17–19]. The lack of kinetic models is one of the reasons why most of the modeling of hydrothermal flames is based on mixing controlled reactions [11, 20]. This approach is valid for non-premixed flames at high temperatures since it assumes that chemical reaction is fast compared to the transport processes in the flow. The characteristics of our system are similar to premixed flames, where fuel and oxidant are totally mixed and chemical reaction is important.

In this work, a new kinetic model for the supercritical water oxidation of isopropyl alcohol in flame regime has been adjusted using our group's previous experimental data [8]. Temperature profiles were used to fit kinetic parameters, by developing a mathematical model. This model is able to reproduce experimental data using either air or oxygen as the oxidant. A parametric analysis showed that the model is in accordance with the work of Serikawa et al. [21]. The adjusted kinetic model has been used to make an analysis of the behavior of a vessel reactor, in particular of the transpiring wall reactor with an internal hydrothermal flame studied at the University of Valladolid.

3.2 Experiments

Experimental data used for adjusting the kinetic parameters of the oxidation of isopropyl-alcohol at hydrothermal flame regime were performed at the University of Valladolid's SCWO pilot plant, which had been adapted to work with tubular mixers as described by Bermejo et al. [8]. The pilot plant has a maximum treatment capacity of 20 kg/h feed and uses air as an oxidant compressed by a four staged reciprocating compressor. Both, air and feed are electrically preheated before being introduced into the tubular reactor, which consists of a commercial Ni-alloy tube of 1/4" diameter and 1.5 m length. The reaction was monitored by measuring temperatures at the mixing point and at several points inside the reactor, and also by determining the total organic carbon (TOC) of the effluent. After leaving the reactor the reaction

mixture is quenched. The products are cooled down to room temperature in the intercoolers, and after depressurization, samples of the liquid and gas effluents can be taken.

Additional experiments using pure O_2 as the oxidant were performed in a similar tubular reactor, installed in a demonstration plant of the University of Valladolid situated in the premises of the CETRANSA company in Santovenia de Pisuerga (Valladolid). In this case, cryogenic O_2 was pumped until reaching operational pressure and brought to room temperature by an evaporator. The reactor was a Ni-alloy tube of 1/4" diameter and 2 m length. The demonstration plant is already described in previous work [22].

To determine the kinetic parameters, data from 24 experiments using air and 8 using O_2, under different inlet conditions were used.

Once the kinetic model was obtained, it was introduced in a previous model of the transpiring wall reactor working at the same University of Valladolid pilot plant as described by Bermejo et al. [23], and the results of simulations were compared to experimental data. The transpiring wall reactor consists of a stainless steel pressure shell with a volume of 10 L. It contains a reaction chamber surrounded by a porous wall through which clean water circulates. The feed and the air are introduced into the reactor through its lower part, and they are fed through the injector into the upper part of the reaction chamber; the reagents flow downwards mixing with the clean water that enters the reactor through the transpiring wall, and decontaminated water leaves the reactor through its lower part. More constructive details of the reactor can be found elsewhere [10, 23]. In order to follow the reaction, the temperature is measured at several points in the reaction chamber.

3.3 Modeling

3.3.1 Tubular reactor

A simple model of the tubular reactor described in section 3.2 was programmed in order to fit the kinetic parameters of IPA oxidation, by minimizing the difference between experimental and calculated temperatures at several points inside the reactor. The following assumptions were made:

1. Plug flow is assumed and the feed and oxidant streams are presumed to be completely mixed at the reactor inlet. There is neither axial nor radial dispersion. This hypothesis of complete mixing was verified by CFD simulation (section 3.4.1).

2. The model assumes that the oxidation of the isopropyl-alcohol (IPA)

takes place in a single step, leading to the formation of carbon dioxide and water as shown in eq. (3.1).

$$C_3H_8O + 4.5O_2 \rightarrow 3CO_2 + 4H_2O \tag{3.1}$$

3. The pressure remains constant at 23 MPa along the reactor.

4. Enthalpy of the mixture is given by the original Peng-Robinson Equation of State (PR-EoS) [24]. Densities are calculated by the PR-EoS with constant volume translation (VTPR-EoS) [25]. In both cases van der Waals mixing rules are used. The volume correction was adjusted for each pure component using density data from the NIST database [26] and from Aspen Plus calculations using the SR-Polar-EoS [27] at operating pressure, similar to the procedure used by Lieball [28]. Table 3.1 presents the volume correction for the five substances that compose the system. Additional information about the volume correction calculation can be found in chapter 2. The translated volume of the mixture is a linear function of the component mole fractions.

Table 3.1: Volume Translation at 23 MPa for application in VTPR-EoS.

	$vt(cm^3/mol)$
H_2O	4.291073
O_2	-2.545861
N_2	-3.743775
CO_2	1.284445
IPA	3.721115

For a differential control volume inside a plug flow reactor, the material balance for the fuel (IPA) results in equation (3.2):

$$\frac{dw_{IPA}}{dz} = -\frac{r \cdot M_{IPA} \cdot S}{\dot{m}} \tag{3.2}$$

Where w_{IPA} is mass fraction of isopropyl-alcohol, z the length of the tubular reactor, r the reaction rate, M_{IPA} the molecular weight of isopropyl-alcohol, S the cross section of the tubular reactor, and $\dot{m}$ the total mass flow.

The energy balance for the same control volume leads to equation (3.3).

$$\frac{dh}{dz} = \frac{\Delta H_r \cdot r \cdot S}{\dot{m}} \tag{3.3}$$

Where h is the specific enthalpy, and ΔH_r is the heat of reaction, calculated from the enthalpies of formation of each component. Assuming no pressure changes $dh = c_p dT$, eq. (3.3) can be rewritten as eq. (3.4).

$$\frac{dT}{dz} = \frac{\Delta H_r \cdot r \cdot S}{\dot{m} \cdot c_p} \tag{3.4}$$

Where c_p is the specific heat capacity of the mixture. In equations (3.2) to (3.4) the reaction rate r can be described according to the Arrhenius law:

$$r = k_0 \exp\left(-\frac{E_a}{RT}\right) C_{IPA} C_{O_2} \tag{3.5}$$

Reaction order regarding IPA is assumed as equal to 1, as suggested in previous works [12, 29]. Oxygen reaction order can not be assumed as 0, since there is no significant excess in experimental data. Therefore, the model assumes first order reaction behavior for both fuel and oxidant. The assumed order of reaction gives the S-shape profiles of temperature observed in experimental data.

In order to improve the optimization process, two auxiliary variables have been defined: $X_1 = \ln(k_0)$ and $X_2 = \frac{E_a}{R \cdot 850}$. Also, for convenience, concentrations were substituted by mass fraction. Thus, equation (3.5) can be rewritten:

$$r = \exp\left(X_1 - \frac{X_2 \cdot 850}{T}\right) \frac{w_{ipa}}{M_{ipa}} \frac{w_{O_2}}{M_{O_2}} \rho^2 \tag{3.6}$$

Where ρ is the density of the mixture. The value 850 is a characteristic temperature and was taken in order to give X_1 and X_2 the same order of magnitude.

The optimization procedure uses the Matlab function `lsqnonlin`, which consists of a non-linear least-square solver with Levenberg-Marquardt algorithm [30, 31]. The function to be minimized is:

$$f_{obj} = \sum_{k=1}^{n} (T_k - \widehat{T_k})^2 \tag{3.7}$$

Where T_k are experimental temperatures and $\widehat{T_k}$ the calculated temperatures. These temperatures are obtained by solving the set of equations for w_{IPA} (eq.(3.2)) and T (eq.(3.4)) simultaneously using Matlab solver `ode15s`. The parameters fitted are X_1 and X_2 from which the Arrhenius parameters can be obtained.

3.3.2 Study of the mixing process of water and air flow

The assumption of instantaneous mixing taking place in the tubular reactor was verified by 3D simulation of the tee-junction. The extent to which air and feed flow are totally mixed was investigated by obtaining the concentration profiles in different lengths of the reactor. In these simulations a non-reacting flow was considered. The geometry of the model includes the tee-junction and a 25 *cm* segment of the reactor and the metallic wall, as shown in figure 3.1. The domain is limited by the longitudinal plane of symmetry and half of the tee and tube wall. The mesh is composed of 436000 mixed cells at the fluid region, and 529000 tetrahedral cells at the solid region. The fluid region mesh is formed by hexahedral cells at the near wall region and tetrahedral cells at core region, assuring an y^+ value below 5. The model includes the five

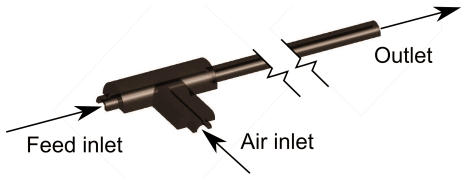

Figure 3.1: 3D tee-junction geometry model used in CFD simulation.

species that constitute the system: water, oxygen, nitrogen, carbon dioxide and isopropyl-alcohol, and solves the Reynolds-averaged transport equations [32] for mass, momentum, energy and species, as shown in equations (3.8) to (3.11):

$$\frac{\partial \rho}{\partial t} + \frac{\partial}{\partial x_i}(\rho u_i) = 0 \tag{3.8}$$

$$\frac{\partial}{\partial t}(\rho u_i) + \frac{\partial}{\partial x_j}(\rho u_i u_j) = -\frac{\partial p}{\partial x_i} + \frac{\partial}{\partial x_j}(\tau_{ij} - \rho\overline{u_i' u_j'}) \tag{3.9}$$

$$\frac{\partial}{\partial t}(\rho E) + \frac{\partial}{\partial x_i}\left[u_i(\rho E + p)\right] = \frac{\partial}{\partial x_j}\left((\lambda + \lambda_t)\frac{\partial T}{\partial x_j}\right) + S_h \tag{3.10}$$

$$\frac{\partial}{\partial t}(\rho w_k) + \frac{\partial}{\partial x_i}(\rho u_i w_k) = -\frac{\partial}{\partial x_i}\left[\rho\left(D + D_t\right)\frac{\partial w_k}{\partial x_i}\right] + R_k \tag{3.11}$$

Where u_i is the fluid velocity in the x_i direction, p the pressure, E is the total energy and w_k the mass fraction of species k. The source terms S_h and R_k represent the heat of reaction and the net rate of species k production

by chemical reaction. Thus, for the non-reacting flow model, their values are zero. The viscous stress tensor τ_{ij} is shown in equation (3.12)

$$\tau_{ij} = \mu \left(\frac{\partial u_i}{\partial x_j} + \frac{\partial u_j}{\partial x_i} - \frac{2}{3}\delta_{ij}\frac{\partial u_l}{\partial x_l} \right) \tag{3.12}$$

Where μ is the molecular viscosity calculated as a mass-fraction average of the properties of the pure components.

In equation (3.10), the total energy E is:

$$E = h - \frac{p}{\rho} + \frac{u^2}{2} \tag{3.13}$$

In equations (3.8) to (3.13) ρ is the mixture density calculated by VTPR-EoS, λ the thermal conductivity calculated by TRAPP method for high pressure fluids [33], D the diffusion coefficient calculated as the mass-fraction average of the pure species, and specific enthalpy h is given by PR-EoS. The turbulent thermal conductivity λ_t, the turbulent diffusion coefficient D_t and the Reynolds stress tensor $-\rho\overline{u_i' u_j'}$ are defined according to the turbulence model being used. In this work, the Realizable k-ϵ model has been used in order to model turbulence, as suggested by Sierra-Pallares et al. [34], with enhanced wall treatment.

The model was solved using the commercial CFD software ANSYS FLUENT 12.0, with segregated pressure based solver, SIMPLE algorithm for pressure-velocity coupling, and second order upwind discretization for energy, momentum, k-ϵ and species equations. The boundary conditions for the fluid region are mass flow inlet, pressure outlet, symmetry and no-slip condition (at the interface with the solid domain).

The test case was modeled also with other near wall treatments, like the low-Reynolds k-ϵ turbulence model [35], and meshes with different refinement levels, but showed no significant differences respect the model described here.

3.3.3 Transpiring wall reactor

A model previously developed for describing the behavior of the transpiring wall reactor [23] was modified in order to describe the performance of the reactor with a hydrothermal flame inside, incorporating the kinetic model obtained in this work. The model assumes stationary conditions considering only mass and energy balances, resolved by the Runge-Kutta method of 4^{th} order, while the momentum equation was neglected. The pressure along the reactor was considered constant and equal to 23 MPa. Enthalpy and heat capacities were calculated using PR-EoS. Densities were calculated by

VTPR-EoS considering the exact composition of the mixture. Global heat transmission coefficients were calculated as a function of the total mass flow, and the coefficient for the heat transmission of the outer wall with the environment was taken as $0.5W \cdot m^{-2} \cdot K^{-1}$. The heat of reaction for IPA oxidation were calculated for different temperatures using a polynomial fit (eq. 3.14).

$$\Delta H_r(T) = \begin{cases} a_0 + a_1 T + a_2 T^2 + a_3 T^3 + a_4 T^4, \; T \leq 404°C \\ b_0 + b_1 T + b_2 T^2 + b_3 T^3 + b_4 T^4, \; T > 404°C \end{cases} \tag{3.14}$$

Where the coefficients of the polynomials are presented in table 3.2.

Table 3.2: Coefficients of polynomial equation fitted for enthalpy of reaction of IPA oxidation as function of temperature at 23 MPa. Temperature in $°C$, enthalpy in J/mol.

a_0	-2.0353 $\cdot 10^6$	b_0	-2.0780 $\cdot 10^6$
a_1	-5.7254 $\cdot 10$	b_1	9.7755 $\cdot 10^2$
a_2	4.5344	b_2	-1.7952
a_3	-2.2537 $\cdot 10^{-2}$	b_3	1.4322 $\cdot 10^{-3}$
a_4	3.4218 $\cdot 10^{-5}$	b_4	-4.1826 $\cdot 10^{-7}$

This model assumes the injector as a PFR, the upper part of the reaction chamber as a CSTR, and the reaction chamber is modeled as a plug flow. The model includes heat exchange between injector and reaction chamber, and heat and mass exchange between reaction chamber and transpiring chamber. A complete description of the base model is given by Bermejo et al. [23].

3.4 Results

3.4.1 Study of Mixing Influence

Figure 3.2 shows the dispersion of species according the result of a non-reacting simulation of the tee-junction. Concentrations (in vertical axis) are normalized by the mass fraction of equilibrium, when the species are completely mixed. The simulation corresponds to an experiment using a feed flow of 5.9 kg/h with 4% mass isopropyl alcohol at 488°C and 3.7 kg/h of air at 389°C, both at 23 MPa, which gives a Reynolds number of 26000. For these conditions the simulation shows that IPA concentrations is stabilized nearly 10 cm after the mixing point. In our facility, the interval between two temperature measuring points was about 20 cm and the total length

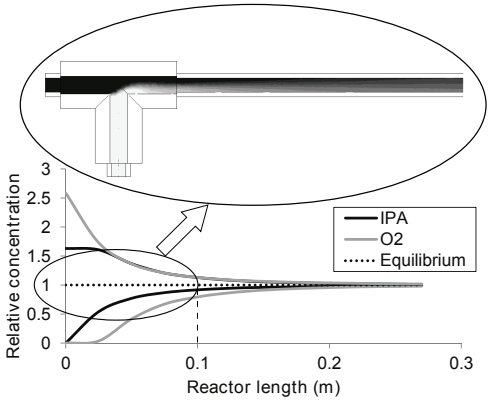

Figure 3.2: Maximum and minimum species concentration relative to equilibrium concentration in the tubular reactor, showing the dispersion along reactor length: IPA (black line), O_2 (grey line). The central dotted line marks the equilibrium value. Above, detail of simulation: IPA (black), O_2 (white).

of the reactor was 1.5 m, making insignificant the mixing length. Thus, the hypothesis of instantaneous mixing is acceptable and the reactor can be modeled as plug flow. Also, a visual reference of the mixing process can be seen on detail in figure 3.2, where the simulated contours of IPA concentration are presented.

3.4.2 Kinetic Model

The fitted parameters and their confidence interval (CI) are presented in equation (3.15). The confidence interval of the parameters was calculated by the Matlab function `nlparci` which calculates the 95% confidence intervals for parameters in nonlinear regression.

$$X = \begin{pmatrix} X_1 \\ X_2 \end{pmatrix} = \begin{pmatrix} 18.34896 \\ 12.65636 \end{pmatrix}, \; CI = \begin{pmatrix} 17.9204 & 18.7775 \\ 12.3087 & 13.0040 \end{pmatrix} \tag{3.15}$$

Thus, the kinetic parameters are shown in eq. (3.16):

$$\begin{aligned} k_0 &= (9.308 \pm 3.989) \cdot 10^7 (m^3\, s^{-1}\, kmol^{-1}) \\ E_a &= 89.441 \pm 2.457 (kJ\, mol^{-1}) \end{aligned} \tag{3.16}$$

Figure 3.3 compares the experimental temperature profile with the prediction of the model using the parameters found in equation (3.16). The data corresponds to experiments at two different inlet temperatures, flows and type of oxidant used: air or oxygen. The model prediction agrees with ex-

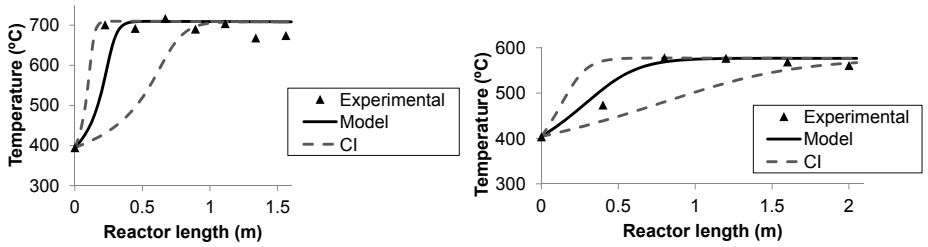

(a) (b)

Figure 3.3: Comparison of experimental temperatures (symbols) along the tubular reactor and model predictions (continuous line) using the fitted kinetics. Dashed lines indicate the predictions in the limits of CI. (a)5.9 kg/h, 4%IPA at 395°C, air as oxidant; (b)10.6 kg/h, 2%IPA at 404°C, O_2 as oxidant.

perimental data, as the experimental temperatures are inside the model's interval of confidence. The least square error over all experimental points used to perform the fitting is 10.8%.

3.4.3 Parametric analysis

The kinetic model was applied in a parametric analysis to study the influence of inlet temperature and fuel concentration on flame formation. Once again, a plug flow reactor was assumed and the results are showed as function of residence time.

Figure 3.4 shows how the fuel concentration affects the flame formation. Three different concentrations where tested at inlet temperature of 350°C, and air in 10% excess. The analysis of the reaction rate shown in figure 3.4a indicates that a feed with 3% IPA at 350°C is slowly oxidized, while a feed with 5% IPA is rapidly oxidized inside a narrow zone that could be recognized as a flame. Figure 3.4b shows the temperature rising for the same cases and suggests a flameless oxidation for 3% IPA and a flame oxidation for 5% IPA. The concentration profiles are shown in figure 3.4c where can be seen a clear separation of reagents and products for the 5% IPA feed. These results are in accordance with the work of Serikawa et al. [21], that found stable hydrothermal flames using a tubular reactor for IPA oxidation, when IPA concentrations were above 4% (or 5% vol, since volume fraction was used in that work instead of mass fraction).

The effects of inlet temperature are shown in figure 3.5. Feeds with 5% IPA and air with 10% excess at three different injection temperatures are compared. Figure 3.5a shows that the injection temperatures have influence on flame position. Reducing injection temperature from 370 to 330°C causes

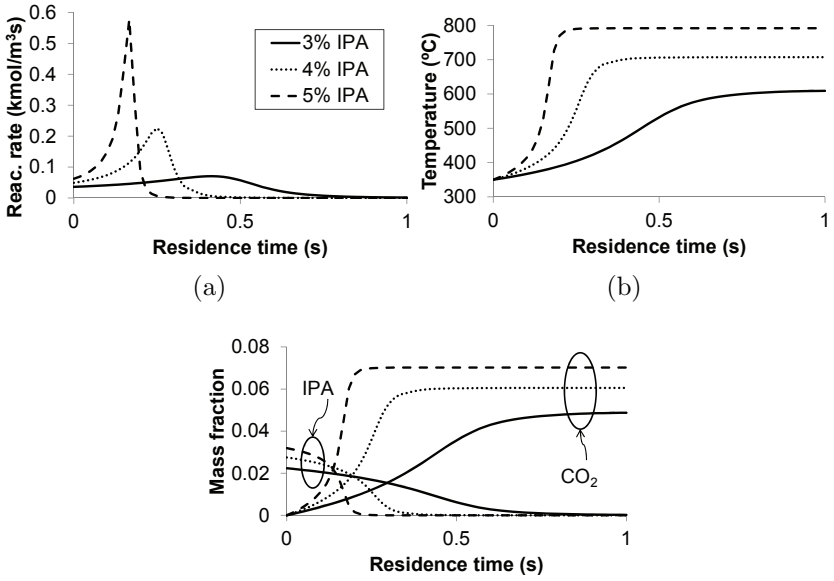

Figure 3.4: (a)Reaction rate, (b)Temperature and (c)Species mass fractions as function of residence time in plug flow reactor at injection temperature of 350°C for different inlet IPA concentrations: 3% (continuous line)), 4% (dotted line) and 5% (dashed line).

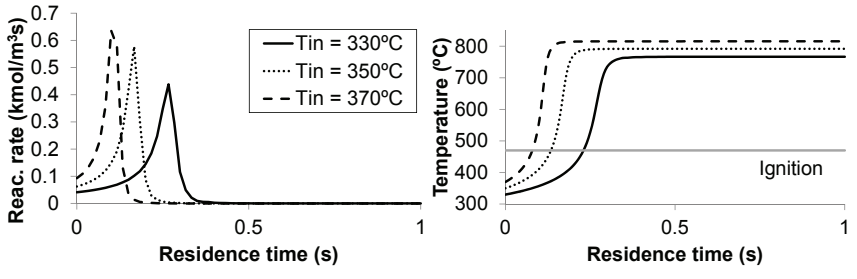

Figure 3.5: (a)Reaction rate, (b)Temperature as function of residence time in plug flow reactor at 5% IPA for different temperatures of injection: 330°C (continuous line)), 350°C (dotted line) and 370°C (dashed line). Grey line corresponds to ignition temperature.

a delay of approximately 0.2 s in the flame ignition. With the characteristics of our experimental plant, this delay is equivalent to a displacement of 60 cm. Figure 3.5b shows temperature profiles for the three cases and the ignition temperature found by Serikawa et al. [21]. This temperature (470°C) corresponds to the beginning of the maximum slope region at temperature profiles predicted in this work.

3.4.4 Simulation of TWR

The result of the transpiring wall reactor simulation shown here corresponds to a piece of experimental data using a feed flow of 27.7 kg/h with 8% mass isopropyl alcohol and 23.9 kg/h of air, an injection temperature of 246°C and a pressure of 23 MPa. The transpiring flow was 16.9 kg/h of water at 25°C.

The results of this simulation show that the model correctly predicts the heating and flameless oxidation inside the injector and also the flame formation at upper part of reaction chamber. In presence of a hydrothermal flame, complete oxidation occurs when injection temperatures are as low as 246°C. Inside the injector, the reagent stream is heated up to 382°C due heat transmission from the reactor chamber through the injector's wall, and slow oxidation. Outside the injector, the reactive mixture reaches a temperature as high as 709°C (experimental value was 694°C). The temperature profile predicted by the model is compared to the experimental temperature data measured inside the injector and at the reaction chamber in figure 3.6a. A good agreement with the experimental data can be observed here.

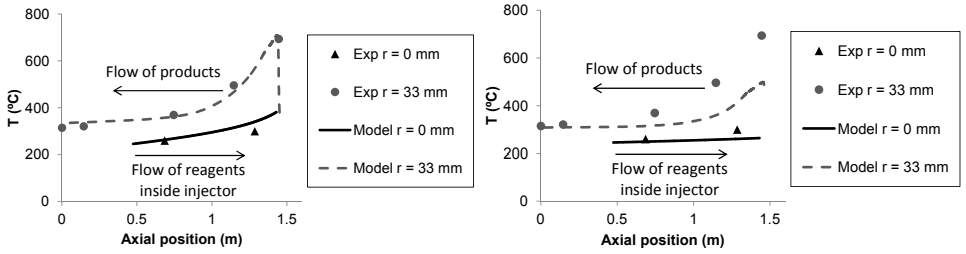

(a) (b)

Figure 3.6: Experimental (symbols) and model (lines) temperature profiles of TWR Simulation: (a)This work, (b) previous model. Black color corresponds to injector; grey color represents reaction chamber.

Figure 3.6b show the same experiment reproduced by the previous model of our group [23]. The kinetic model adopted in that previous work was able to reproduce experimental data for inlet temperatures of 300°C and above, but failed at lower injection temperatures. Other models existing in

literature, fitted for systems at lower temperatures, are not fast enough to correctly predict the rapid reaction rate at flame zone. Nevertheless, the model developed in this work shows satisfactory results for a wide range of inlet temperatures and concentrations.

3.5 Conclusions

A new simple kinetic model for supercritical water oxidation of isopropyl-alcohol in hydrothermal flame regime was determined by adjusting the temperature profile in tubular SCWO reactors. The model is able to predict temperature profiles in tubular reactors at different IPA concentrations, feed flows and using air or oxygen as the oxidant.

A 3D CFD model confirmed the hypothesis that the mixing process occurs in the first centimeters of the tubular reactor. Thus, the initiation of the reaction is not affected by the mixing process, being the reaction controlled by the kinetics.

Given the inlet conditions, the model can estimate if the oxidation will be flame or flameless regime, and is capable of reproducing both.

This kinetic model was applied to a model for the transpiring wall reactor developed by the University of Valladolid and the experimental data were successfully described. According to the results, in the presence of a hydrothermal flame, the reactor can be maintained in steady state regime, with total destruction of fuel, even for subcritical feed injections (246°C).

The new kinetic model, allied with modeling and simulation, allows for a better understanding of SCWO reactors and can lead to improving their design and optimization.

Acknowledgments

The authors thank the Spanish Ministry of Science and Innovation for the CTQ2010-15475 Project (subprogram PPQ). J.P.S.Queiroz thanks the Spanish Ministry of Education's FPU program (AP2009-0399) for his PhD grant.

Bibliography

[1] M. D. Bermejo, M. J. Cocero, Supercritical water oxidation: A technical review, AIChE Journal 52 (2006) 3933–3951.

Nomenclature

C	molar concentration ($kmol\,m^{-3}$)
E_a	activation energy ($kJ\,mol^{-1}$)
ΔH_r	heat of reaction ($J\,kmol^{-1}$)
M	molecular weight ($kg\,kmol^{-1}$)
R	universal gas constant ($J\,mol^{-1}K^{-1}$)
R_k	species source ($kmol\,m^{-3}s^{-1}$)
S	cross section (m^2)
S_h	energy source ($J\,m^{-3}s^{-1}$)
T	temperature (K)
V	molar volume ($m^3\,mol^{-1}$)
X	auxiliary parameter
c_p	constant pressure heat capacity ($J\,kg^{-1}K^{-1}$)
f_{obj}	objective function
h	specific enthalpy ($J\,kg^{-1}$)
k_0	Arrhenius pre-exponential factor ($s\,m^3\,kmol^{-1}$)
$\dot{m}$	mass flow ($kg\,s^{-1}$)
r	reaction rate ($kmol\,m^{-3}s^{-1}$)
t	time (s)
u	velocity ($m\,s^{-1}$)
vt	translated volume ($cm^3\,mol^{-1}$)
w	mass fraction
y^+	dimensionless wall distance
z	longitudinal coordinate (m)
Greek symbols	
λ	thermal conductivity ($W\,m^{-1}K^{-1}$)
ρ	density ($kg\,m^{-3}$)
τ	stress tensor ($N\,m^{-2}$)
Subscripts	
i, j, l	directions
k	species
t	turbulent
Abbreviations	
CFD	computational fluid dynamics
CI	confidence interval
PR	Peng-Robinson equation of state
IPA	isopropyl-alcohol
SCW	supercritical water
SCWO	supercritical water oxidation
TOC	total organic carbon
TWR	transpiring wall reactor
VTPR	volume translated Peng-Robinson equation of state

[2] G. Brunner, Near and supercritical water. part II: oxidative processes, Journal of Supercritical Fluids 47 (2009) 382–390.

[3] C. Augustine, J. Tester, Hydrothermal flames: From phenomenological

experimental demonstrations to quantitative understanding, Journal of Supercritical Fluids 47 (2009) 415–430.

[4] W. Schilling, E. Franck, Combustion and diffusion flames at high-pressures to 2000 bar, Berichte Der Bunsen-Gesellschaft-Physical Chemistry Chemical Physics 92 (1988) 631–636.

[5] C. Oh, R. Kochan, T. Charlton, A. Bourhis, Thermal-hydraulic modeling of supercritical water oxidation of ethanol, Energy & Fuels 10 (1996) 326–332.

[6] B. Wellig, M. Weber, K. Lieball, K. Prikopsky, P. von Rohr, Hydrothermal methanol diffusion flame as internal heat source in a SCWO reactor, Journal of Supercritical Fluids 49 (2009) 59–70.

[7] B. Wellig, K. Lieball, P. von Rohr, Operating characteristics of a transpiring-wall SCWO reactor with a hydrothermal flame as internal heat source, Journal of Supercritical Fluids 34 (2005) 35–50.

[8] M. D. Bermejo, P. Cabeza, M. Bahr, R. Fernandez, V. Rios, C. Jimenez, M. J. Cocero, Experimental study of hydrothermal flames initiation using different static mixer configurations, Journal of Supercritical Fluids 50 (2009) 240–249.

[9] M. D. Bermejo, C. Jimenez, P. Cabeza, A. Matias-Gago, M. J. Cocero, Experimental study of hydrothermal flames formation using a tubular injector in a refrigerated reaction chamber. influence of the operational and geometrical parameters, Journal of Supercritical Fluids 59 (2011) 140–148.

[10] M. D. Bermejo, P. Cabeza, J. P. S. Queiroz, C. Jimenez, M. J. Cocero, Analysis of the scale up of a transpiring wall reactor with a hydrothermal flame as a heat source for the supercritical water oxidation, Journal of Supercritical Fluids 56 (2011) 21–32.

[11] C. Narayanan, C. Frouzakis, K. Boulouchos, K. Príkopský, B. Wellig, P. Rudolf von Rohr, Numerical modelling of a supercritical water oxidation reactor containing a hydrothermal flame, Journal of Supercritical Fluids 46 (2008) 149–155.

[12] F. Vogel, J. Blanchard, P. Marrone, S. Rice, P. Webley, W. Peters, K. Smith, J. Tester, Critical review of kinetic data for the oxidation of methanol in supercritical water, Journal of Supercritical Fluids 34 (2005) 249–286.

[13] R. K. Helling, J. W. Tester, Oxidation of simple compounds and mixtures in supercritical water: carbon monoxide, ammonia and ethanol, Environmental Science & Technology 22 (1988) 1319–1324.

[14] L. Li, P. Chen, E. Gloyna, Kinetic-model for wet oxidation of organic-compounds in subcritical and supercritical water, Supercritical Fluid Engineering Science - Fundamentals and Applications 514 (1993) 305–313.

[15] J. Ploeger, P. Bielenberg, J. Dinaro-Blanchard, R. Lachance, J. Taylor, W. Green, J. Tester, Modeling oxidation and hydrolysis reactions in supercritical water-free radical elementary reaction networks and their applications, Combustion Science and Technology 178 (2006) 363–398.

[16] P. Webley, J. Tester, H. Holgate, Oxidation-kinetics of ammonia and ammonia-methanol mixtures in supercritical water in the temperature-range 530-degrees-c 700-degrees-c at 246 bar, Industrial & Engineering Chemistry Research 30 (1991) 1745–1754.

[17] T. Hunter, S. Rice, R. Hanush, Raman spectroscopic measurement of oxidation in supercritical water .2. conversion of isopropyl alcohol to acetone, Industrial & Engineering Chemistry Research 35 (1996) 3984–3990.

[18] S. P. Maharrey, D. R. Miller, A direct sampling mass spectrometer investigation of oxidation mechanisms for acetic acid in supercritical water, The Journal of Physical Chemistry A 105 (2001) 5860–5867.

[19] S. Rice, T. Hunter, A. Ryden, R. Hanush, Raman spectroscopic measurement of oxidation in supercritical water .1. conversion of methanol to formaldehyde, Industrial & Engineering Chemistry Research 35 (1996) 2161–2171.

[20] J. Sierra-Pallares, M. Parra-Santos, J. Garcia-Serna, F. Castro, M. Cocero, Numerical analysis of high-pressure fluid jets: Application to RTD prediction in supercritical reactors, Journal of Supercritical Fluids 49 (2009) 249–255.

[21] R. M. Serikawa, T. Usui, T. Nishimura, H. Sato, S. Hamada, H. Sekino, Hydrothermal flames in supercritical water oxidation: investigation in a pilot scale continuous reactor, Fuel 81 (2002) 1147–1159.

[22] P. Cabeza, M. D. Bermejo, C. Jimenez, M. J. Cocero, Experimental study of the supercritical water oxidation of recalcitrant compounds

under hydrothermal flames using tubular reactors, Water Research 45 (2011) 2485–2495.

[23] M. D. Bermejo, F. Fernandez-Polanco, M. J. Cocero, Modeling of a transpiring wall reactor for the supercritical water oxidation using simple flow patterns: Comparison to experimental results, Industrial & Engineering Chemistry Research 44 (2005) 3835–3845.

[24] D.-Y. Peng, D. B. Robinson, A new two-constant equation of state, Industrial & Engineering Chemistry Fundamentals 15 (1976) 59–64.

[25] A. Peneloux, E. Rauzy, R. Freze, A consistent correction for redlich-kwong-soave volumes, Fluid Phase Equilibria 8 (1982) 7–23.

[26] E. W. Lemmon, M. O. McLinden, D. G. Friend, Thermophysical properties of fluid systems, in: P. J. Linstrom, W. G. Mallard (Eds.), NIST Chemistry WebBook, NIST Standard Reference Database, 69, National Institute of Standards and Technology, Gaithersburg MD, 20899, 2011. Last access: 05/24/2013.

[27] J. Schwartzentruber, H. Renon, S. Watanasiri, Development of a new cubic equation of state for phase equilibrium calculations, Fluid Phase Equilibria 52 (1989) 127–134.

[28] K. S. Lieball, Numerical Investigations on a Transpiring Wall Reactor for Supercritical Water Oxidation, Doctor of technical sciences, Swiss Federal Institute of Technology Zurich, Zurich, 2003.

[29] L. Li, P. Chen, E. Gloyna, Generalized kinetic-model for wet oxidation of organic-compounds, AIChE Journal 37 (1991) 1687–1697.

[30] K. Levenberg, A method for the solution of certain problems in least squares, The Quarterly of Applied Mathematics 2 (1944) 164–168.

[31] D. Marquardt, An algorithm for least-squares estimation of nonlinear parameters, SIAM Journal on Applied Mathematics 11 (1963) 431–441.

[32] ANSYS, ANSYS FLUENT theory guide release 12, 2009.

[33] B. E. Poling, J. M. Prausnitz, J. P. O'Connell, The Properties of Gases and Liquids, McGraw-Hill, New York, 5 th edition, 2007.

[34] J. Sierra-Pallares, M. Parra-Santos, J. Garcia-Serna, F. Castro, M. Cocero, Numerical modelling of hydrothermal flames. micromixing effects over turbulent reaction rates, Journal of Supercritical Fluids 50 (2009) 146–154.

[35] B. E. Launder, B. I. Sharma, Application of the energy-dissipation model of turbulence to the calculation of flow near a spinning disc, Letters in Heat and Mass Transfer 1 (1974) 131–138.

Chapter 4

Numerical simulation of premixed hydrothermal flames using a RANS-pdf approach

Abstract

Effects of turbulence on a premixed hydrothermal flame produced inside a supercritical water oxidation reactor are studied. Turbulent mean reaction rate is computed assuming a fixed shape for the probability density function and the results are compared to the laminar (Arrhenius) mean reaction rate.

4.1 Introduction

The study of hydrothermal flames began in the 80s after a series of studies of professor Franck, who called the oxidation process in dense aqueous environment as "hydrothermal combustion" [1]. Augustine and Tester [2] defined hydrothermal flames as combustion flames produced in aqueous environments at conditions above the critical point of water (P > 22.1 MPa and T > 374°C). Above these conditions, species involved in oxidation reactions, such as O_2, N_2, CO_2 and organic compounds, are completely miscible with water, forming a single homogeneous phase. Hydrothermal flames operate in the regime of thermal runaway [2], in which species enter the reaction zone at significantly lower temperatures before being heated to the reaction temperature and undergoing the combustion process.

One of the engineering applications of hydrothermal flames is as internal heat source in supercritical water oxidation (SCWO) process. The purpose is to confine a self-sustaining hydrothermal flame reaction zone inside a vessel within a co-flowing or transpiring stream of subcritical water that protects the reactor walls from corrosion and salt plugging. Serikawa et al. [3] developed a continuous refrigerated facility for observing hydrothermal flames oxidizing isopropyl alcohol. The ETH Zurich has been developing different continuous hydrothermal burners working with non premixed flames [4–6]. They used the hydrothermal flame as an internal heat source in a transpiring wall reactor. Reactors developed in the University of Valladolid, can be described as working at hydrothermal flame regime with a premixed flame [7, 8]. The direct injection of the waste into a hydrothermal flame is a solution to avoid the external preheating of the feed up to supercritical conditions, eliminating the problems of corrosion and plugging in the preheating section. Due to the high flame temperatures, the combustion reaction would proceed very quickly, requiring residence times of only 10-100 ms to completely oxidize organic compounds [2]. Another benefit of the high temperatures achieved by hydrothermal flames is the enhancement of energy recovery, which traditionally is a challenge in SCWO processes [9].

In addition to SCWO, hydrothermal flames have been applied to thermal spallation drilling [2] systems, for drilling deep wells in hard rocks. Flame jet thermal spallation uses high heat fluxes to rapidly heat a rock surface, inducing thermal stresses that lead to the formation of rock fragments, or spalls [2]. In boreholes that are more than 2000 m deep and filled with water, the hydrostatic pressure exceeds the critical pressure of water. In such a situation, hydrothermal flames can provide the required heat to spall the rock [10].

Mathematical modeling provides a comprehensive way to understand ex-

perimental results, equipment design and scaling-up processes. Computational fluid dynamics (CFD) has been used to model hydrothermal flames in SCWO reactors (e.g. [11–13]). Some simplifying assumptions normally applied to reactive flow transport models cannot be used with hydrothermal flames due the particular properties of supercritical media. These assumptions include constant density or unit Schmidt number, for example. There are a few works that try to overcome those restrictions. Schuler et al. [14] applied a variable turbulent Prandtl number (usually constant on CFD tools) to simulating submerged supercritical water jets. Sierra-Pallares et al. [15] used a micromixing model developed for liquids (Schmidt number higher than unity) to modeling a non-remixed hydrothermal flame.

The prediction of chemical reactions in turbulent flows is not an easy task. Oxidation reaction rates depend on species concentration and temperature, and that dependence is usually non-linear. Thus, the effect of turbulent fluctuations in species concentration and/or temperature on the reaction rate is not clear. Little modeling research is available on turbulent-chemistry interactions in supercritical environments. For safety reasons, most of the experimental setups for producing hydrothermal flames feed fuel and oxidant separately. Thus, existing work on modeling is focused on diffusion flames models, where the mixing process needs more attention than the reaction itself. The new SCWO reactor operating in University of Valladolid [16] mixes the cold reagents before the injection on reaction chamber, being similar to a premixed flame burner. In this work, the turbulence-chemistry interactions in a premixed hydrothermal flame are studied. To the best of our knowledge, for the first time a RANS-pdf model is applied in this context.

4.2 Governing equations

The flow of supercritical fluids can be described by fundamental conservation equations for mass, momentum, energy and species. Balance equations for the mean quantities in Reynolds-averaged Navier-Stokes (RANS) simulations are obtained by averaging the instantaneous balance equations. This averaging procedure introduces unclosed quantities that have to be modeled, using turbulent combustion models [17].

For variable density flows, the Favre average is defined as:

$$\widetilde{f} = \frac{\overline{\rho f}}{\bar{\rho}} \tag{4.1}$$

Any quantity f may be split into mean and fluctuating components as:

$$f = \widetilde{f} + f'' \text{ with } \widetilde{f''} = 0 \tag{4.2}$$

Using this formalism, the averaged balance equation for chemical species become:

$$\frac{\partial}{\partial t}(\bar{\rho}\widetilde{y_k}) + \frac{\partial}{\partial x_i}(\bar{\rho}\widetilde{u_i}\widetilde{y_k}) = -\frac{\partial}{\partial x_i}\left[\bar{\rho}\bar{D}\frac{\partial \widetilde{y_k}}{\partial x_i} + \bar{\rho}\widetilde{u_i''y_k''}\right] + \overline{\dot{w}}_k \tag{4.3}$$

The species turbulent flux is closed using the classical gradient assumption:

$$\bar{\rho}\widetilde{u_i''y_k''} = -\frac{\mu_t}{Sc_t}\frac{\partial \widetilde{y_k}}{\partial x_i} \tag{4.4}$$

The conservation equations of mass, momentum and energy, and their respective closures, are not presented here, and can be found elsewhere [17]. The objective of this study is to model the mean reaction rate $\overline{\dot{w}}_k$. All the other turbulent unknown quantities are treated in classical way [17, 18].

4.3 Closure of turbulent reaction rate

Turbulent premixed flames usually are characterized by the Damköhler number, which corresponds to the ratio of the integral turbulent time scale to the chemical time scale.

$$Da = \frac{\tau_t}{\tau_c} \tag{4.5}$$

The turbulent time scale is estimated from the turbulence model ($\tau_t = \epsilon/k$), while the chemical time scale depends on the Arrhenius law. We assume a reaction rate of first order for fuel and oxygen, giving:

$$\dot{w} = k_0 exp\left(\frac{-E_a}{RT}\right) C_a C_b \text{ and } \frac{1}{\tau_c} = k_0 exp\left(\frac{-E_a}{RT}\right)\frac{C_a C_b}{C_a + C_b} \tag{4.6}$$

If $Da \gg 1$, the reaction is fast compared to the turbulence, and the reaction zone is viewed as a collection of fresh and burnt pockets transported by turbulent eddies. If $Da \ll 1$, the turbulence is fast and all the species are mixed before reaction occurs.

Preliminary calculations point to slow rates of reaction, with $Da \sim 1$. Thus, we studied two models which chemical reaction rate is important and cannot be neglected.

4.3.1 Arrhenius approach

In the lower limit of Da, the effects of turbulence can be neglected. This is equivalent to suppose that the mean reaction rate corresponds to the reaction rate obtained using mean local values $\bar{C}$ and $\bar{T}$.

$$\overline{\dot{w}} = \overline{k_0 exp(-E_a/RT) C_a C_b} = k_0 exp(-E_a/R\overline{T})\overline{C}_a\overline{C}_b \tag{4.7}$$

4.3.2 Probability density function (pdf) model

This approach does not require assumptions on the flame structure such as mixing-controlled combustion: mean reaction rates are expressed combining instantaneous reaction rates given from Arrhenius law (Eq. 1.24), with the joint probability density function p(N) to have given values of the thermochemical variables (i.e. species mass fractions, temperature.

$$\widetilde{\dot{w}} = \int_0^1 \dot{w}(c)p(c)dc \tag{4.8}$$

In the second approach used, the effects of turbulence over the rate of reaction are studied through a progress variable c, which is assumed to follow a probability density function (pdf). In general, a pdf function can take any shape and exhibit multiple extrema. It contains information not only on the mean value of the variable but also on its variance. For many combustion applications, however, pdf functions often present common features, suggesting that these functions can be described using a limited number of parameters [19]. A possible approach is to suppose that the pdf has a fixed shape, parametrized using, for example, only one or two parameters. The logical parameters to use are the moments of the variable: mean quantities and/or variance. The most popular pdf shape is the so-called β-function:

$$p(c) = \frac{c^{(a-1)} \cdot (1-c)^{(b-1)}}{\int_0^1 c^{(a-1)} \cdot (1-c)^{(b-1)} dc} \tag{4.9}$$

Where, c is the progress variable, based on fuel mass fraction, and the variance of this distribution corresponds to the turbulent fluctuations of the progress variable [19]. The parameters a and b are determined by mean and variance of progress variable:

$$a = \tilde{c}\left[\frac{\tilde{c}(1-\tilde{c})}{\widetilde{c''^2}} - 1\right];\ b = \frac{a}{\tilde{c}} - a \tag{4.10}$$

The mean value of progress variable is obtained directly from RANS calculation of fuel mass fraction:

$$\tilde{c} = 1 - \frac{\tilde{y}_{\text{fuel}}}{\tilde{y}_{\text{fuel},o}} \tag{4.11}$$

One additional transport equation is solved for the variance:

$$\frac{\partial \bar{\rho}\widetilde{c''^2}}{\partial t} + \frac{\partial\left(\bar{\rho}\tilde{u}_i\widetilde{c''^2}\right)}{\partial x_i} = \underbrace{\frac{\partial}{\partial x_i}\left(\overline{\rho D\frac{\partial \widetilde{c''^2}}{\partial x_i}}\right) + \overline{2c''\frac{\partial}{\partial x_i}\left(\rho D\frac{\partial \tilde{c}}{\partial x_i}\right)}}_{\text{molecular diffusion}} - \underbrace{\frac{\partial}{\partial x_i}\left(\overline{\rho u_i'' c''^2}\right)}_{\text{turbulent transport}} - \underbrace{2\overline{\rho u_i'' c''}\frac{\partial \tilde{c}}{\partial x_i}}_{\text{production}} - \underbrace{2\overline{\rho D\frac{\partial c''}{\partial x_i}\frac{\partial c''}{\partial x_i}}}_{\text{dissipation}} + \underbrace{2\overline{c''\dot{w}}}_{\text{reaction}} \tag{4.12}$$

Where the three last terms are closed as:

$$\overline{\rho u_i'' c''}\frac{\partial \tilde{c}}{\partial x_i} = -\bar{\rho}\frac{\nu_t}{Sc_t}\frac{\partial \tilde{c}}{\partial x_i}\frac{\partial \tilde{c}}{\partial x_i} \tag{4.13}$$

$$\overline{\rho D\frac{\partial c''}{\partial x_i}\frac{\partial c''}{\partial x_i}} = -\rho\frac{\epsilon}{k}\widetilde{c''^2} \tag{4.14}$$

$$\overline{c''\dot{w}} = \int_0^1 (c^* - \tilde{c})\,\dot{w}(c^*)p(c^*)dc^* \tag{4.15}$$

For an adiabatic, single reaction, with unity Lewis number, temperature and fuel concentration are correlated, and the mean reaction rate is function only of the progress variable:

$$\widetilde{\dot{w}} = \int_0^1 \dot{w}(c)p(c)dc \tag{4.16}$$

4.4 Results

The source terms for the variance transport equation, and the calculations of reaction rate were implemented by user-defined functions in ANSYS FLUENT. The integrals in equations (4.15) and (4.16) are pre-calculated and tabulated for values of $\tilde{c}$ and $\widetilde{c''^2}$, in order to reduce computational effort. The geometry used as model is shown in figure 4.1, and it is a simplification of a SCWO reactor developed in University of Valladolid [8].

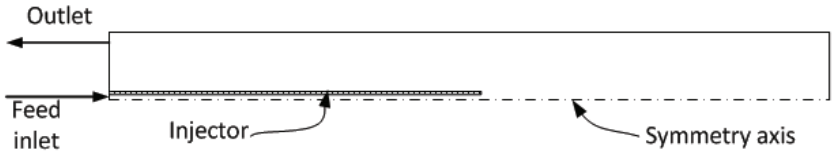

Figure 4.1: Geometry of reactor.

Realizable k-ϵ turbulence model was used with enhanced wall treatment. Property calculations are described in Chapter 2, and Arrhenius reaction rate is described in Chapter 3. Inlet conditions are given in table 4.1.

Table 4.1: Feed stream characteristics.

Flow	27.1	kg/h
P	23	MPa
T	150	°C
H_2O	43.0	%w/w
C_3H_8O	5.0	%w/w
O_2	12.1	%w/w
N_2	39.9	%w/w

Figure 4.2 compares the rate of reaction using the pdf approach and the Arrhenius laminar one. It can be observed that the inclusion of turbulent effects results in a wider and larger flame.

As it is expected, the zone more sensitive to turbulence is not the center of the jet, but the shear layer. Figure 4.3 shows the profiles of mean reaction rate for both Arrhenius and pdf methods. Figure 4.3a presents the rate of reaction at centerline as function of length L/d_o starting from injector's outlet, where d_o is the internal diameter of the injector. Both approaches predict almost the same behavior. In figure 4.3b the radial profile of mean reaction rate is presented as function of radius, corresponding to a section 20 mm above the injector's exit. It can be seen that ignoring the turbulence effects makes the reaction rate to be overpredicted by a factor of 3.

The effect of a slower reaction rate is evidenced in figure 4.4, where the mass fraction of fuel (IPA) is shown as function of residence time. According the pdf model, the reaction needs more time to consume all the fuel.

At the conditions tested here, the total residence time is about 20 s, much higher than the delay showed by an improvement on reaction rate calculation. Thus at reactor outlet the elimination efficiency, and the final temperature are not changed.

4.5 Conclusions

A turbulent premixed flame model based on presumed probability density function has been applied to a hydrothermal flame maintained in a supercritical water oxidation reactor. The method was applied in a simplified model of a real pilot scale reactor.

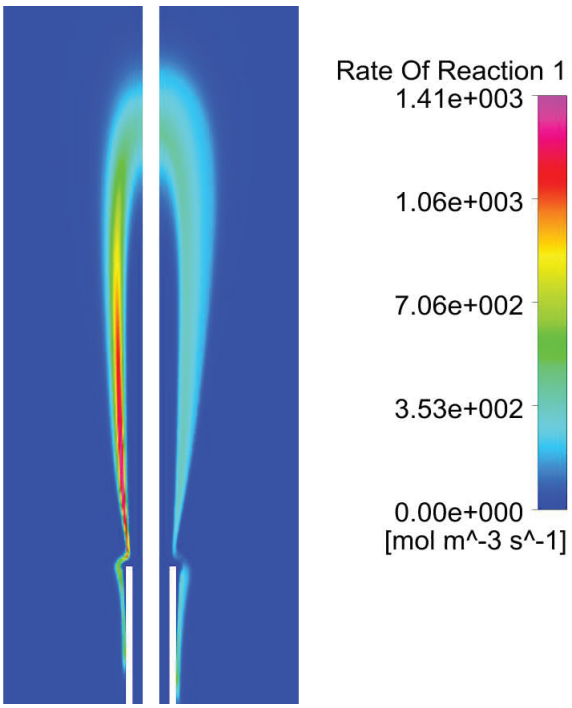

(a) (b)

Figure 4.2: Simulation contours of rate of reaction: (a)Arrhenius approach. (b)Pdf approach.

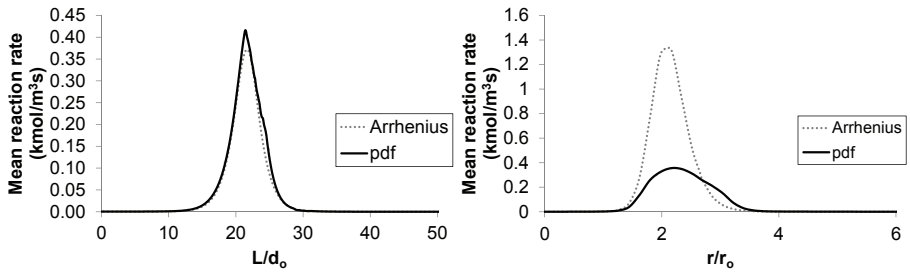

(a) (b)

Figure 4.3: Profiles of mean rate of reaction. (a)Axial profile at centerline. $d_o = 3.86mm$. (b)Radial profile 20 mm above the injector's outlet. $r_o = d_o/2$.

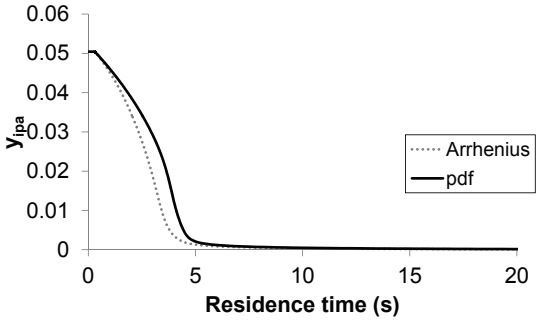

Figure 4.4: Mass fraction of IPA at reactor centerline as function of residence time.

The analysis of the results indicates that the turbulence greatly affects the reaction rate in the shear layer, but not at the core of the jet. The effects could modify the efficiency of the reactor on eliminating residues or producing energy, depending on the residence times involved. Also, when dealing with other fuels (and real waste) the turbulence-chemistry interaction could be more noticeable.

Bibliography

[1] W. Schilling, E. Franck, Combustion and diffusion flames at high-pressures to 2000 bar, Berichte Der Bunsen-Gesellschaft-Physical Chemistry Chemical Physics 92 (1988) 631–636.

[2] C. Augustine, J. Tester, Hydrothermal flames: From phenomenological experimental demonstrations to quantitative understanding, Journal of Supercritical Fluids 47 (2009) 415–430.

[3] R. M. Serikawa, T. Usui, T. Nishimura, H. Sato, S. Hamada, H. Sekino, Hydrothermal flames in supercritical water oxidation: investigation in a pilot scale continuous reactor, Fuel 81 (2002) 1147–1159.

[4] B. Wellig, K. Lieball, P. von Rohr, Operating characteristics of a transpiring-wall SCWO reactor with a hydrothermal flame as internal heat source, Journal of Supercritical Fluids 34 (2005) 35–50.

[5] K. Príkopský, B. Wellig, P. R. von Rohr, SCWO of salt containing artificial wastewater using a transpiring-wall reactor: Experimental results, The Journal of Supercritical Fluids 40 (2007) 246–257.

[6] B. Wellig, M. Weber, K. Lieball, K. Prikopsky, P. von Rohr, Hydrothermal methanol diffusion flame as internal heat source in a SCWO reactor, Journal of Supercritical Fluids 49 (2009) 59–70.

[7] M. D. Bermejo, P. Cabeza, M. Bahr, R. Fernandez, V. Rios, C. Jimenez, M. J. Cocero, Experimental study of hydrothermal flames initiation using different static mixer configurations, Journal of Supercritical Fluids 50 (2009) 240–249.

[8] M. D. Bermejo, C. Jimenez, P. Cabeza, A. Matias-Gago, M. J. Cocero, Experimental study of hydrothermal flames formation using a tubular injector in a refrigerated reaction chamber. influence of the operational and geometrical parameters, Journal of Supercritical Fluids 59 (2011) 140–148.

[9] M. D. Bermejo, Á. Martín, J. P. S. Queiroz, P. Cabeza, F. Mato, M. J. Cocero, Chapter 15 supercritical water oxidation (SCWO) of solid, liquid and gaseous fuels for energy generation, in: Z. Fang, C. C. Xu (Eds.), Near-critical and Supercritical Water and Their Applications for Biorefineries, number 2 in Biofuels and Biorefineries, Springer Verlag, 2014.

[10] G. Brunner, Chapter 10 - oxidation in high-temperature and supercritical water, in: Gerd Brunner (Ed.), Hydrothermal and Supercritical Water Processes, number 5 in Supercritical Fluid Science and Technology, Elsevier, 2014, pp. 525–568.

[11] K. S. Lieball, Numerical Investigations on a Transpiring Wall Reactor for Supercritical Water Oxidation, Doctor of technical sciences, Swiss Federal Institute of Technology Zurich, Zurich, 2003.

[12] C. Narayanan, C. Frouzakis, K. Boulouchos, K. Príkopský, B. Wellig, P. Rudolf von Rohr, Numerical modelling of a supercritical water oxidation reactor containing a hydrothermal flame, Journal of Supercritical Fluids 46 (2008) 149–155.

[13] J. P. S. Queiroz, M. D. Bermejo, M. J. Cocero, Numerical study of the influence of geometrical and operational parameters in the behavior of a hydrothermal flame in vessel reactors, Chemical Engineering Science 112 (2014) 47–55.

[14] M. J. Schuler, T. Rothenfluh, P. Rudolf von Rohr, Simulation of the thermal field of submerged supercritical water jets at near-critical pressures, The Journal of Supercritical Fluids 75 (2013) 128–137.

[15] J. Sierra-Pallares, M. Parra-Santos, J. Garcia-Serna, F. Castro, M. Cocero, Numerical modelling of hydrothermal flames. micromixing effects over turbulent reaction rates, Journal of Supercritical Fluids 50 (2009) 146–154.

[16] P. Cabeza, J. P. S. Queiroz, S. Arca, C. Jiménez, A. Gutiérrez, M. D. Bermejo, M. J. Cocero, Sludge destruction by means of a hydrothermal flame. optimization of ammonia destruction conditions, Chemical Engineering Journal 232 (2013) 1–9.

[17] D. Veynante, L. Vervisch, Turbulent combustion modeling, Progress in Energy and Combustion Science 28 (2002) 193–266.

[18] ANSYS, ANSYS FLUENT theory guide release 12, 2009.

[19] T. Poinsot, D. Veynante, Theoretical and Numerical Combustion, Second Edition, R.T. Edwards, Inc., Philadelphia, 2 edition, 2005.

Chapter 5

Numerical study of the influence of geometrical and operational parameters in the behavior of a hydrothermal flame in vessel reactors

Abstract

The influence of the internal configuration of vessel reactors for the Supercritical Water Oxidation Process is evaluated by simulation and compared to experimental data. A one equation model is used to close the RANS equations and allow the reproduction of the experimental results. The model can be used for designing reactors working under hydrothermal flame looking at performance and flame stabilization. Geometrical parameters studied here are the distance between injector's outlet and reactor's ceiling and the injector inner diameter. Influence of operational parameters like flow velocity and inlet temperature are also verified.

Keywords: Hydrothermal flames, CFD modeling, Supercritical water oxidation, RTD Analysis

Chemical Engineering Science 112 (2014), 47-55

5.1 Introduction

Supercritical water oxidation (SCWO) is a useful technology for the destruction of waste with residence times lower than one minute. It takes advantage of the special solvation properties of water above its critical point (374°C, 22.1 MPa) to achieve the complete destruction of organic waste. Oxidation of organics dissolved in supercritical water can be carried out in a homogeneous phase due to the complete miscibility of all involved species (O_2, N_2, CO_2 and organics) with supercritical water. Due to these advantages it has also been proposed as a technology for replacing combustion in power generation [1, 2]. However, some challenges still have to be overcome for the successful and profitable commercialization of this technology: corrosion, salt deposition and high energetic demand [3]. Corrosion and salt deposition problems can be avoided, and heat recovery can be optimized, by the use of appropriate materials and reactor designs. The application of reactors working with a hydrothermal flame as a heat source addresses many of the challenges present in supercritical water oxidation technology. Hydrothermal flames are flames produced in aqueous environments at conditions above the critical point of water [4]. Injection of the reagents over a hydrothermal flame can avoid preheating problems, such plugging and corrosion, since the feed can be injected at lower temperatures (even room temperature). Also the kinetics are much faster allowing complete destruction of the pollutants in residence times lower than 1 s [4, 5]. Furthermore, the high temperatures associated to the hydrothermal flames contribute to a better energy recovery of the reaction heat for shaft work production. Due to safety and material limitations the flame has to be properly insulated or kept at a distance from the pressure vessel wall. The configuration of the reactor and fluid injection nozzle has to be specially projected for this purpose.

Several research groups have developed reactors working with a hydrothermal flame as a heat source [5, 6], since the formation of hydrothermal flames was proved by Franck and coworkers [7]. The High Pressure Process Group (HPPG) of the University of Valladolid (UVa) (Spain) showed the formation of hydrothermal flames in tubular and vessel reactors [8, 9]. Vessel reactors have demonstrated more success than tubular ones at maintaining steady stable hydrothermal flames with injection temperatures near to room temperature [5, 6, 9]. Vessel reactors provide low flow velocities, that are compatible with slow flame speed at hydrothermal conditions [10].

To enhance the development of SCWO processes for industrial-scale applications, it is necessary to understand the reactor performance and develop reliable simulation models. Bermejo et al. [11] classify these models into three main categories. The simplest kind of models assumes some level of

conversion (without kinetic modeling) and solves mass and energy balances [12, 13]. This kind of model is useful for analysis of energy efficiency in SCWO, and it just needs accurate values of enthalpies and heat capacities. Increasing complexity, models that include simple flow patterns (plug flow or perfect mixing) can give more information about the behavior of particular reactors [14–18]. Models like those need a kinetic model for the reaction and also good predictions of densities. Due their simplicity they can easily solve non-stationary reactors and can be used in control systems that demands fast responses [18, 19]. To overcome the problems of corrosion and salt deposition several reactors with complex designs have been developed. These reactors can present flow patterns quite different from plug flow or perfectly mixed. Models for these new reactors are also more complicated and usually use CFD tools [6, 20–23]. Thus, this family of models solves conservation equations, the applicable constitutive equations, and dynamically calculates transport properties at different conditions as needed. CFD models can describe temperatures and conversions, show recirculation areas, and predict how the salt deposition occurs.

In this work a CFD model has been used to analyze the behavior of vessel reactors working with an internal hydrothermal flame. The model was validated with the new cooled wall reactor design (CWR) developed in the University of Valladolid [9]. The geometry of the injector and operational parameters have been analyzed.

5.2 Experimental Data

The results of CFD model were validated using experimental data provided by the new cooled wall reactor working at the pilot plant of the University of Valladolid [9]. The cooled wall reactor consists of a vertical reaction chamber of 2.2 L (1 m length and 53 mm internal diameter), limited by a Ni-alloy wall contained in a stainless steel pressure shell with a volume of 4.3 L. Cold water flows in the annular space between the reaction chamber and the pressure shell in order to keep the pressure vessel at temperatures lower than 400°C. Feed and air are introduced into the reactor through its lower part, and flow through an injector up to the upper part of the reaction chamber, where the reaction takes place. The stream flows down and decontaminated water leaves the reactor through its lower part. In order to follow the reaction, the temperature is measured at several points of the reaction chamber. A scheme of the reactor including the position of the temperature measurements used for validation is shown in Figure 5.1. The position of the thermocouples shown in Figure 5.1 was slightly different when injectors with

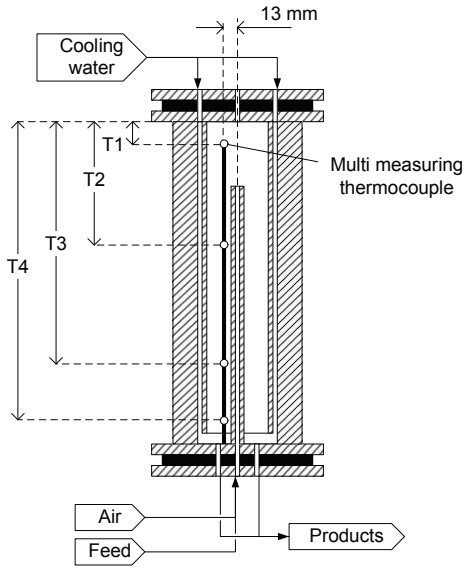

Figure 5.1: Scheme of CWR showing position of thermocouples. Details in Table 5.1.

different configurations were tested. Table 5.1 summarizes the characteristics of the injectors and the position of thermocouples. For each configuration a series of experiments at different flows and temperatures was performed, in order to obtain a set of measurements. All the injectors are Ni-alloy empty tubes. The experiments were performed using isopropyl-alcohol (IPA) as contaminant-model, and air as oxidant. Details concerning operation procedure and measurements can be found in the work of Bermejo et al. [9].

Table 5.1: Dimensions of injectors and positions of temperature measurements. Distances of measuring points are related to the top of reactor, as shown in Figure 5.1.

	Inj. 1	Inj. 2	Inj. 3
Length (mm)	950	950	500
Diameter (mm)	3.86	2.16	3.86
T1 (mm)	20	30	120
T2 (mm)	120	120	430
T3 (mm)	520	520	520
T4 (mm)	945	945	945

5.3 Modeling

Governing equations

The flow of supercritical fluids can be described by fundamental conservation equations for mass, momentum, energy and species. The turbulent flow is calculated using the Reynolds-averaged transport equations [24] as shown in equations (5.1) to (5.4):

$$\frac{\partial \rho}{\partial t} + \frac{\partial}{\partial x_i}(\rho u_i) = 0 \tag{5.1}$$

$$\frac{\partial}{\partial t}(\rho u_i) + \frac{\partial}{\partial x_j}(\rho u_i u_j) = -\frac{\partial p}{\partial x_i} + \frac{\partial}{\partial x_j}(\tau_{ij} - \rho\overline{u_i' u_j'}) \tag{5.2}$$

$$\frac{\partial}{\partial t}(\rho E) + \frac{\partial}{\partial x_i}\left[u_i(\rho E + p)\right] = \frac{\partial}{\partial x_j}\left[(\lambda + \lambda_t)\frac{\partial T}{\partial x_j}\right] + S_h \tag{5.3}$$

$$\frac{\partial}{\partial t}(\rho w_k) + \frac{\partial}{\partial x_i}(\rho u_i w_k) = -\frac{\partial}{\partial x_i}\left[\rho\left(D + D_t\right)\frac{\partial w_k}{\partial x_i}\right] + R_k \tag{5.4}$$

Where u_i is the averaged fluid velocity in the x_i direction, p the pressure, E is the total energy $(h - p/\rho + u^2/2)$ and w_k the mass fraction of species k. The source terms S_h and R_k represent the heat of reaction and the net rate of species k production by chemical reaction, respectively. The viscous stress tensor τ_{ij} is shown in equation (5.5):

$$\tau_{ij} = \mu\left(\frac{\partial u_i}{\partial x_j} + \frac{\partial u_j}{\partial x_i} - \frac{2}{3}\delta_{ij}\frac{\partial u_l}{\partial x_l}\right) \tag{5.5}$$

The Reynolds stress tensor $-\rho\overline{u_i' u_j'}$ is modeled assuming the Boussinesq approach. The turbulent thermal conductivity $\left(\lambda_t = \frac{c_p \mu_t}{Pr_t}\right)$ and the turbulent diffusion coefficient $\left(D_t = \frac{\mu_t}{\rho S c_t}\right)$ are defined according to the Spalart-Allmaras turbulence model. This model solves one equation for the kinematic turbulent viscosity, being faster than traditional two-equation models. This model was initially developed for aerodynamic flows. However, it has been also used for compressible flow cases (e.g. Allmaras et al. [25], Zhao et al. [26]). Bardina et al. [27] compared the performance of this model against other two-equation models in 10 different cases, including compressible flows and complex geometries. The best overall model was judged to be the SST model, followed by the Spalart-Allmaras model. It is also flexible using wall functions when the mesh is not sufficiently fine or solving the boundary layer when it is possible. Furthermore, the near-wall gradients of the transported

turbulent variable in the model are much smaller than the gradients of the transported variables in the $k-\epsilon$ or $k-\omega$ models. This might make the model less sensitive to numerical instabilities when non-layered meshes are used near walls [24]. Sierra-Pallares et al. [28] compared the performance of different turbulence models reproducing experimental data of temperature and density for supercritical fluids, and found that this model, although it is not conceived to deal with confined jets, exhibits an acceptable accuracy.

Thermodynamic properties

The density of the supercritical mixture ρ is calculated by Peng-Robinson equation of state with Boston-Mathias alpha function, Van der Waals mixing rules, and volume translation (VTPR-EoS) [29]. The volume translation used in density calculations was fitted for each component that constitute the system (H_2O, O_2, N_2, CO_2 and IPA), at the operation pressure of 23 MPa. Details about the fitting can be found at Queiroz et al. [30]. The volume translation has no influence on enthalpy calculations, thus specific enthalpy h (and also c_p) is given by original Peng-Robinson equation of state (PR-EoS) [31].

Transport properties

The thermal conductivity λ is calculated by TRAPP method for high pressure fluids (Transport Properties Prediction, described by Poling et al. [32]), and the molecular viscosity of the mixture μ is calculated as a mass-fraction average of the viscosities of the pure components as function of temperature.

The turbulent diffusion D_t (described above, after equation 5.5) overwhelms laminar diffusion, and the specification of detailed laminar diffusion properties in turbulent flows is not necessary. Thus, the diffusion coefficient D is admitted constant and equals to $10^{-7}m^2/s$. In fact, the laminar diffusion coefficient estimated using the method of Mathur and Thodos [32] assumes values between 10^{-9} and $10^{-6}m^2/s$, while the turbulent one is around $10^{-4}m^2/s$.

Kinetic model

The oxidation of isopropyl-alcohol is modeled as a single-step reaction:

$$C_3H_8O + 4.5O_2 \rightarrow 3CO_2 + 4H_2O \tag{5.6}$$

It has been assumed that kinetics follow Arrhenius law. The parameters were fitted from tubular reactor data of our group [30]:

$$R_k = 9.308 \cdot 10^7 \cdot C_{IPA} \cdot C_{O_2} \cdot \exp\left(\frac{-89441}{RT}\right) \ (kmol \cdot m^{-3} \cdot s^{-1}) \qquad (5.7)$$

Other studies apply Eddy Dissipation models [22, 33] assuming that reaction's rate is controlled by mixing /turbulence. This assumption is not adopted in this work because low injection temperatures produce slow reaction rates, making the chemical time higher than mixing time (which means Damköhler number less than 1).

Numerical procedure

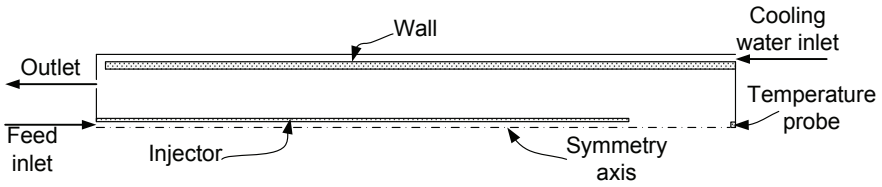

Figure 5.2: Scheme of geometry and boundaries of the model.

The main elements of the reactor have been included in the model geometry, including the metallic injector, the reaction chamber, and the space between the pressure shell and the chamber (Figure 5.2). A simplification, consisting of the assumption that the effluent leaves the reactor through an annular channel on its lower section, was considered. This assumption was essential to allow modeling the reactor as an axisymmetric 2D system instead of as a 3D system, which considerably reduces the complexity and computer-time requirements of the model. Nevertheless, the simplification has no further influence on results since the reaction zone is located in the region of flame formation, which means the injector outlet and the upper part of reactor. The model was solved for steady-state using the commercial CFD software ANSYS FLUENT 12.0, with segregated pressure based solver, SIMPLE algorithm for pressure-velocity coupling, and second order upwind discretization for the convective terms in energy, momentum, turbulent-viscosity and species equations. The boundary conditions for the fluid region are prescribed mass flow at inlets; prescribed pressure (gauge) at outlet; axial symmetry at the centerline; and no-slip condition with coupled thermal conditions at the walls. Heat transfer by conduction through both the metallic walls of the injector and of the reaction chamber has been considered in the energy equation. As initial condition, the temperature at the

entire domain was set to 427°C (700 K), and the mass fraction of water at the fluid region was set to 1.0.

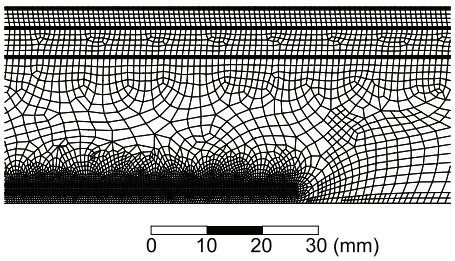

Figure 5.3: Detail of mesh showing the refinement at near-wall regions.

Unstructured meshes have been constructed with the meshing tool present in ANSYS 12, using quadrilateral dominant elements and inflation layers near the walls. Further refinements were performed for each case in order to achieve mesh-independent solutions, around 10^5 cells. The dimensionless wall distance y^+ is greater than 30 or lower than 1 in all the cases, allowing the application of Spalart-Allmaras turbulence model. A piece of mesh is shown in figure 5.3.

Residence time distribution

To predict the residence time distribution in the reactor, experiments with a virtual tracer substance were simulated. For this purpose, the concentration of tracer, with a diffusion coefficient equal to its turbulent diffusivity, was simulated using a scalar transport equation like equation (5.4), without source terms. The pulse input was modeled as a injection of tracer during 0.01 s at inlet. With the frozen flow approximation, only the tracer transport equation was solved over the fluid field previously calculated, and the RTD curve is obtained averaging the value of the tracer concentration at the outlet, following the theory developed by Danckwerts [34].

5.4 Results

Changing the injector configuration and the feed flow lead to a list of 12 model cases that show the behavior of the reactor (Table 5.2). The mass fraction of IPA presented in the table corresponds to the feed composition (preceding the injection of air). All the cases assume stoichiometric amount of oxidant.

Table 5.2: Cases simulated for parameter study of cooled wall reactor. All the cases assume stoichiometric amount of oxidant.

Feed (kg/h)	Injector	Inlet T ($°C$)	% IPA (mass)	Air (kg/h)	Case #
13	Inj. 1	150	8.8	11.7	S1
		300	4.6	6.2	S2
	Inj. 2	150	8.8	11.7	S3
		300	4.6	6.2	S4
	Inj. 3	150	10.5	14.1	S5
		300	9.5	12.7	S6
23	Inj. 1	150	8.8	20.7	S7
		300	4.6	11.0	S8
	Inj. 2	150	8.8	20.7	S9
		300	4.6	11.0	S10
	Inj. 3	150	10.5	24.9	S11
		300	9.5	22.5	S12

5.4.1 Model Validation

Figure 5.4 shows a comparison of experimental and predicted temperatures for two cases where the injector has different lengths. In the figure, dashed lines correspond to temperature inside the injector ($r = 0$) and arises slowly due to heat transfer through injector's wall. Continuous lines are the prediction for the temperature on the reaction chamber ($r = 13mm$), which is higher at injector outlet, where flame is formed. The triangles are experimental measurements of temperature. Figure 5.4a corresponds to case S1 and figure 5.4b to case S5. Both cases have the same inlet temperatures and the same flow rates, but case S5 has a shorter injector. Simulations are in accordance with experimental data, and the mean deviation on temperature prediction relative to experimental measurements are 14% and 9% respectively.

Simulations show a strong dependence between the maximum temperature reached at reaction chamber and the elimination of organic material. Figure 5.5 shows this relation for the set of cases compared and indicates poor elimination when the maximum reaction temperature is below 650°C. The same result was found experimentally [9]. Figure 5.5b shows some points with high elimination at low temperatures. These points probably correspond to experiments where the position of thermocouples do not fit the point of maximum temperature inside the reactor. Here, elimination is equivalent to IPA conversion.

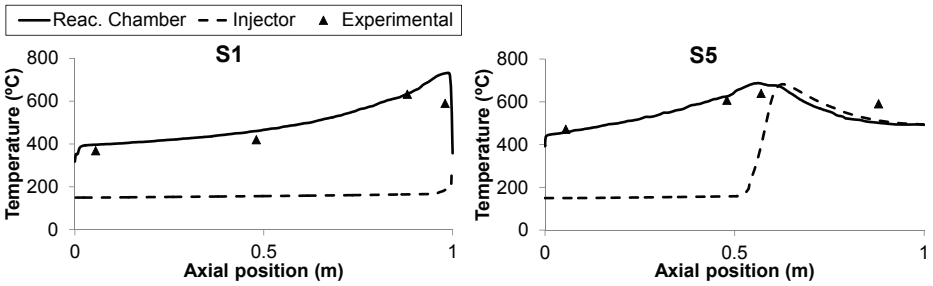

(a) (b)

Figure 5.4: Temperature profile inside the CWR: Experimental points and simulation profile predictions. (a)Case S1 - injector length = 0.95 m. (b)Case S5 - injector length = 0.50 m.

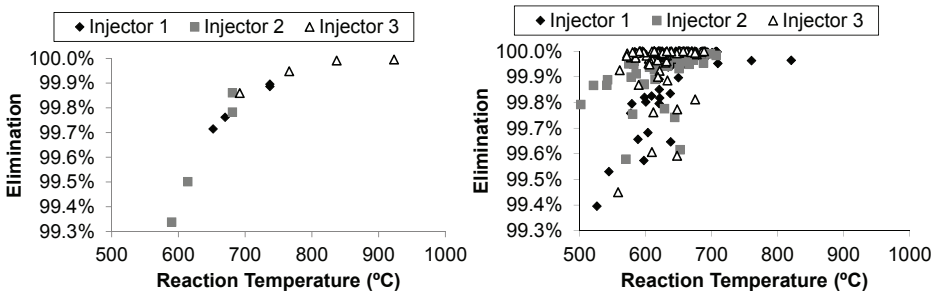

(a) (b)

Figure 5.5: Elimination efficiencies as function of maximum temperature inside reaction chamber. (a)Predicted by simulation. (b)Experimental data from Bermejo et al. [9].

The model also provides detailed information regarding the internal behavior of the reactor. Figure 5.6 presents the contours of reaction rate and mass fraction of IPA, at upper section of the reactor (first 230 mm). The shape of contours points to the existence of a flame at injector outlet. In figure 5.6a it is observed that most of the reaction takes place in a surface separating reagents from products. In figure 5.6b it can be observed that beyond the flame area, the concentration of fuel (IPA) decreases to zero. It should be noted that the maximum mass fraction of IPA which appears in this figure (4.6%) is related to feed plus air mass flow; while table 5.2 shows mass fractions related only to feed mass flow (8.8%). The flame is maintained

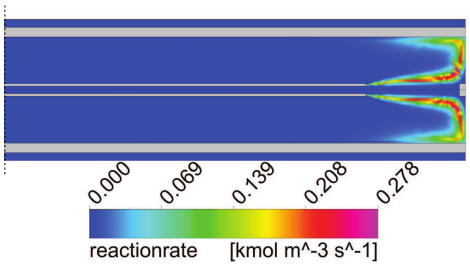

(a)

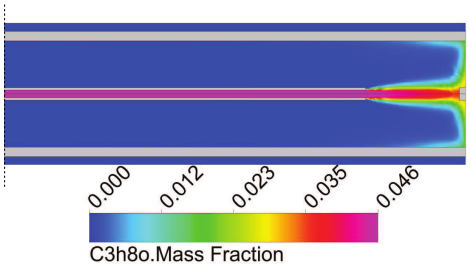

(b)

Figure 5.6: Simulation contours at top of reaction chamber for case S1: (a)Rate of reaction and (b)Mass fraction of IPA.

by the recirculation zone at upper part of reaction chamber that allows cold feed to be brought in contact with hot products. The recirculation zone is observable through the streamlines plotted over temperature contour (Figure 5.7a, first 230 mm are shown). At the lower section, the streamlines show the path of the cooled flow until the outlet (Figure 5.7b, last 230 mm are shown).

As general result, model indicates that the cooling water stream protects the pressure vessel from high temperatures, reducing problems of material safety. Also, the injection at low temperatures (150°C), far from the critical region, keeps the salts dissolved inside the injector, avoiding plugging and corrosion. Finally, the cooling water entering the reaction chamber at the

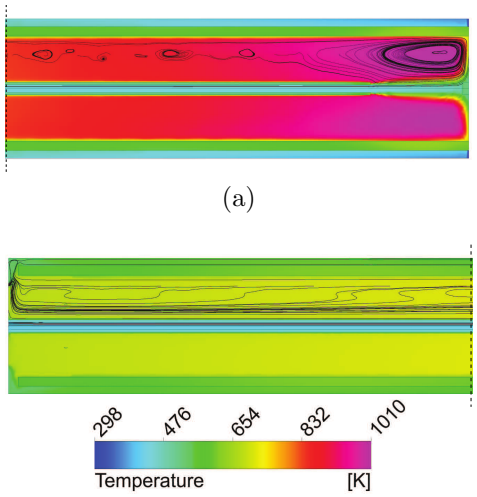

(a)

(b)

Figure 5.7: Simulation contours of temperature and streamlines for case S1: (a)Top of reaction chamber, (b)Bottom of reaction chamber.

bottom forms a pool at subcritical temperature capable of redissolving salts (if they are present) before leaving the reactor.

5.4.2 Influence of injector's diameter and feed flow

The effects of variations on diameter and flow rate can be studied together, through the Reynolds number inside the injector.

In first place the influence in the heat transfered is studied. Figure 5.8 shows the heat transfer coefficient through the injector's wall as function of Reynolds number, where black diamonds represent simulations with injector's diameter of 1/4", and grey squares correspond to cases with diameter of 1/8". The coefficient is calculated as the heat flux through the inner wall of the injector (given by the simulation) divided by the mean temperature difference between the wall and the flow core. The lines link cases with the same feed flow (13 or 23 kg/h). The general trend shown in figure 5.8 is that heat transfer coefficient increases with Reynolds number. Looking only to the effect of feed flow, the increment of Re has a small effect on heat transfer coefficient for injector 1 (compare S1 and S7, for example). Injector 2 is more sensitive to changes in feed flow.

In second place, the influence of the Reynolds number at the exit of the injector in the shape of the flame is studied. Figures 5.9 and 5.10 shows the rate of reaction for cases S6 and S12, which compare different flow rates. It indicates that, at higher mass flow, the flame starts later and is extended to the upper part of reactor. These two cases are compared because the

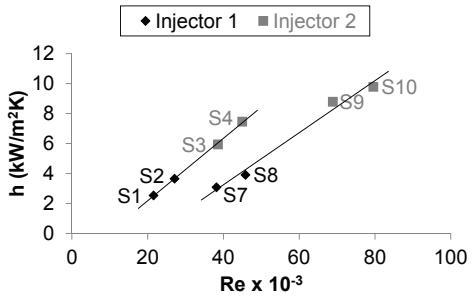

Figure 5.8: Heat transfer coefficient at internal wall of injector as function of Reynolds number. Black diamonds correspond to injector 1 (1/4"), grey squares correspond to injector 2 (1/8"), lines show the tendency for sets of same flow rate of feed.

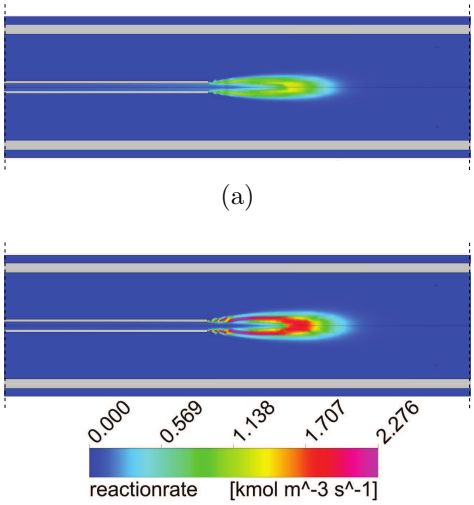

(a)

(b)

Figure 5.9: Simulation contours of rate of reaction: (a)Case S6 - Feed mass flow = 13 kg/h. (b)Case S12 - Feed mass flow = 23 kg/h.

displacement of the flame is more evident with the shorter injector, far from the reactor's ceiling. The use of very high mass flows could "lift" the flame and make it unstable, leading to the extinction of the reaction. This effect was not tested in experiments due to pumping limitations, and it also cannot be represented in steady-state simulations due to its transient nature.

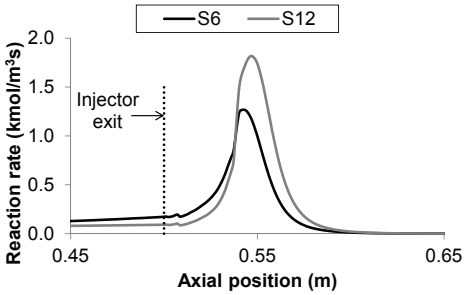

Figure 5.10: Profiles of reaction's rate calculated at axial line for cases S6 and S12. Central section of the reaction chamber.

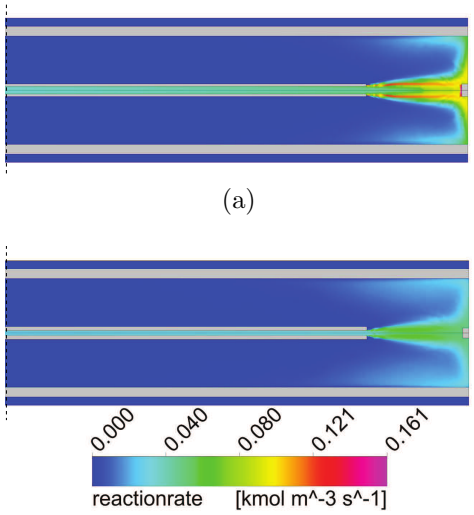

(a)

(b)

Figure 5.11: Simulation contours of rate of reaction: (a)Case S2 - Injector diameter = 1/4". (b)Case S4 - Injector diameter = 1/8".

The effects of reducing diameter over the reaction zone can be observed in figure 5.11, which shows the reaction rate for cases S2 and S4. Reducing the diameter of the injector causes more turbulence at outlet, which reduces the flame stability. The result is a dispersed reaction zone, which is more similar to a flameless oxidation regime. Reaction temperatures in cases with injector 1 are 60°C higher than cases with injector 2.

5.4.3 Influence of injector's length

Experimental measurements and simulations suggest that the flow of reagents "collides" against reactor's ceiling, which could be the cause for the back mixing phenomena when the injector is 0.95 m long. In order to evaluate the influence of distance between injector outlet and reactor's ceiling, the injector was reduced to 0.50 m. With that configuration, the flow has sufficient space for stabilizing with no influence of ceiling. Figures 5.4a and 5.4b show the temperature profiles inside the injector and at reaction chamber for cases S1 and S5 that have the same inlet temperature and flow but different injectors. The distance to walls and ceiling allows a smooth rising on temperature, and the cooling of products is not so efficient in S5 as in S1. The design of the reactor aims to provide a subcritical zone at the bottom to enhance salt recovery. Thus, case S1 is closer to our objective, showing high temperatures at upper part and low temperatures at bottom. Results show that even far from the reactor's ceiling, the flow regime generates a recirculation area at injector outlet, allowing the formation and stabilization of the flame, as shown in figures 5.12a and 5.12b, and the flame is not deformed. It should

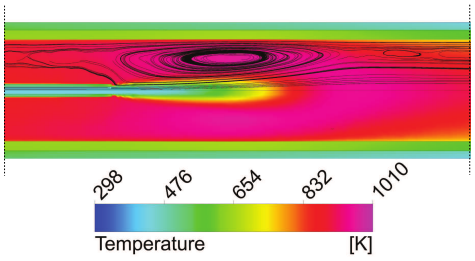

(a)

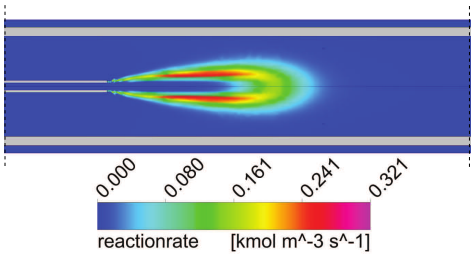

(b)

Figure 5.12: Simulation contours of CWR for case S5: (a)Temperature and streamlines, (b)Rate of reaction.

be observed that the configuration with a shorter injector needs higher fuel concentration to reach the reaction temperature. The same behavior was found by experiments [9] and it can be explained by the smaller surface of injector 3 for heat transfer from reaction chamber.

5.4.4 Influence of inlet temperature

Changes at inlet temperature are associated with changes in IPA concentration, in order to reach the same reaction temperature. Increasing inlet temperature makes the reaction start inside the injector as shown in figure 5.13. The initial consumption of IPA inside the injector reduces its concentration at the reaction chamber and the rate of reaction is lower. High inlet temperatures accelerate the beginning of the reaction, but may be not necessary if the reactor hydrodynamics can stabilize the flame (as is the case in our reactor).

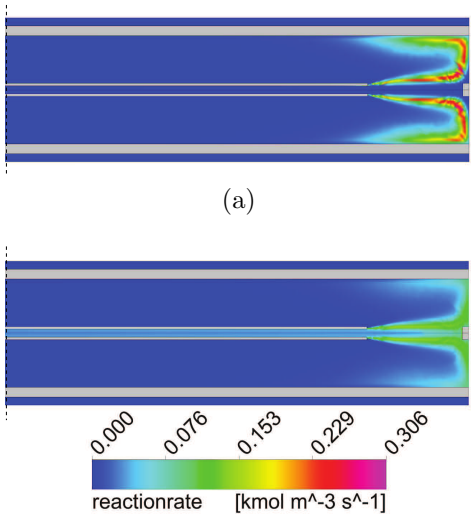

(a)

(b)

Figure 5.13: Simulation contours of rate of reaction: (a)Case S7 - Inlet temperature = 150°C. (b)Case S8 - Inlet temperature = 300°C.

5.4.5 Study of residence time

The complexity of the reactor, together with the influence of the natural convection induced by the sharp temperature changes, indicates that the flow field inside the reactor is not simple. A residence time distribution analysis of the reactor, in order to determine the flow patterns as well as deviations of ideal behavior, like dead areas would be very convenient. Nevertheless the harsh operational conditions make very difficult to perform this analysis experimentally. The CFD model used here allows us to perform this useful analysis in a simple way. In order to analyze the flow characteristics of the reactor a tracer injection was simulated to obtain the residence time distribution curves theoretically. The RTD results are shown in terms of

E(t) (the exit age distribution of flow) in figure 5.14. The curves are very similar for injectors 1 and 2, giving mean residence times (t_m) of 47s and 52s, respectively. However, the use of injector 3 gives a shorter t_m, 24s, and its RTD curve has a long tail which means a deviation from ideal behavior. The hold-back (χ) and the segregation (σ) are parameters that measure the

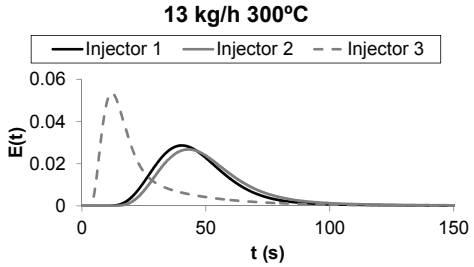

Figure 5.14: Residence time distribution curves for 13 kg/h of feed at 300°C. Injectors 1, 2 and 3 correspond to cases S2, S4 and S6, respectively.

deviation from ideal reactors, PFR and CSTR, respectively [34]. χ varies from 0 for PFR to 1 when most of the reactor is occupied by dead zones, and it is equal to $1/e$ for a CSTR. σ is 0 for a CSTR and equals $1/e$ for PFR. Figure 5.15 shows that, with long injectors, our reactor presents a PFR character with a small CSTR zone. For the short injector, however, the behavior of the reactor is most like a CSTR with small plug flow zones. The hypothesis of describing such kind of reactors as a combination of simple flow patterns was already proposed by Bermejo et al. [14]. Fauvel et al. [17] and Plugatyr and Svishchev [35] also used simple flow patterns to model SCWO reactors, although the design of both reactors is quite different from the cooled wall reactor used in this work.

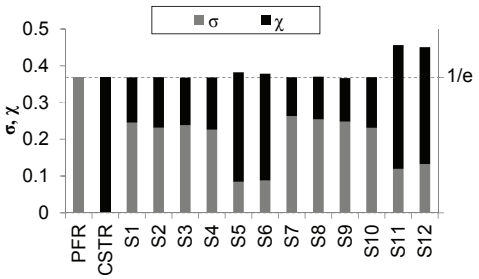

Figure 5.15: Deviation from ideal reactors. σ: segregation, χ: hold-back.

Robinson and Tester [36] defined the degree of stagnancy based on the cumulative internal RTD, as presented in equation (5.8), where c defines a

cutoff residence time.

$$S\left(ct_m\right) = 1 - \frac{1}{t_m}\int_0^{ct_m} tE(t)dt \tag{5.8}$$

Physically, $S(2t_m)$ represents the fraction of the internal contents which will remain in the system for a time greater than twice the mean value. Figure 5.16 shows that the degree of stagnancy is increased with the short injector, and there is no apparent dependence of flow rate nor inlet temperature. These results, together with the observation of streamlines in figures 5.7a

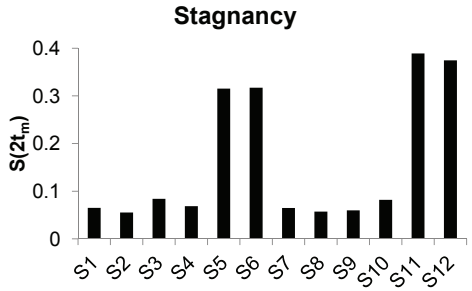

Figure 5.16: Degree of stagnancy.

and 5.12a, show that the stagnancy is caused by a dead volume at the upper part of the reactor. Thus, when designing this kind of reactor, one should try to keep the flame far from the walls and the ceiling (protecting the material and not deforming the flame) but also avoiding the formation of dead zones (caused by an injector too short).

5.5 Conclusions

A CFD model for supercritical water oxidation reactors was developed and it was validated with the cooled wall reactor constructed by University of Valladolid. The model correctly predicts experimental temperature profiles and was applied to study the influence of operational and geometrical factors in the hydrodynamics of hydrothermal flame formation.

According to the model, the use of long injectors produces higher temperatures than the shorter one, but the hydrothermal flame is slightly deformed due the proximity to the reactor's ceiling. When using shorter injectors, on the other hand, the flame is not deformed, and the reactor temperature is reduced at upper part, reducing the stress for the construction material. A drawback of short injector is the reduction of cooling effect necessary for salt recovery.

Injector's diameter and feed flow have influence on fluid velocity, but reducing the diameter can increase the turbulence at injector's outlet and makes the flame unstable. When injection velocity was increased the flame front was slightly pushed by the flow. In the cases presented here, that effect was more dependent on feed flow than injector's diameter. High inlet temperatures accelerate the beginning of the reaction, but may be not necessary if the reactor hydrodynamics can stabilize the flame.

The use of a CFD model allows to perform a RTD analysis of this complex system that would be difficult to perform experimentally. The RTD study shows a stagnant area in the top of the reactor, when short injectors are used. When designing this kind of reactors a compromise in the length of the injector must be adopted between avoiding the wall's stress due to the high temperature of the flames and reducing the dead volume of the reactor. The reactor behavior can be described as a combination of simple flow patterns.

Based on the results, the model showed to be useful for the design of new reactors and optimization of operating conditions.

Acknowledgments

The authors thank to Spanish Ministry of Science and Innovation for the CTQ2011-23293 Project (subprogram PPQ) and Project ENE2012-33613. J.P.S. Queiroz thanks the Spanish Education Ministry for the FPU Grant (FPU AP2009-0399).

Bibliography

[1] M. D. Bermejo, M. J. Cocero, F. Fernandez-Polanco, A process for generating power from the oxidation of coal in supercritical water, Fuel 83 (2004) 195–204.

[2] F. Donatini, G. Gigliucci, J. Riccardi, M. Schiavetti, R. Gabbrielli, S. Briola, Supercritical water oxidation of coal in power plants with low CO2 emissions, Energy 34 (2009) 2144–2150.

[3] G. Brunner, Near and supercritical water. part II: oxidative processes, Journal of Supercritical Fluids 47 (2009) 382–390.

[4] C. Augustine, J. Tester, Hydrothermal flames: From phenomenological experimental demonstrations to quantitative understanding, Journal of Supercritical Fluids 47 (2009) 415–430.

Nomenclature

D	diffusion coefficient $(m^2\,s^{-1})$
$E(t)$	exit age distribution
R	universal gas constant $(J\,mol^{-1}K^{-1})$
R_k	species source therm $(kmol\,m^{-3}s^{-1})$
$S(ct_m)$	degree of stagnancy
S_h	energy source therm $(J\,m^{-3}s^{-1})$
T	temperature (K)
h	specific enthalpy $(J\,kg^{-1})$
t	time (s)
u	velocity $(m\,s^{-1})$
w	mass fraction
y^+	dimensionless wall distance
Greek symbols	
λ	thermal conductivity $(W\,m^{-1}K^{-1})$
μ	viscosity (Pa, s)
ρ	density $(kg\,m^{-3})$
σ	segregation
τ	stress tensor $(N\,m^{-2})$
χ	hold-back
Subscripts	
i, j, l	directions
k	species
t	turbulent
Abbreviations	
CFD	computational fluid dynamics
CWR	cooled wall reactor
IPA	isopropyl-alcohol
PR	Peng-Robinson equation of state
SCWO	supercritical water oxidation
VTPR	volume translated Peng-Robinson equation of state

[5] B. Wellig, M. Weber, K. Lieball, K. Prikopsky, P. von Rohr, Hydrothermal methanol diffusion flame as internal heat source in a SCWO reactor, Journal of Supercritical Fluids 49 (2009) 59–70.

[6] C. Oh, R. Kochan, T. Charlton, A. Bourhis, Thermal-hydraulic modeling of supercritical water oxidation of ethanol, Energy & Fuels 10 (1996) 326–332.

[7] W. Schilling, E. Franck, Combustion and diffusion flames at high-pressures to 2000 bar, Berichte Der Bunsen-Gesellschaft-Physical Chemistry Chemical Physics 92 (1988) 631–636.

[8] M. D. Bermejo, P. Cabeza, M. Bahr, R. Fernandez, V. Rios, C. Jimenez, M. J. Cocero, Experimental study of hydrothermal flames initiation using different static mixer configurations, Journal of Supercritical Fluids 50 (2009) 240–249.

[9] M. D. Bermejo, C. Jimenez, P. Cabeza, A. Matias-Gago, M. J. Cocero, Experimental study of hydrothermal flames formation using a tubular injector in a refrigerated reaction chamber. influence of the operational and geometrical parameters, Journal of Supercritical Fluids 59 (2011) 140–148.

[10] M. D. Bermejo, P. Cabeza, J. P. S. Queiroz, C. Jimenez, M. J. Cocero, Analysis of the scale up of a transpiring wall reactor with a hydrothermal flame as a heat source for the supercritical water oxidation, Journal of Supercritical Fluids 56 (2011) 21–32.

[11] M. D. Bermejo, D. Rincón, V. Vazquez, M. J. Cocero, Supercritical water oxidation: Fundamentals and reactor modeling, Chemical Industry and Chemical Engineering Quarterly 13 (2007) 79–87.

[12] M. J. Cocero, E. Alonso, M. T. Sanz, F. Fdz-Polanco, Supercritical water oxidation process under energetically self-sufficient operation, The Journal of Supercritical Fluids 24 (2002) 37–46.

[13] E. D. Lavric, H. Weyten, J. De Ruyck, V. Pleşu, V. Lavric, Supercritical water oxidation improvements through chemical reactors energy integration, Applied Thermal Engineering 26 (2006) 1385–1392.

[14] M. D. Bermejo, F. Fernandez-Polanco, M. J. Cocero, Modeling of a transpiring wall reactor for the supercritical water oxidation using simple flow patterns: Comparison to experimental results, Industrial & Engineering Chemistry Research 44 (2005) 3835–3845.

[15] P. Chen, L. Li, E. Gloyna, Simulation of a concentric tube reactor for supercritical water oxidation, in: Innovations in supercritical fluids, number 608 in ACS Symposium Series, Americal Chemical Society, Washington, DC, 1995, pp. 348–363.

[16] A. Ermakova, V. I. Anikeev, Modeling of the oxidation of organic compounds in supercritical water, Theoretical Foundations of Chemical Engineering 38 (2004) 333–340.

[17] E. Fauvel, C. Joussot-Dubien, E. Pomier, P. Guichardon, G. Charbit, F. Charbit, S. Sarrade, Modeling of a porous reactor for supercritical

water oxidation by a residence time distribution study, Industrial & Engineering Chemistry Research 42 (2003) 2122–2130.

[18] K. R. Muske, J. D. Littell, P. C. Dell'Orco, L. A. Le, R. L. Flesner, Hydrothermal treatment of C-N-O-H wastes: Model-based reactor effluent control, Industrial & Engineering Chemistry Research 40 (2001) 1397–1405.

[19] P. Dutournié, J. Mercadier, Unsteady behaviour of hydrothermal oxidation reactors: theoretical and numerical studies near the critical point, The Journal of Supercritical Fluids 35 (2005) 247–253.

[20] M. D. Bermejo, A. Martin, J. P. S. Queiroz, I. Bielsa, V. Rios, M. J. Cocero, Computational fluid dynamics simulation of a transpiring wall reactor for supercritical water oxidation, Chemical Engineering Journal 158 (2010) 431–440.

[21] K. S. Lieball, Numerical Investigations on a Transpiring Wall Reactor for Supercritical Water Oxidation, Doctor of technical sciences, Swiss Federal Institute of Technology Zurich, Zurich, 2003.

[22] S. Moussière, A. Roubaud, O. Boutin, P. Guichardon, B. Fournel, C. Joussot-Dubien, 2D and 3D CFD modelling of a reactive turbulent flow in a double shell supercritical water oxidation reactor, The Journal of Supercritical Fluids 65 (2012) 25–31.

[23] N. Zhou, A. Krishnan, F. Vogel, W. A. Peters, A computational model for supercritical water oxidation of organic toxic wastes, Advances in Environmental Research 4 (2000) 75–90.

[24] ANSYS, ANSYS FLUENT theory guide release 12, 2009.

[25] S. R. Allmaras, F. T. Johnson, P. R. Spalart, Modifications and clarifications for the implementation of the spalart-allmaras turbulence model, Big Island, Hawaii. Seventh International Conference on Computational Fluid Dynamics.

[26] L. Zhao, Y. Liu, J. Yang, Y. Zhao, J. Zheng, H. Bie, X. Liu, Numerical simulation of temperature rise within hydrogen vehicle cylinder during refueling, International Journal of Hydrogen Energy 35 (2010) 8092–8100.

[27] J. Bardina, P. Huang, T. Coakley, Turbulence modeling validation, NASA Tech. Memo. 110446, American Institute of Aeronautics and Astronautics, 1997.

[28] J. Sierra-Pallares, M. Parra-Santos, J. Garcia-Serna, F. Castro, M. Cocero, Numerical analysis of high-pressure fluid jets: Application to RTD prediction in supercritical reactors, Journal of Supercritical Fluids 49 (2009) 249–255.

[29] A. Peneloux, E. Rauzy, R. Freze, A consistent correction for redlich-kwong-soave volumes, Fluid Phase Equilibria 8 (1982) 7–23.

[30] J. Queiroz, M. Bermejo, M. Cocero, Kinetic model for isopropanol oxidation in supercritical water in hydrothermal flame regime and analysis, The Journal of Supercritical Fluids 76 (2013) 41–47.

[31] D.-Y. Peng, D. B. Robinson, A new two-constant equation of state, Industrial & Engineering Chemistry Fundamentals 15 (1976) 59–64.

[32] B. E. Poling, J. M. Prausnitz, J. P. O'Connell, The Properties of Gases and Liquids, McGraw-Hill, New York, 5 th edition, 2007.

[33] J. Sierra-Pallares, M. Parra-Santos, J. Garcia-Serna, F. Castro, M. Cocero, Numerical modelling of hydrothermal flames. micromixing effects over turbulent reaction rates, Journal of Supercritical Fluids 50 (2009) 146–154.

[34] P. Danckwerts, Continuous flow systems: Distribution of residence times, Chemical Engineering Science 2 (1953) 1–13.

[35] A. Plugatyr, I. M. Svishchev, Residence time distribution measurements and flow modeling in a supercritical water oxidation reactor: Application of transfer function concept, The Journal of Supercritical Fluids 44 (2008) 31–39.

[36] B. A. Robinson, J. W. Tester, Characterization of flow maldistribution using inlet-outlet tracer techniques: An application of internal residence time distributions, Chemical Engineering Science 41 (1986) 469–484.

Chapter 6

SCWO for energy production by hydrothermal flame as internal heat source. Experimental results and energetic study

Abstract

This work presents experimental and model results obtained with a new configuration of a cooled wall reactor working with two outlets: an upper outlet through which a hot effluent (500 - 600°C) free of salts is obtained and lower outlet through which an effluent at subcritical temperature dissolving the precipitated salts is obtained. Different flow distributions were tested in order to find the optimal conditions. TOC removal over 99.99% was obtained at injection temperatures as low as room temperature, when the fraction of products leaving the reactor in the upper effluent is lower than 70% of the feed flow. The performance of the reactor was tested with the oxidation of a recalcitrant compound such as ammonia, using isopropyl alcohol as co-fuel. Removals higher than 99% of N-NH_4^+ were achieved in both effluents, working with temperatures near 700°C. Slightly better eliminations were obtained in the bottom effluent because its residence time in the reactor is longer. The behaviour of the reactor working with feeds with a high concentration of salts was also tested. Feeds containing up to 2.5% wt Na_2SO_4 could be injected in the reactor without plugging problems and a TOC removal of 99.7% was achieved in these conditions. Upper effluent always presented a

concentration of salt lower than 100 ppm. Finally, a theoretical analysis of the energy recovery of the reactor working with two outlets was made.

6.1 Introduction

Since Franck and coworkers discovered hydrothermal flames [1] and it could be applied to the Supercritical Water Oxidation (SCWO), new challenges came up to the study of SCWO. For flammable compounds such as methane or methanol, hydrothermal flame can occur at temperatures as low as 400°C [2]. SCWO in the presence of hydrothermal flames can reduce residence times to the order of milliseconds [3] without the production of sub-products typical of conventional combustion such as NOx [4] or dioxins [5].

SCWO with a hydrothermal flame has a number of advantages over the flameless process. Some of these advantages permit overcoming the traditional challenges that make the successful and profitable commercialization of SCWO technology difficult. The advantages include the following [3]:

- The reduced residence times (in the order of milliseconds) allows the construction of smaller reactors.
- It is possible to carry out the reaction with feed injection temperatures near to room temperature when using vessel reactors [6, 7]. This avoids problems such as plugging and corrosion in a preheating system, having an advantage from the operational and energy integration perspective.
- Higher operation temperatures improve the energy recovery.

The first reactor probably working with a hydrothermal flame inside was the MODAR reactor, working in conditions of concentration, temperature and pressure above the ignition conditions of methanol and being able to work with injection temperatures of 25°C and injecting the air at 220°C [7]. In the ETH of Zurich, the direct injection of the waste into a diffusion hydrothermal flame generated inside the reactor was developed as a solution to avoid the external preheating of the waste up to supercritical conditions [8, 9]. Príkopský and coworkers investigated the feasibility of injecting feeds with a 3%wt of sodium sulfate (Na_2SO_4) in the transpiring wall reactor with a diffusion hydrothermal flame as internal heat source [10]. No plugging was observed during the experiments, but salt deposits were detected in the upper hot zone of the reactor. In a previous investigation of our research group [6], it was found that using a transpiring wall reactor, a premixed hydrothermal flame inside the reaction chamber could be maintained when injecting the feed at a temperature as low as 110°C. Using a similar reactor, feeds with up to 4.74% wt Na_2SO_4 could be injected [11]. The reactor worked without plugging, but the recovery of salts was only between 5% and 50%. Both research groups reported an increase in the temperature when salt was injected in the reactor [10, 11].

It has been proved that injection of cold feeds over a hydrothermal flame is only possible when working with vessel reactors [9–11] and it is not possible when working with tubular reactors [12]. This behavior was due to the low flame front velocities in hydrothermal flames that is lower than 0.1 m/s, in comparison to the higher flame front velocities at atmospheric conditions (0.4-3 m/s). This is the reason why flow velocities lower than 0.1 m/s are necessary to keep a stable hydrothermal flame where cold reagents can be injected [13]. Recently our group has succeeded in keeping working continuously a vessel reactor injecting feeds at temperatures as low as 25°C [14].

Even though the most immediate application of hydrothermal flames is in the SCWO process for waste destruction, which is the most industrially developed hydrothermal process, it is possible to move from the idea of hydrothermal flame as a technology for the destruction of wastes to consider it as a technology for the generation of clean energy, which could eventually substitute the actual technologies based on atmospheric combustion. The efficiency in energy production by SCWO of coal and direct expansion of the effluent was compared to the efficiencies of other conventional power plants by Bermejo et al. [15]. If the steam was produced at 650°C and 30 MPa, efficiencies as high as 38% were obtained by SCWO. Efficiency was as high as 41% if the effluent was reheated and expanded a second time. The efficiencies at the same steam conditions for pulverized coal power plant and pressurized fluidized bed power plant were 32 and 34% respectively. Comparison is more favourable using oxygen enriched or even using pure oxygen as the oxidant. In this last option the cost of the oxidant must be assumed. Nevertheless it is known that the use of oxygen as an oxidant is investigated to improve the efficiency of combustion in power plants.

In his proposal for a sustainable society with a decentralized production based on renewable resources, Arai et al. [16] proposed the supercritical oxidation of biomass wastes and other sustainable fuels with a hydrothermal flame as a clean energy source. Augustine and Tester [3] also propose its utilization with low grade fuels. In general, this technology can be applied to the valorization of waste such as waste water treatment plant sludge, biomass or plastic wastes and in general any kind of waste with high energetic content. To form these flames it is necessary to use aqueous mixtures with a heat content of at least 1250 kJ/L. One important challenge about working with hydrothermal flames is improving energy recovery in SCWO system [15]. Hydrothermal flames allow new reactor designs that not only are able to inject feeds without preheating because of the possibility of injecting reactants at room temperature but also use the heat released by the flame for other purposes as the energetic integration of the process or for production

of electricity by turbines [17]. The high temperature effluent can also be used as heat source in other hydrothermal processes, such as liquefaction or gasification, where the heat recovery is a critical issue [18, 19]. In the case of waste with high concentration of inorganic substances, new reactor designs able to separate these salts from the effluent must be developed in order to make it possible to directly expand the effluent in an electricity production turbine.

The main goal of this work is the study of the behavior of new cooled wall reactor with the main particularity of having two outlets in order to try to keep the maximum heat released by the flame in a clean and high temperature flow leaving the reactor from the upper zone and other flow at subcritical conditions with the salts dissolved going out for the bottom of the reactor. In this way the optimum upper/lower effluent relation was optimized taking into account the temperature profiles inside the reactor and the organic matter elimination in both streams. The performance of the reactor with recalcitrant pollutants such as ammonia was tested as well as the performance of the reactor with feeds containing salts. A CFD model is also used to describe the behaviour of the reactor. Finally, a theoretical energetic study of the process with the new reactor was performed.

6.2 Experimental

6.2.1 Experimental setup

All the experiments analyzed in this research have been carried out in the SCWO facility installed in the University of Valladolid. It consists of a continuous facility working with a feed flow of 22.5 L/h, and air supplied by a four stage compressor, with a maximum feed rate of 36 kg/h is used as the oxidant. The reactor consist of a pressure vessel made of AISI 316 stainless steel able to stand a maximum pressure of 30 MPa and a maximum wall temperature of 400°C, containing a reaction chamber made of Ni-alloy 625 where the temperature be as high as 700°C. Waste water feed and air are previously pressurized and preheated with electrical resistances to the desired temperature before being injected by the bottom of the reactor. The reagents are conducted to the top of the reactor chamber by means of a tubular injector. At the outlet of the injector the hydrothermal flame is formed. Cooling water, previously pressurized is circulating between the pressure vessel and the reaction chamber introduced by the top of the reactor in order to cool down the vessel at a temperature lower than 400°C. This cooling water is entering in the reaction chamber through its lower part and

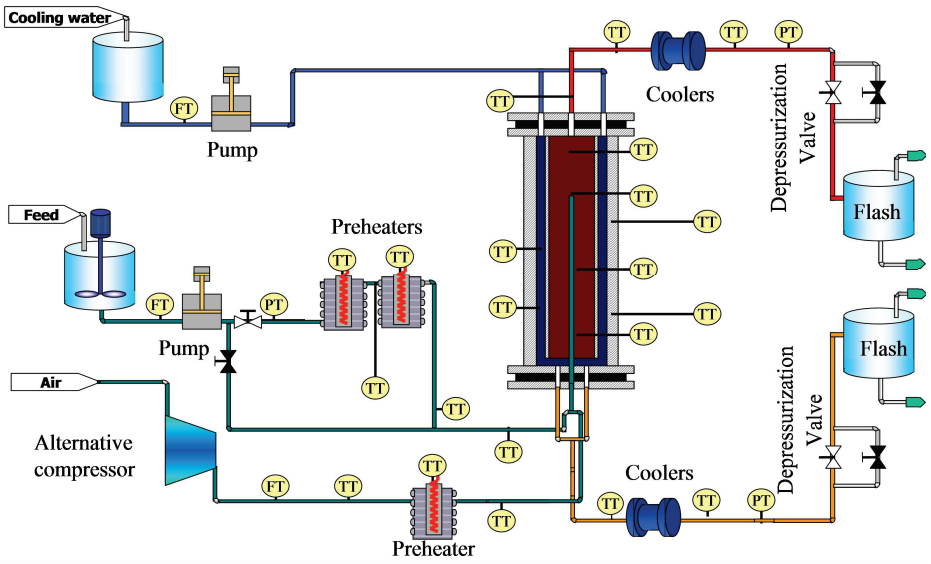

Figure 6.1: Diagram of SCWO facility with two outlets.

leaving the reactor by the bottom together with a fraction of the products. The rest of the products leave the reactor by another outlet situated in the top of the reactor chamber. After leaving the reactor, both effluents are cooled down in the intercoolers and depressurized. The flow diagram of the facility with two outlets is shown in Figure 6.1. More information about the facility can be found elsewhere [6, 12]. Figure 6.2 shows a scheme of the reactor with the different position of thermocouples inside the reaction chamber. The different temperature profiles are referred at the position of these four thermocouples. Each effluent (top and bottom flow) is measured with a rotameter in order to know the distribution of the feed flow respect the two outlets.

6.2.2 Experimental procedure

Previous to the beginning of the experiment the reactor must be preheated electrically to 400°C. The reaction is initiated by injected air and waste water streams preheated electrically up to a temperature higher than 400°C. A few minutes after continuous injecting of IPA solution and air stream the hydrothermal flame is ignited. At that moment a sharp increase the temperatures at the top of the reactor (T1 and T2) is registered. Then, the electrical heating of the wall of the reactor is turned off and the cooling water flow is connected. For keeping the maximum temperature constant in values around 600-700°C till the desired injection temperature is reached, IPA

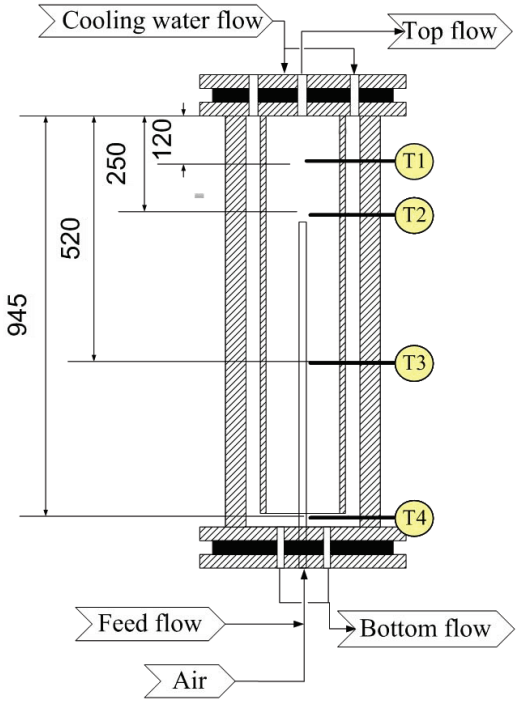

Figure 6.2: Scheme of the reactor with the positions of the temperature measurement inside the reaction chamber and the flow distribution.

concentration was increased as the injection temperature was decreased down to the selected injection temperature. After the target injection temperature is reached (from 300°C till room temperature, around 20-30°C), the upper flow and bottom flow are regulated opening or closing the decompression valves keeping the air and the pressure constant. Pressure must be stabilized around 23 MPa. Several stationary states with different prepared feeds and different flow up/bottom ratio are reached and samples of the liquid effluent are taken.

Total Organic Carbon (TOC) and Total Nitrogen (TN) analysis of the samples were performed with a TOC 5050 SHIMADZU Total Organic Carbon Analyzer which uses combustion and IR analysis. The detection limit is 1 ppm. Salt concentration is measured using a conductimeter Basic 30 provided by Crison. For doing this, conductivities of solutions of known Na_2SO_4 concentration are measured obtaining a linear calibration line between conductivity and Na_2SO_4 concentration. Nitrates and nitrites were characterized in the liquid effluent by ionic chromatography with an IC PAK A column of Waters. The detection limit is 1 ppm. NH_3 and NO_x at the gas effluent were analyzed with Dräger tubes detectors Lab Safety Supply CH29401 and CH31001. The NO_x detection limits for these tubes ranged from 0.5 to 100 ppm and the NH_3 detection limits ranged from 5 to 70 ppm (standard deviation for both tubes are between 10 and 15%).

6.2.3 Materials

The experiments analyzed in this research were performed using feeds prepared with isopropyl alcohol (IPA, 99% purity) supplied by COFARCAS (Spain) and tap water without further purification. For experiments made with ammonia it was used ammonia (25% in mass) supplied by COFARCAS (Spain). Synthetic waste containing salts were prepared using Na_2SO_4 supplied by COFARCAS (purity > 98%) (Spain).

6.3 Modeling

A CFD model was performed in order to study the internal behavior of the new reactor. The main elements of the reactor have been included in the model geometry, like the injector, the reaction chamber, and the space between the pressure shell and the chamber. The reactor is modeled as an axisymmetric 2D system. The turbulent flow dynamics is modeled by Reynolds-Averaged-Navier-Stokes equations, using the Realizable k-ϵ turbulence model with enhanced wall treatment [20]. The density of the super-

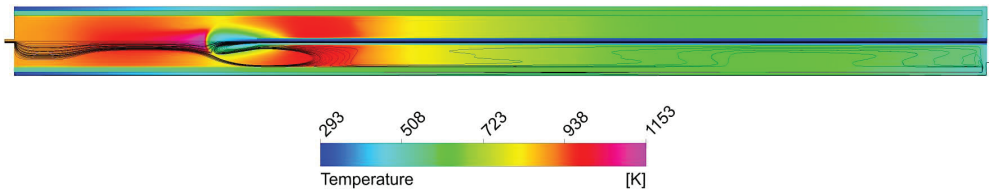

Figure 6.3: Model contours of temperature and pathlines.

critical mixture is calculated by Peng-Robinson equation of state with Van der Waals mixing rules, and volume translation (VTPR-EoS) [21]. The volume translation used in density calculations was fitted for each component that constitutes the system (H_2O, O_2, N_2, CO_2 and IPA), at the operation pressure of 23 MPa. The volume translation has not influence on enthalpy calculations, thus, specific enthalpy (and also cp) is given by original Peng-Robinson equation of state (PR-EoS) [22]. The thermal conductivity and the molecular viscosity of the mixture are calculated as a mass-fraction average of the properties of the pure components as function of temperature. The laminar diffusion coefficient is estimated using the method of Mathur and Thodos [23], although turbulent diffusion usually overwhelms laminar diffusion, and the specification of detailed laminar diffusion properties in turbulent flows is not necessary.

6.4 Results and discussion

As general result, the new reactor with two outlets successfully eliminates organic material and provides a clean stream with high energy content. The injection at low temperatures (20°C), far from the critical region, keeps the salts dissolved inside the injector, avoiding plugging and corrosion. Finally, the cooling water entering the reaction chamber at the bottom forms a pool at subcritical temperature capable of redissolving salts (if they are present) before leaving the reactor. Figure 6.3 shows the temperature field predicted by the CFD model and validated with experimental data in section 6.4.2. Pathlines are also shown.

6.4.1 Description of parameters

The performance of the reactor is studied by a set of parameters described in this section. The fraction of flow leaving the reactor by the top outlet is defined as the ratio of the upper effluent liquid flow, measured after decom-

pression, to the feed flow, as shown in eq. (6.1).

$$\text{Upper effluent fraction (\%)} = \frac{F_{\text{top,liq}}}{F_{\text{feed,liq}}} \cdot 100 \tag{6.1}$$

As the cooling water mixes the flow that comes out the reactor at the bottom outlet, the samples taken at the bottom flow must be corrected in order to know the real concentration of TOC and TN at the bottom effluent. The concentration of top effluent does not have to be corrected since this flow is not mixed with the cooling water flow:

$$TOC_{\text{bottom}} = TOC_{\text{bottom measured}} \frac{F_{\text{feed}} + F_{\text{cooling}} - F_{\text{top}}}{F_{\text{feed}} - F_{\text{top}}} \tag{6.2}$$

$$TN_{\text{bottom}} = TN_{\text{bottom measured}} \frac{F_{\text{feed}} + F_{\text{cooling}} - F_{\text{top}}}{F_{\text{feed}} - F_{\text{top}}} \tag{6.3}$$

Once the TOC and TN are corrected, it can be calculated the removal efficiency for each effluent:

$$TOC\_\text{removal}_{\text{top/bottom}} = \left(1 - \frac{TOC_{\text{top/bottom}}}{TOC_{\text{feed}}}\right) \cdot 100 \tag{6.4}$$

$$N - NH_4^+\_\text{removal}_{\text{top/bottom}} = \left(1 - \frac{N - NH_{4\ \text{top/bottom}}^+}{N - NH_{4\ \text{feed}}^+}\right) \cdot 100 \tag{6.5}$$

N-NH_4^+ concentration in the effluent is obtained from the difference of TN and the concentration of nitric Nitrogen (N-NO_3 and N-NO_2). The fraction of Na_2SO_4 recovered in the effluents is defined in eq. (6.6).

$$\text{Salt recovery top/bottom flow} = \frac{C_{Na_2SO_4,\text{top/bottom}} \cdot F_{\text{top/bottom}}}{C_{Na_2SO_4,\text{feed}} \cdot F_{\text{feed}}} \cdot 100 \tag{6.6}$$

Where $C_{Na_2SO_4,\text{top/bottom}}$ and $C_{Na_2SO_4,\text{feed}}$ are the concentration of Na_2SO_4 in % wt in the top/bottom effluent and in the feed respectively.

6.4.2 Influence of the upper effluent fraction.

Temperature profiles inside the reactor. With the new configuration of the reactor, the first point was the study of the influence of upper flow fraction (eq. (6.1)) in order to check how the new outlet affects the behavior of the hydrothermal flame. Experiments were made with injections at room temperature and at 200°C. In order to analyze the results, the experimental

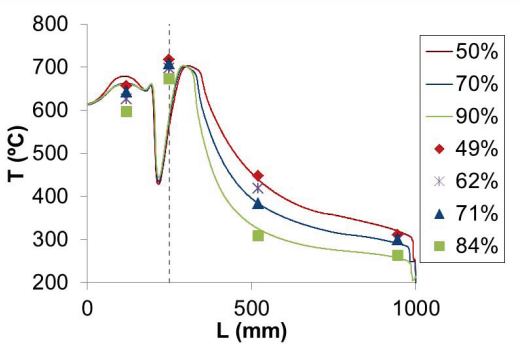

Figure 6.4: Temperature profiles for different upper effluent fractions at 20°C. Symbols stand for experimental data, while continuous lines come from CFD model. The vertical dashed line indicates the position of the outlet of the injector.

temperature profiles registered along the reactor for the different flow distributions were compared in figure 6.4, which shows experimental and model results for temperature at different lengths of the reactor. It can be observed that when the upper flow increases, all the temperatures inside the reactor decrease. This is because the top outlet is closer to the injector outlet and when a higher fraction is leaving the reactor by the top a low amount of products in flowing down the reactor. Thus, the heat content of this flow fraction is not transmitted to the reaction chamber and to the reagents entering through the injector.

TOC Removal. In the figure 6.5 the TOC concentration in both effluents was plotted as a function of the upper flow fraction. In figure 6.5a the feed inlet temperature is 20°C (room T) and in figure 6.5b the feed inlet temperature is 200°C. In both experiments TOC removals higher than 99.99% were obtained in both effluents when the fraction of effluent leaving the reactor by its upper part is below 70%. Thus, the optimum upper effluent fraction is around this value. This behavior could be explained because the increasing the upper flow fraction can elongate the flame and making that some bottom products do not react completely because they do not pass through the flame.

6.4.3 Influence of the IPA concentration

Temperature profiles inside the reactor. In order to analyze the influence of the IPA concentration in the temperatures profile along the reactor, experiments at injection temperature of 200°C and at 85% upper effluent fraction condition were carried out in order to try to improve the removal of TOC at

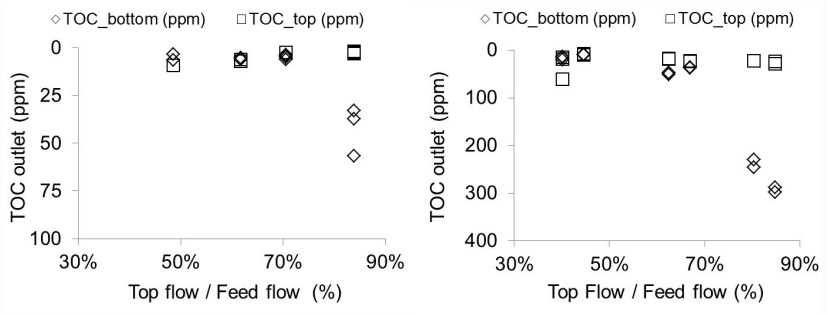

(a) (b)

Figure 6.5: Values of TOC in the top and bottom effluent as a function of the upper effluent fraction at injection temperature of (a) 20°C and 13.5% of IPA, (b) 200°C and 10.5% of IPA.

the bottom flow for the highest upper flow fractions. As it can be observed in the figure 6.6, higher IPA concentration generates higher temperatures in the top of the reactor. However, at the bottom of the reactor the temperatures are similar for both IPA concentrations when the upper effluent fraction remains constant. The values of TOC in both cases were lower than 10 ppm at the top flow and lower than 100 ppm at the bottom flow, but no improvements in the TOC bottom removal were observed.

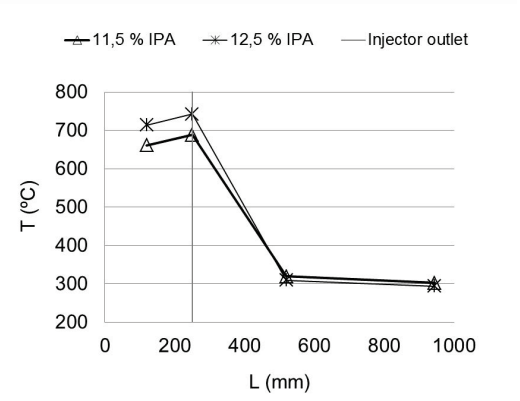

Figure 6.6: Temperature profile for different feed concentrations and with a relation of 85% of upper effluent fraction and an injection temperature of 200°C.

6.4.4 Influence of the cooling water

Temperature profiles inside the reactor. A study was performed trying to know the influence of the cooling water flow in the temperatures profiles along the reactor. The injection temperature of the experiment was 200°C and the ratio top flow/total flow was fixed at 48%. Three cooling water flows were studied: 5.2, 6.8 and 9.1 kg/h. (keeping the feed flow at 13.5 kg/h). The evolution of the temperature profiles along the reactor is shown in the figure 6.7a. The figure shows that temperatures along the whole reactor decrease when the cooling flow increases with a consequence reduction of the TOC removal in the bottom effluent as can be appreciated in figure 6.7b where the values of TOC concentration are plotted as a function of the cooling flow. It is observed that from cooling flows higher than 9.1 kg/h TOC concentration increases as much as 500 ppm in the bottom effluent. With these results it can be noticed that a flow of 5-6 kg/h of cooling water is enough to have good removals and keep the temperature at the bottom of the reactor below the supercritical temperature (374°C), and that if a lower bottom temperature is required, an increase of the cooling flow could be worth but taking care with not decrease the TOC removal.

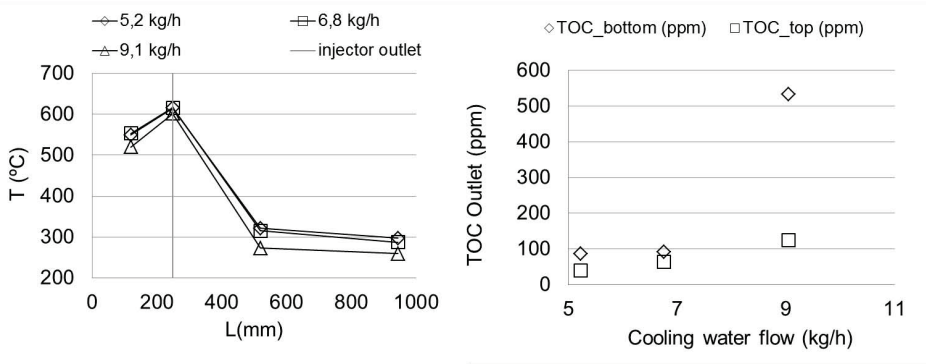

Figure 6.7: (a) Temperature profiles for different cooling water flows. (b) TOC values in top and bottom effluents for different cooling water flows.

6.4.5 Ammonia removal

Different mixtures of IPA and ammonia were tested with the new configuration of the reactor. The main results obtained with this new configuration, were compared with results obtained with mixtures of ammonia and IPA tested in the same reactor working with only the bottom outlet [4]. Figure 6.8 shows Ammonia and TOC removal represented versus maximum tem-

perature registered inside the reactor. The upper effluent fraction was kept constant at values around 50% which means that the 50% of the feed injected (liquid) has been taken out by the upper outlet. It can be appreciated that

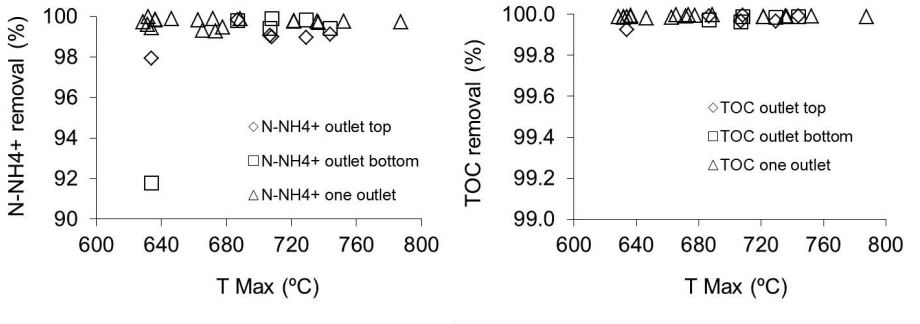

Figure 6.8: Ammonia removal (a) and TOC removal (b) vs max temperature inside the reactor for feeds with concentrations between 0.5-3% of ammonia and 9-11.5% of IPA working with 100% bottom flow and with 50% top flow.

temperatures higher than 700°C are required to achieve N-NH_4^+ removals over 99%. These temperatures are higher than those needed to obtain the same removal with the reactor working with only one outlet. Table 6.1 summarises the average results for removal of the different experiments made with mixtures of ammonia and IPA. Working with two outlets, it is observed that

Table 6.1: Removal results from the experiments made with different concentrations of ammonia.

NH_4^+o (%)	IPAo (%)	T_{max} (°C)	TOC Rem.(%) top	TOC Rem.(%) bottom	N-NH_4^+ Rem.(%) top	N-NH_4^+ Rem.(%) bottom	N-NO_3^- top (ppm)	N-NO_3^- bottom (ppm)
0.5	11.5	744	99.99	99.99	99.13	99.41	49	38
0.5	10.5	706	99.97	99.96	99.07	99.41	47	21
0.5	10.0	634	99.93	94.71	97.94	91.77	50	14
1.0	10.0	708	99.99	99.99	98.99	99.88	36	74
3.0	9.0	686	99.99	99.97	99.83	99.79	186	78
3.0	9.5	729	99.97	99.98	99.29	99.82	26	27

ammonia removal is slightly higher in the bottom effluent than in the top effluent, probably because the residence time for the products comprising the lower effluent is longer than the one of the top effluent, that it seems to be too short to have complete oxidation of ammonia [4]. Nitrate concentration is in general higher in the top effluent due to the higher temperatures. The concentrations of NOx and NH_4^+ in the gas effluent were under the detection limit of 0.5 and 5 ppm respectively for all the experimental conditions tested.

6.4.6 Behavior of the reactor working with high salt content feeds

The main goal of this new design of the reactor is to obtain a top effluent at high temperature and free of salts, becoming this way available to be used in systems to produce energy. To achieve that, salts contained in the feed must precipitate and fall, leaving the reactor dissolved in the bottom effluent while the top effluent is free of salts. For this purpose, feeds with Na_2SO_4 concentrations until 2.5% (25000 ppm) were injected in the reactor, using IPA as fuel to obtain reaction temperatures of 700°C, and at feed flow rates of 13-14 kg/h. In table 6.2 the main results of the experiments made with feed containing salts are summarized. Equation (6.6) explains how the salt recovery is calculated. As can be observed in table 6.2, it is possible to

Table 6.2: Main results for the experience made with feed containing 2.5% wt of Na_2SO_4.

F_{top} (kg/h)	F_{bottom} (kg/h)	TOC top (ppm)	TOC bottom (ppm)	T_{max} (°C)	T_{bottom} (°C)	Na_2SO_4 top (ppm)	Na_2SO_4 Recovery bottom (%)
7.2	10.2	1.0	209	749	239	77	2.4
7.2	10.2	0.3	352	712	244	73	32.1
7.2	10.2	0.5	599	740	250	77	21.1
7.2	10.2	0.8	23	742	254	72	1.8
7.2	10.2	0.7	69	683	258	75	45.5
7.2	10.2	0.7	16	691	258	85	0.7
Average		0.7	211	719	251	76	17.3

recover a top effluent almost free of salts (with conductivities below values of the tap water, equivalent to concentrations of Na_2SO_4 lower than 100 ppm) and at temperatures over 500°C, available to be expanded in a turbine or for the production of steam at high temperature that could be also expanded in a turbine. Paying attention to the salt recovery at the bottom flow, it was possible to obtain an average of 17% of salt recovery. This recovery is higher than the obtained with the reactor working with only one outlet [14] (average of 10%) but it was not possible to improve and stabilize the recovery during long times. This fact could be interpreted as the possible formation of solid clusters of salts swept away by the outlet stream and dissolved in the cooling systems.

6.4.7 Energy recovery

In order to analyze the possibility of using the high temperature of the effluent of SCWO reactors to produce energy, an analysis of the options for generating

energy was performed.

6.4.7.1 Parameter calculations

The following equations explain how the different parameters for the study were calculated. Firstly, the amount of energy released by the waste and fuel contained in the feed is calculated as shown in eq. (6.7).

$$\text{kW injected at the feed} = \frac{F_{\text{feed}} C_{\text{fuel}} \Delta H_{\text{c,fuel}}}{3600} \tag{6.7}$$

where $\Delta H_{\text{c,fuel}}$ is the enthalpy of combustion for IPA (3750 kJ/kg).
The energy consumed is due mainly to the pumping equipment (pumps and compressors). The fraction of energy consumed with respect of the energy contained in the feed is calculated as shown in eq. (6.8).

$$\text{Consumption} = \frac{\text{kW Cosumed}}{\text{kW injected at the feed}} \cdot 100 \tag{6.8}$$

The energy production is calculated using Peng-Robinson Equation of State with Boston-Mathias alpha function considering an isentropic turbine with an efficiency of 72 %. The fraction of energy produced with respect to the energy introduced in the feed is calculated as shown in eq. (6.9).

$$\text{Relative production} = \frac{\text{kW produced}}{\text{kW injected at the feed}} \cdot 100 \tag{6.9}$$

kW produced is the energy produced by direct expansion or steam expansion production.
From the production and consumption is obtained the percentage of the efficiency in energy production of the system of each reactor and kind of oxidant as shown in eq. (6.10).

$$\text{Efficiency} = \frac{\text{kW produced} - \text{kW Cosumed}}{\text{kW injected at the feed}} \cdot 100 \tag{6.10}$$

Mass and energy balances were solved considering thermal and volumetric properties calculated using Peng-Robinson Equation of State.

6.4.7.2 Energy produced by steam expansion

The most conventional method for electric generation is using the products stream as heat source for a Rankine cycle. In table 6.3 the characteristics of the steam than can be produced from the heat contained in the effluent

of the reactor based on T-S diagram for water are shown. The low pressure steam could be produced with effluents at temperatures up to 400°C (typical effluent temperatures of vessel reactors like the transpiring wall reactor and cooled wall reactor) and the high pressure steam by the effluents up to 700°C (effluents of tubular reactors or the effluent of the new cooled wall reactor described in this work).
Comparison of the recovery energy for different reactors by steam production:

- Tubular reactor [4, 12]
  This reactor consisted on a straight and empty tube made of Ni alloy C-276 with a total length of 5400 mm and a diameter of 1/4" (i.d. 3.86 mm) giving an internal volume of 63.2 ml and it was thermally isolated. In this case (figure 6.9), the effluent is used firstly to preheat the feed until the injection temperature (around 400°C) and the remaining heat flow is used to produce steam.

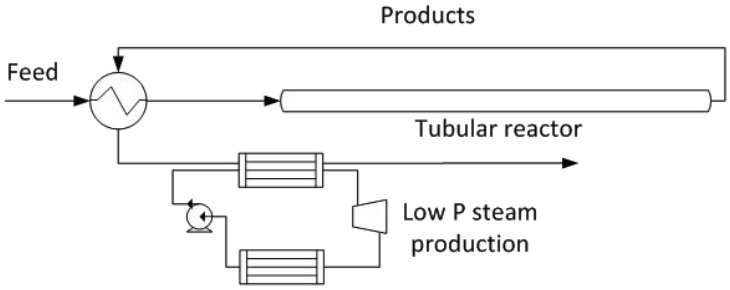

Figure 6.9: System recovery design for a tubular reactor.

- Original cooled wall reactor designed in the University of Valladolid (Valladolid, Spain) [24]
  This reactor is composed by two concentric tubes; the inner one is made of Inconel 625, and the outer shell is made of SS 316. Oxidation reaction takes place inside the inner tube (reaction chamber). In the gap between both tubes, the pressurized feed stream is going down and cooling the reaction media at the same time. In such way, the inner tube does not withstand any pressure at all; having the same

Table 6.3: Characteristics of the steam.

	Pressure (bar)	Temperature (°C)
High Pressure Steam	46	600-700
Low Pressure Steam	10	350-400

pressure in one side than on the other, and the thickness of the inner tube (Inconel 625) can be reduced. The effluent of the original CWR (at 400°C) can be used in a Rankine cycle as it is shown in figure 6.10.

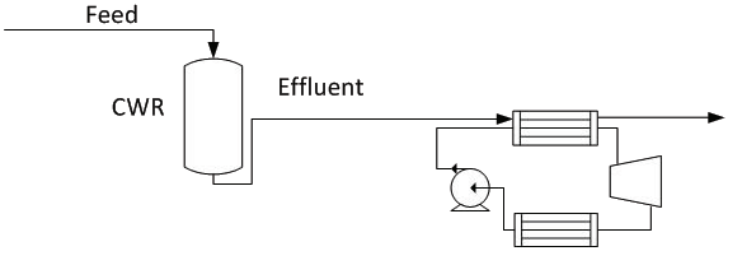

Figure 6.10: System recovery design for the original CWR.

- New cooled wall reactor design [14]
  The new reactor consists of a vertical Ni-alloy reaction chamber that is inside of a pressure vessel made of AISI 316 able to stand a maximum pressure of 30 MPa and 400°C. Between the walls of the two vessels a stream of cold water refrigerates the reaction vessel. The reagents (feed and oxidant) are introduced in the reactor through a tubular injector up to the top of the reaction chamber. The flame is produced outside of the injector, normally at the top of the reaction chamber, where the maximum temperature is registered. Reaction chamber is refrigerated with room temperature pressurized water that flowed between the reaction chamber wall and the inner wall which supported the pressure, keeping the pressurized wall at temperatures lower than 400°C, and entering in the reaction chamber by its lower part mixing with the reaction products. The products flowed down the reactor leaving it by its lower part together with the cooling water. Following the idea of

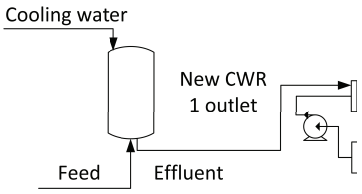

Figure 6.11: System recovery designed for the new CWR with the configuration with one outlet.

the original CWR, the products come out the reactor at temperatures

around 325°C and can produce steam to be expanded in a Rankine cycle (figure 6.11).
Other configuration of this reactor is working with an outlet at the top of the reactor, thus having two outlets: one at high temperature and other at subcritical temperatures with the salt dissolved with the cooling water (figure 6.12). For performing the comparative energetic

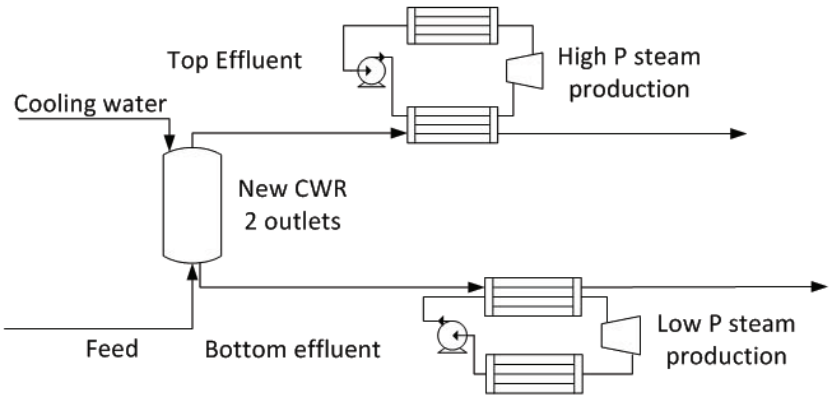

Figure 6.12: System recovery designed for the new CWR with the configuration with two outlets.

analysis among the different reactors types, typical operational parameters for each reactor such as fuel concentration, oxidant excess over the stoichiometric amount (based on the average excess used in the majority of the experiments and the acceptable oxidant excess to oxidize nitrogen compounds), the percentage of cooling water and the effluent temperature were fixed. These parameters are shown in table 6.4. In first place, the analysis was performed considering that the effluents are used to generate steam for a Rankine cycle. The results are also shown in table 6.4, at the last two columns. As can be observed, producing electricity through Rankine cycles present only positive efficiencies (be able to cover the energy consumption required by the pumping equipment) when the system is using oxygen as the oxidant. This is due to the much higher consumption of air compressors compared to liquid oxygen cryogenic pumps. Actually, the energy required (defined in equation (6.8)) when using air and oxygen ascends to 28% and 0.2%, respectively.

6.4.7.3 Energy recovery with the new cooled wall reactor

Focusing on the new CWR reactor design, a detailed analysis of the energetic recovery possibilities is shown above. In figure 6.13 it is shown another pos-

Table 6.4: Conditions fixed for the study of each reactor, recovering energy through a Rankine cycle. 5% excess of oxidant is assumed in all cases.

Type of reactor	Heat flow feed (kW)	Cooling water (% of feed)	Injection T (°C)	Effluent T (°C)	Efficiency	
					Air	O_2
Original CWR	1202	0	Room T	400	-16.9%	8.6%
New CWR 1 outlet	1202	35	Room T	325	-16.8%	4.8%
Tubular reactor	372	0	350-400	700	-21.1%	5.7%
New CWR 2 outlets 100%	1208	35	Room T	Top 700 Bot. 300	-8.0%	19.0%
New CWR 2 outlets 70%	1208	35	Room T	Top 700 Bot. 300	-11.0%	14.0%

sibility of energy recovery for each effluent of the new CWR design, besides scheme shown in figure 6.12. It was assumed, as observed experimentally,

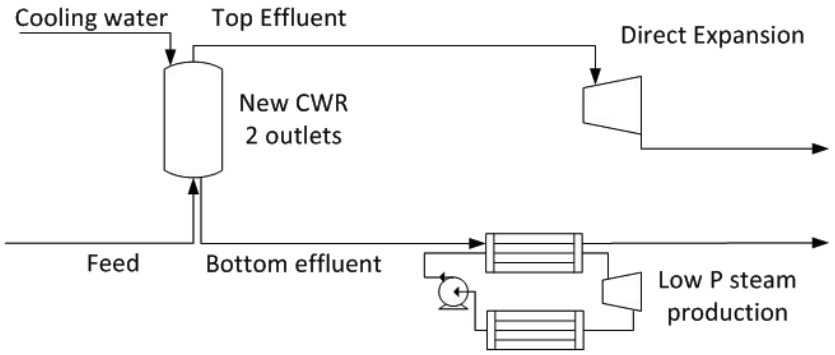

Figure 6.13: Scheme of the direct expansion of top effluent for the recovery energy with the CWR with 2 outlets.

that all the gases involved in the combustion leaves the reactor with the top effluent: CO_2 produced in the reaction, N_2 (when air is used as oxidant) and O_2 from the oxidant mixed with the water flow, being the bottom effluent considered as pure water.

Influence of the distribution flow through different parameters

To analyze the electricity production with the new CWR reactor, the conditions assumed are: 5% oxidant excess; 1208 kW of heat flow feed; flow of cooling water equivalent to 35% of feed flow; and effluent temperatures of 700°C and 300°C, at top and bottom outlets, respectively. The selected percentage of cooling water is based on the optimal operational parameters obtained with the new reactor.

Influence of the kind of energy production system

Table 6.5 shows the efficiency of the new reactor obtained by direct expan-

sion of the flow and steam production working with air and with oxygen. Different flow distributions are assumed. As can be observed, the energy

Table 6.5: Values of efficiency obtained with the new reactor by direct expansion of the flow and steam production working with air and with oxygen for different proportion in top effluent /feed.

Oxidant	Energy production	Upper effluent fraction (%) 50	60	70	80	90	100
Air	Rankine Cycle	-14%	-12%	-14%	-10%	-9%	-8%
	Direct Expansion	-0.7%	3%	7%	11%	15%	19%
Oxygen	Rankine Cycle	11%	12%	14%	16%	17%	19%
	Direct Expansion	15%	17%	20%	22%	25%	27%

produced by direct expansion of the flow from the reactor is bigger than the energy obtained by the production of steam in a Rankine cycle that could be expanded afterwards.

Influence of the oxidant

In figure 6.14 is represented how the efficiency varies with the top effluent/feed relation. It is observed that when the top effluent is directly ex-

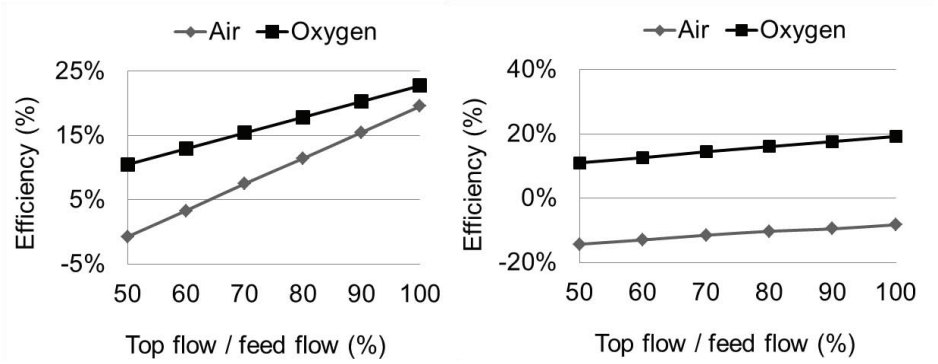

Figure 6.14: Efficiency of the recovery energy of the new reactor with (a) direct expansion and (b) steam production.

panded in a turbine, working with air would be a possible option if flow distribution is over 65% (top flow / feed flow). In the case of the expansion with the steam produced in the Rankine cycle, the consumption of the facility working with air as the oxidant is always higher than the energy produced. In both cases, oxygen offers better theoretical results with respect the energy production and energy pumping requirements.

6.5 Conclusions

We have presented a new cooled wall design for supercritical water oxidation, capable of producing a high energy products stream with very low content of salts. Total elimination of organics and nitrogen compounds is achieved without needing of preheating the feed thanks to the hydrothermal flame inside the reactor. Other important advantage of the new reactor is that reaction and salt precipitation take place in one equipment.
Using IPA as fuel TOC removal was higher than 99.9% in both effluents while the percentage of products leaving the reactor in the top effluent was lower than 70%. At higher top effluents total TOC removal is not achieved in the bottom effluent. Removals of ammonia higher than 99% were possible with intermediate upper flow fractions and temperatures over 700°C but the removal of ammonia in the upper flow was lower than in the bottom flow probably due to the necessity of higher residence times for the oxidation of products coming out the reactor trough the top outlet.
Experimental results using IPA as fuel and Na_2SO_4 as a model salt show that is possible to obtain a top effluent at 600°C, with a salt content lower than 100 ppm and a bottom effluent which allows recovering an average of 17% of salts at a temperature of 300°C.
Initial estimations about the energy recovery of the top flow indicates that the process can be self-sustained and could be integrated in conventional plants for waste treatment and/or energy generation.

6.6 Acknowledgments

The authors thank to the Spanish Ministry of Economy and Competitiveness for the projects CTQ2011-23293 and ENE2012-33613. P.C. thanks Junta de Castilla y León for predoctoral grant. J.P.S.Q thanks the Spanish Education Ministry for the FPU grant (FPU AP2009-0399). C.J. thanks the Spanish Economy and Competitiveness Ministry for her predoctoral grant BES-2011-046496.

Bibliography

[1] W. Schilling, E. Franck, Combustion and diffusion flames at high-pressures to 2000 bar, Berichte Der Bunsen-Gesellschaft-Physical Chemistry Chemical Physics 92 (1988) 631–636.

[2] G. M. Pohsner, E. U. Franck, Spectra and temperatures of diffusion

flames at high pressures to 1000 bar, Berichte der Bunsengesellschaft für physikalische Chemie 98 (1994) 1082–1090.

[3] C. Augustine, J. Tester, Hydrothermal flames: From phenomenological experimental demonstrations to quantitative understanding, Journal of Supercritical Fluids 47 (2009) 415–430.

[4] P. Cabeza, M. D. Bermejo, C. Jimenez, M. J. Cocero, Experimental study of the supercritical water oxidation of recalcitrant compounds under hydrothermal flames using tubular reactors, Water Research 45 (2011) 2485–2495.

[5] R. M. Serikawa, T. Usui, T. Nishimura, H. Sato, S. Hamada, H. Sekino, Hydrothermal flames in supercritical water oxidation: investigation in a pilot scale continuous reactor, Fuel 81 (2002) 1147–1159.

[6] M. D. Bermejo, E. Fdez-Polanco, M. J. Cocero, Experimental study of the operational parameters of a transpiring wall reactor for supercritical water oxidation, Journal of Supercritical Fluids 39 (2006) 70–79.

[7] C. Oh, R. Kochan, T. Charlton, A. Bourhis, Thermal-hydraulic modeling of supercritical water oxidation of ethanol, Energy & Fuels 10 (1996) 326–332.

[8] B. Wellig, K. Lieball, P. von Rohr, Operating characteristics of a transpiring-wall SCWO reactor with a hydrothermal flame as internal heat source, Journal of Supercritical Fluids 34 (2005) 35–50.

[9] B. Wellig, M. Weber, K. Lieball, K. Prikopsky, P. von Rohr, Hydrothermal methanol diffusion flame as internal heat source in a SCWO reactor, Journal of Supercritical Fluids 49 (2009) 59–70.

[10] K. Príkopský, B. Wellig, P. R. von Rohr, SCWO of salt containing artificial wastewater using a transpiring-wall reactor: Experimental results, The Journal of Supercritical Fluids 40 (2007) 246–257.

[11] M. D. Bermejo, F. Fdez-Polanco, M. J. Cocero, Effect of the transpiring wall on the behavior of a supercritical water oxidation reactor: Modeling and experimental results, Industrial & Engineering Chemistry Research 45 (2006) 3438–3446.

[12] M. D. Bermejo, P. Cabeza, M. Bahr, R. Fernandez, V. Rios, C. Jimenez, M. J. Cocero, Experimental study of hydrothermal flames initiation using different static mixer configurations, Journal of Supercritical Fluids 50 (2009) 240–249.

[13] M. D. Bermejo, P. Cabeza, J. P. S. Queiroz, C. Jimenez, M. J. Cocero, Analysis of the scale up of a transpiring wall reactor with a hydrothermal flame as a heat source for the supercritical water oxidation, Journal of Supercritical Fluids 56 (2011) 21–32.

[14] M. D. Bermejo, C. Jimenez, P. Cabeza, A. Matias-Gago, M. J. Cocero, Experimental study of hydrothermal flames formation using a tubular injector in a refrigerated reaction chamber. influence of the operational and geometrical parameters, Journal of Supercritical Fluids 59 (2011) 140–148.

[15] M. D. Bermejo, M. J. Cocero, F. Fernandez-Polanco, A process for generating power from the oxidation of coal in supercritical water, Fuel 83 (2004) 195–204.

[16] K. Arai, R. L. Smith Jr., T. M. Aida, Decentralized chemical processes with supercritical fluid technology for sustainable society, The Journal of Supercritical Fluids 47 (2009) 628–636.

[17] E. D. Lavric, H. Weyten, J. De Ruyck, V. Pleşu, V. Lavric, Supercritical water oxidation improvements through chemical reactors energy integration, Applied Thermal Engineering 26 (2006) 1385–1392.

[18] A. A. Peterson, F. Vogel, R. P. Lachance, M. Fröling, J. Michael J. Antal, J. W. Tester, Thermochemical biofuel production in hydrothermal media: A review of sub- and supercritical water technologies, Energy & Environmental Science 1 (2008) 32–65.

[19] M. Gassner, F. Vogel, G. Heyen, F. Maréchal, Optimal process design for the polygeneration of SNG, power and heat by hydrothermal gasification of waste biomass: Thermo-economic process modelling and integration, Energy & Environmental Science 4 (2011) 1726–1741.

[20] ANSYS, ANSYS FLUENT theory guide release 12, 2009.

[21] A. Peneloux, E. Rauzy, R. Freze, A consistent correction for redlich-kwong-soave volumes, Fluid Phase Equilibria 8 (1982) 7–23.

[22] D.-Y. Peng, D. B. Robinson, A new two-constant equation of state, Industrial & Engineering Chemistry Fundamentals 15 (1976) 59–64.

[23] G. P. Mathur, G. Thodos, The self-diffusivity of substances in the gaseous and liquid states, AIChE Journal 11 (1965) 613–616.

[24] M. J. Cocero, D. Vallelado, R. Torio, E. Alonso, F. Fdez-Polanco, Optimisation of the operation variables of a supercritical water oxidation process, Water Science and Technology 42 (2000) 107–113.

Conclusions & Future work

The overall objective of this thesis has been achieved and new developments and tools regarding hydrothermal flames and supercritical water oxidation process have been presented. A summary of the conclusions extracted from this work is described below:

1. *Property estimation methods.* Methods of calculation of thermodynamic and transport properties have been reviewed and a set of models has been applied:

    - Peng-Robinson equation of state with volume translation is able to predict densities of pure components and mixtures, in liquid and supercritical phases.
    - Residual enthalpy retrieved from Peng-Robinson equation of state (in its original form) is in agreement with reference values.
    - Most of the transport properties methods available are only valid for liquid or gas phase, not for both. TRAPP method is reported to be applicable in the liquid phase, but it has shown poor results for water.
    - The property methods have been applied in simple balance-based models and in CFD simulations using the software ANSYS FLUENT.

2. *Kinetics in hydrothermal flame supercritical water oxidation.* A simple method of estimation of kinetic parameters using temperature profiles measured in a tubular adiabatic reactor has been proposed:

    - An Arrhenius type kinetic model for supercritical water oxidation of isopropyl-alcohol in hydrothermal flame regime has been determined by adjusting the temperature profile in tubular SCWO reactors. The model is able to predict temperature profiles in tubular reactors at different IPA concentrations, feed flows and using air or oxygen as the oxidant.
    - Given the inlet conditions, the model can estimate if the oxidation will be flame or flameless regime, and is capable of reproducing both.
    - This kinetic model was applied to a model for the transpiring wall reactor developed by the University of Valladolid and the experimental data were successfully described. According to the results, in the presence of a hydrothermal flame, the reactor can be maintained in steady state regime, with total destruction of fuel, even for subcritical feed injections.

- The application of turbulent combustion models has showed that hydrothermal flames inside SCWO reactors are in the limit between chemical controlled and mixing controlled. Both, kinetic model and turbulence, are important and influence hydrothermal flames.

3. *Operational parameters effects in chamber reactors.* A CFD model for supercritical water oxidation reactors has been developed and can be used as designing tool:

   - The model correctly predicts experimental temperature profiles of the cooled wall reactor constructed by University of Valladolid.
   - It was found that the hydrothermal flame is affected by geometrical parameters such as injector diameter and length, or distance to reactor's ceiling.
   - The use of a CFD model has allowed to study a RTD analysis of this complex system that would be difficult to perform experimentally. The RTD study shows a stagnant area in the top of the reactor, when short injectors are used.
   - When designing this kind of reactors a compromise in the length of the injector must be adopted between avoiding the wall's stress due to the high temperature of the flames and reducing the dead volume of the reactor.
   - The behavior of this particular reactor can be described as a combination of simple flow patterns.

4. *Energetic study of a new design rector.* A new cooled wall design for supercritical water oxidation reactor has been presented:

   - The reactor is capable of producing a high energy products stream with very low content of salts. Total elimination of organics and nitrogen compounds is achieved without needing of preheating the feed thanks to the hydrothermal flame inside the reactor. Reaction and salt precipitation take place in one equipment.
   - The CFD model predicts quantitatively the temperature profiles inside the reactor and how these temperatures are affected by flow distribution.
   - TOC removal was higher than 99.9% in both effluents while the percentage of products leaving the reactor in the top effluent was lower than 70%. At higher top flows total TOC removal is not

achieved in the bottom effluent. Top effluent at 600°C, with a salt content lower than 100 ppm has been obtained, and an average of 17% of salts has been recovered in the bottom effluent.

- It has been found that the process can be self-sustained and could be integrated in conventional plants for waste treatment and/or energy generation.

This thesis aimed to select existing tools and develop new ones for a better understanding on hydrothermal flames in supercritical water reactors. However, the results bring new research needs which could be satisfied in the future:

1. It would be interesting to obtain experimental/reference data of transport properties for aqueous mixtures in sub and supercritical states, in order to test the existing methods of estimation and to develop new ones.

2. We have presented tools for SCWO modeling assuming one phase flows, what is a good approximation to real reactors but neglects the low temperature zones. It would be useful to couple multiphase CFD models with the appropriate mass transfer and phase equilibria models. It would help to comprehend the mechanisms of evaporation of fuel drops and reaction initiation.

3. A turbulent premixed flame model has been applied to hydrothermal flames based on a presumed probability density function (β-pdf) for the turbulent fluctuations in fuel concentration. It would be interesting to study the effect of fluctuations in other variables, like temperature and density, using joint probability density functions.

4. The methods presented for energy recovery/power generation are based on usual technologies of expansion of high pressure streams. New technologies for turbines and expansion systems should be studied to optimize the usage of the high energy content of SCWO effluent reactors.

Resumen

Introducción

La oxidación en agua supercrítica (OASC) es una tecnología conocida y ya se ha contrastado su eficiencia en la destrucción total de residuos en tiempos de residencia de unos pocos segundos. Esto se debe a las propiedades disolventes del agua por encima de su punto crítico (374°C, 22,1 MPa) que permiten la completa miscibilidad entre la materia orgánica y el oxígeno, propiciando un medio homogéneo para la reacción de oxidación. Sin embargo, aún existen algunos desafíos del punto de vista práctico que pueden reducir la eficiencia o la rentabilidad de esta tecnología: corrosión, deposición de sales y alta demanda energética. El uso de las llamas hidrotermales como fuente de calor interna permite contrarrestar muchos de los problemas existentes en el proceso de oxidación en agua supercrítica.

La formación de llamas hidrotermales se demostró por primera vez en los años 80 por el profesor Ernst Franck. Desde entonces muchos grupos de iinvestigación han desarrollado reactores que trabajan con una llama hidrotermal como fuente de calor. Entre las ventajas de la OASC con llama hidrotermal, se destacan la eliminación de contaminantes en milisegundos y la posibilidad de mantener la reacción con temperaturas de inyección de alimentación cercanas a la temperatura ambiente. Esto se traduce en:

- Reducción del tamaño de los reactores, debido a la reducción de los tiempos de reacción.
- Reducción de los problemas de corrosión y deposición de sales, debido a la inyección de reactivos a temperatura baja que evita el precalentamiento externo.
- Mejora del aprovechamiento energético, debido a las altas temperaturas producidas en la llama.

Objetivos

El objetivo general de esta tesis es profundizar el conocimiento del proceso de Oxidación en Agua Supercrítica (OASC) en régimen de llama hidrotermal, a través de herramientas de modelado y simulación. La investigación debe enfocarse en las posibilidades de generación de energía de esta tecnología. Los objetivos parciales necesarios para una descripción completa del proceso se enumeran abajo.

Estudiar los métodos de estimación de propiedades para sustancias puras en estado supercrítico y sus mezclas acuosas, y su aplicación en herramientas de simulación.

- Estudiar la disponibilidad de métodos de cálculo de propiedades capaces de describir propiedades térmicas y de transporte de mezclas en condiciones supercríticas.

- Construir una biblioteca de rutinas de métodos de propiedades que pueda ser utilizada en modelos CFD y en balances y modelos sencillos de llamas hidrotermales en el contexto de los reactores OASC.

Estudio de la cinética de la OASC en llama hidrotermal.

- Desarrollar un método para la determinación de parámetros cinéticos a partir de datos experimentales de fácil obtención, tal como variaciones de temperatura.

- Utilizando este método, ajustar un modelo cinético para la oxidación en agua supercrítica de isopropanol en régimen de llama hidrotermal, reduciendo así la escasez de datos cinéticos en estas condiciones.

- Validar el modelo cinético con distintos conjuntos de datos experimentales y distintos tipos de reactor.

- Estudiar como las interacciones con la turbulencia afectan las llamas hidrotermales.

Estudiar como la configuración del reactor y las condiciones de operación afectan el comportamiento de la llama hidrotermal.

- Construir un modelo CFD realista para reactores de tipo tanque que funcionan con una llama hidrotermal.

- Validar el modelo con datos experimentales del nuevo reactor de pared enfriada diseñado y operado en la Universidad de Valladolid.

- Analizar los efectos de la geometría del inyector y los parámetros de operación sobre el comportamiento de una llama hidrotermal.

- Utilizar el modelo para obtener información adicional (no accesible experimentalmente) como curvas de distribución de tiempos de residencia.

Aplicar el modelo CFD a un nuevo reactor para la predicción de la distribución de flujos para obtener eficiencia energética.

- Estudiar el comportamiento del nuevo reactor de pared enfriada con dos corrientes de salida con el objetivo de optimizar la recuperación energética.

- Estudiar los efectos de la relación entre los flujos de las salidas superior e inferior en los perfiles de temperatura dentro del reactor y en la eliminación de materia orgánica en ambas corrientes.
- Encontrar las condiciones para mantener la máxima cantidad del calor liberado por la llama en una corriente limpia a alta temperatura que sale del reactor por su parte superior.
- Utilizar los resultados de CFD y los métodos de propiedades para realizar predicciones realistas de la eficiencia energética del proceso OASC.

Resultados

En el **capítulo 1**, se ha revisado el estado del arte de la tecnología, con especial atención a la producción de energía. En lo que se refiere a la descripción de propiedades (termodinámicas y de transporte) existen métodos recomendados para sustancias puras pero su validez para mezclas en condiciones supercríticas no está del todo clara. La mayoría de los trabajos existentes en literatura utilizan ecuaciones cúbicas de estado para el cálculo de densidades y entalpías, y reglas de mezcla lineales para viscosidades y conductividades térmicas. Cuanto al diseño de reactores, éstos han evolucionado con el objetivo de reducir los problemas de corrosión y deposición de sales, casi siempre optando por diluir los productos de reacción. Para que el proceso sea rentable energéticamente otras estrategias deben ser utilizadas para mantener los productos a la temperatura más alta posible sin perjudicar el funcionamiento del reactor, y las llamas hidrotermales estabilizadas adecuadamente son ideales para este fin. Esta revisión deja claras las necesidades de investigación en diversos campos relacionados con la OASC, a parte de las soluciones técnicas en las etapas de bombeo y pre-tratamiento de biomasa real. El modelado es esencial cuando llamas hidrotermales están presentes, ya que su comportamiento no siempre se puede observar directamente, y estos modelos requieren mejoras en otros sub-modelos de cinética química, turbulencia, ecuaciones de estado y propiedades de transporte para mezclas. Finalmente, se deben desarrollar y construir equipos de expansión apropiados a la naturaleza y condición de las corrientes de salida, que además sean eficientes en la recuperación de trabajo.

En el **capítulo 2**, se describen los métodos de estimación de propiedades utilizados en esta tesis. Una simple ecuación cúbica de estado ha mostrado buena exactitud y rapidez de cálculo para la estimación de propiedades termodinámicas de mezclas supercríticas. La densidad es calculada con la ecuación de estado de Peng-Robinson con la modificación de la traslación

del volumen, mientras la entalpía es calculada con la ecuación original de Peng-Robinson.

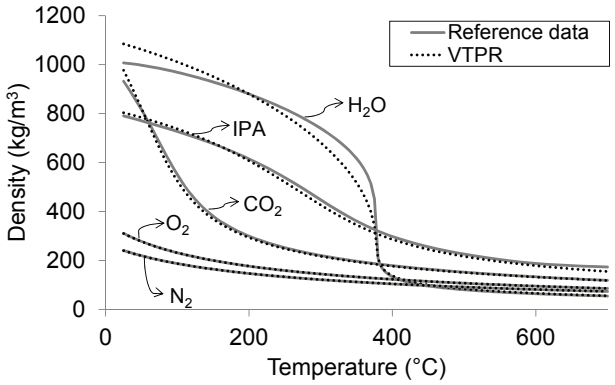

Figura R1: Densidades de los componentes puros en función de la temperatura a 23 MPa.

Los parámetros de traslación del volumen (tabla R1) se han ajustado para minimizar la desviación en la densidad calculada para los compuestos puros respecto a valores de referencia. Una vez ajustados los volúmenes para los componentes puros, la densidad de la mezcla se ha calculado utilizando reglas de mezcla dependientes de la composición para los parámetros de entrada de la ecuación de Peng-Robinson.

Tabla R1: Traslación del volumen a 23 MPa para utilización en la ecuación de estado VTPR.

	$vt(cm^3/mol)$
H_2O	4.291073
O_2	-2.545861
N_2	-3.743775
CO_2	1.284445
IPA	3.721115

Las propiedades de transporte se podrían predecir con una exactitud razonable a altas temperaturas. Sin embargo, en el rango de baja temperatura (altas densidades), los métodos presentan resultados pobres y en su lugar se han usado reglas de mezcla basadas en fracciones másicas.

En la tercera parte de la tesis se hace un estudio de la cinética de la OASC en régimen de llama hidrotermal. En el **capítulo 3**, se presenta un método para determinar parámetros cinéticos a partir de datos experimentales de fácil medición. El método consiste en ajustar los parámetros

cinéticos minimizando el error en la predicción de los perfiles de temperatura obtenidos experimentalmente. Usando este método, se ha ajustado una nueva ecuación para la velocidad de reacción de oxidación de isopropanol en régimen de llama hidrotermal: $r = k_0 \exp\left(-\frac{E_a}{RT}\right) C_{IPA} C_{O_2}$, donde $k_0 = (9{,}308 \pm 3{,}989) \cdot 10^7 (m^3 \cdot s^{-1} \cdot kmol^{-1})$ y $E_a = 89{,}441 \pm 2{,}457 (kJ \cdot mol^{-1})$. La desviación media del ajuste es de 10,8 %, y ejemplos de la aplicación del modelo con aire y oxígeno se muestran en la figura R2.

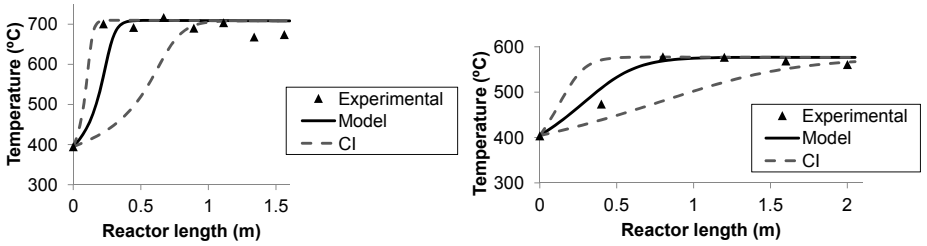

(a) (b)

Figura R2: Comparación de temperaturas experimentales (símbolos) a lo largo del reactor tubular y predicciones del modelo (línea continua) con la cinética ajustada. Las líneas discontinuas indican las predicciones en los límites del intervalo de confianza. (a)5,9 kg/h, 4 %IPA a 395°C, aire como oxidante; (b)10,6 kg/h, 2 %IPA a 404°C, O_2 como oxidante.

Con el modelo cinético se ha realizado un análisis paramétrico de la formación de la llama, y el modelo se ha utilizado en la descripción de un reactor de tipo tanque operando en estado estacionario en régimen de llama hidrotermal con inyección a temperaturas subcríticas (figura R3). El modelo desarrollado representa una gran mejora respecto a anteriores modelos estudiados en nuestro grupo.

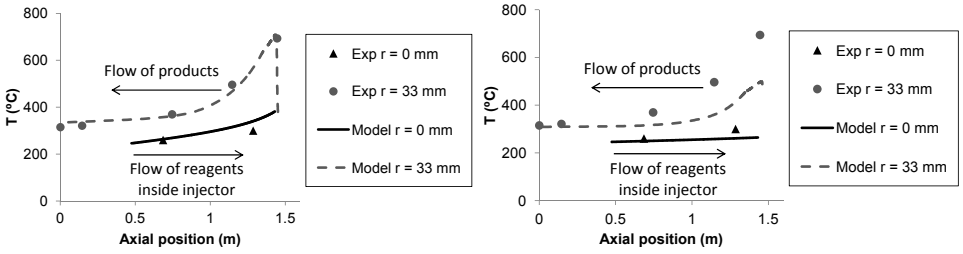

(a) (b)

Figura R3: Perfiles de temperatura experimental (símbolos) y simulado (líneas) del reactor de pared transpirable: (a)Este modelo, (b)modelo anterior. El color negro corresponde al inyector; el gris representa la cámara de reacción.

En el **capítulo 4** las interacciones entre la turbulencia y el flujo reactivo son evaluadas con un modelo de combustión turbulenta basado en cuantificar las fluctuaciones turbulentas a través de probabilidades. Los resultados se comparan en la figura R4.

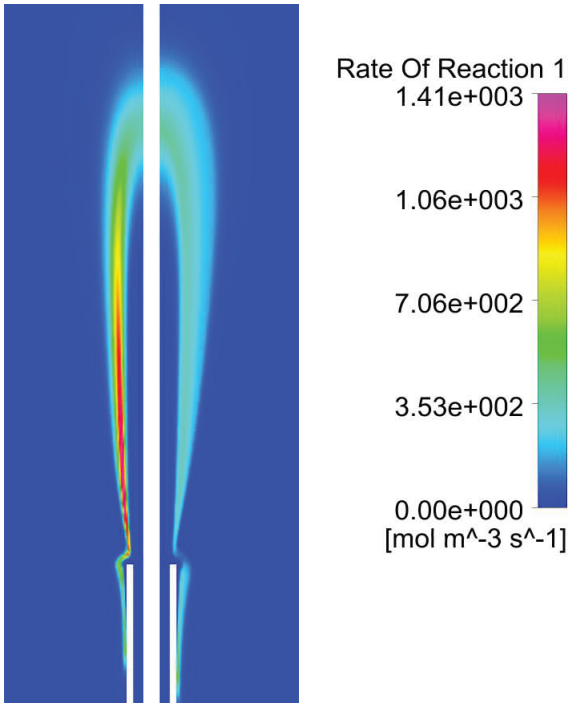

(a) (b)

Figura R4: Contornos de velocidad de reacción resultantes de la simulación: (a)Modelo de Arrhenius. (b)Modelo pdf.

Se ha encontrado que estas fluctuaciones, a pesar de que alteran la estructura de la llama, no tienen influencia sobre la eficiencia de eliminación de residuos (figura R5) o la generación de energía. Esto se puede explicar por el hecho de que el volumen de este reactor está sobredimensionado, permitiendo tiempos de residencia mucho más grandes que los tiempos de reacción.

En el **capítulo 5** se simula la influencia de la configuración interna de reactores de tanque para el proceso OASC y los resultados son comparados a los datos experimentales. El modelo y los datos experimentales utilizados corresponden al nuevo reactor de pared enfriada desarrollado en la Universidad de Valladolid (figura R6).
El modelo CFD desarrollado ofrece una buena predicción de los resultados experimentales (desviaciones del orden de 10 % para perfiles de temperatura) y puede ser utilizado para el diseño de reactores que funcionen con una llama

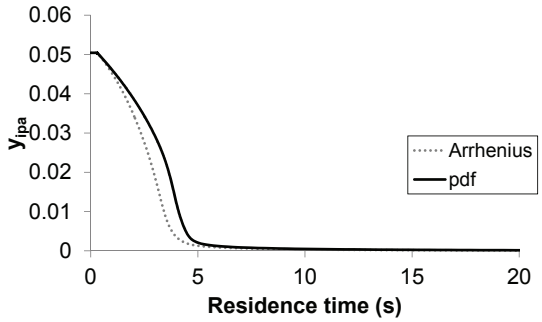

Figura R5: Fracción másica de IPA en el centro del reactor en función del tiempo de residencia.

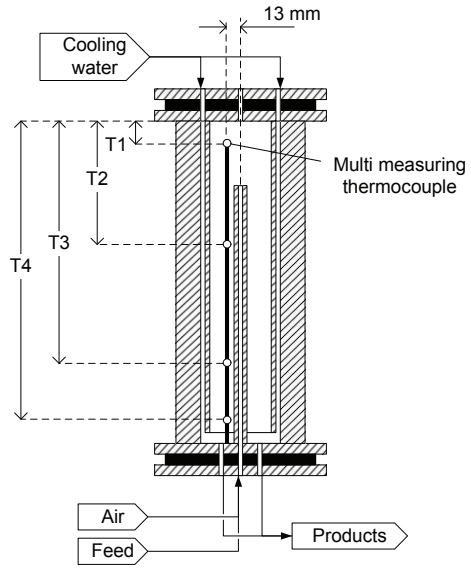

Figura R6: Esquema del reactor de pared enfriada indicando la posición de los termopares. Detalles en la tabla 5.1.

hidrotermal, como se observa en la figura R7.

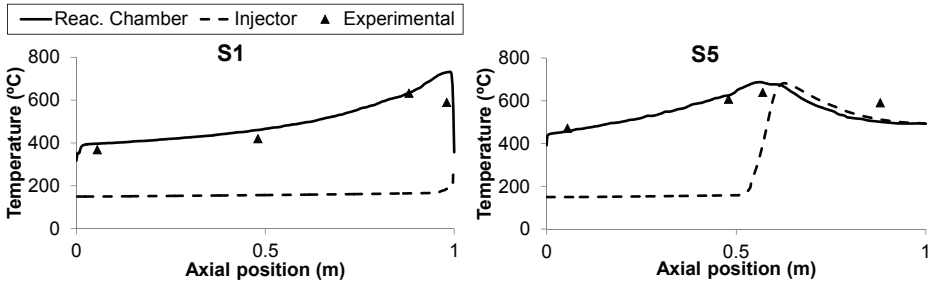

(a) (b)

Figura R7: Perfil de temperatura dentro del reactor de pared enfriada: puntos experimentales y perfiles resultantes del modelado. (a)Caso S1 - longitud del inyector = 0,95 m. (b)Caso S5 - longitud del inyector = 0,50 m.

Del modelo se obtienen curvas de distribución de tiempos de residencia dando información adicional acerca del comportamiento no-ideal del reactor (figura R8).

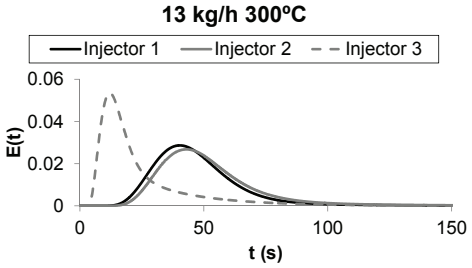

Figura R8: Curvas de distribución de tiempos de residencia para una alimentación de 13 kg/h a 300°C. Inyectores 1, 2 y 3 corresponden a los casos S2, S4 y S6, respectivamente.

Las metodologías desarrolladas en este trabajo se aplican a una nueva configuración de reactor especialmente diseñado para la generación de energía en el **capítulo 6**. Los resultados experimentales se describen brevemente y se aplica el modelo al estudio del comportamiento interno del reactor y como éste es afectado por la existencia de dos salidas. Un ejemplo se observa en la figura R9.
Finalmente, se estudia la integración energética y se muestra que tanto el aprovechamiento de calor, como la generación de vapor de alta presión, y la generación de electricidad por expansión directa de los productos, son teóricamente factibles en OASC (tabla R2).

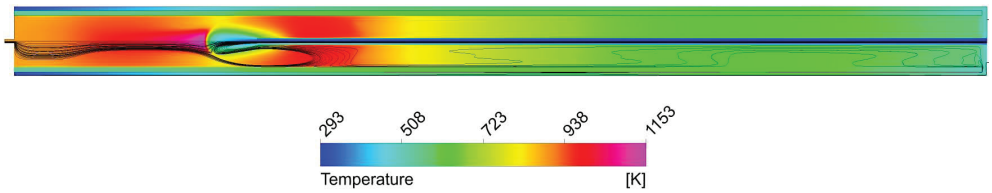

Figura R9: Contornos de temperatura y líneas de flujo producidos por el modelo.

Tabla R2: Eficiencias obtenidas con el nuevo reactor por expansión directa de los productos y por producción de vapor, utilizando aire y oxígeno para diferentes valores del ratio efluente superior/alimentación.

Oxidant	Energy production	Upper effluent fraction (%) 50	60	70	80	90	100
Air	Rankine Cycle	-14 %	-12 %	-14 %	-10 %	-9 %	-8 %
	Direct Expansion	-0.7 %	3 %	7 %	11 %	15 %	19 %
Oxygen	Rankine Cycle	11 %	12 %	14 %	16 %	17 %	19 %
	Direct Expansion	15 %	17 %	20 %	22 %	25 %	27 %

Conclusiones y trabajo futuro

El objetivo global de esta tesis ha sido cumplido y nuevos desarrollos y herramientas relacionadas a las llamas hidrotermales y al proceso de oxidación en agua supercrítica han sido presentados. Un resumen de las conclusiones extraídas de este trabajo se describe a continuación:

1. *Métodos de estimación de propiedades.* Métodos de cálculo de propiedades termodinámicas y de transporte se han revisado y un conjunto de modelos se ha aplicado:

   - La ecuación de estado de Peng-Robinson con la modificación del volumen trasladado es capaz de predecir densidades de componentes puros y de mezclas, tanto en fase líquida como supercrítica.
   - La entalpía residual obtenida de la ecuación de estado de Peng-Robinson (en su forma original) está en concordancia con los valores de referencia.
   - La mayoría de los métodos existentes para propiedades de transporte son válidos solamente para fase gaseosa o fase líquida, no

para ambas. El método TRAPP está clasificado como aplicable también en la fase líquida, pero ha mostrado resultados pobres para el agua.

- Las rutinas para cálculos de propiedades se han aplicado a modelos sencillos basados en balances de materia y energía y también en simulaciones CFD usando el software ANSYS FLUENT.

2. *Cinéticas en oxidación en agua supercrítica en llamas hidrotermales.* Un método sencillo para la estimación de parámetros cinéticos usando perfiles de temperatura medidos en un reactor tubular adiabático ha sido propuesto:

   - Se han determinado los parámetros para un modelo cinético del tipo Arrhenius para la oxidación de isopropanol en agua supercrítica en régimen de llama. Los parámetros se han obtenido ajustando perfiles de temperatura a los datos experimentales de reactores OASC tubulares. El modelo describe perfiles de temperatura en reactores tubulares a distintas concentraciones de IPA, distintos flujos de alimentación y usando aire u oxígeno como oxidante.
   - Fijadas las condiciones de entrada, el modelo pude estimar si la reacción de oxidación se dará en régimen de llama o no, y es capaz de reproducir ambos casos.
   - La cinética fue aplicada a un modelo sencillo del reactor de pared transpirable desarrollado en la Universidad de Valladolid y los datos experimentales se han reproducido con éxito. Según los resultados, en presencia de una llama hidrotermal la reacción se puede mantener en estado estacionario, con total destrucción de materia orgánica, incluso a temperaturas de inyección subcríticas.
   - La inclusión de un modelo de combustión turbulenta ha demostrado que las llamas hidrotermales dentro de los reactores OASC están en la región entre los procesos limitados por el tiempo de reacción y los limitados por el tiempo de mezcla. Ambos, cinética y turbulencia, son importantes e influencian las llamas hidrotermales.

3. *Efecto de parámetros operacionales en reactores de tanque.* Un modelo CFD para reactores de oxidación en agua supercrítica ha sido desarrollado:

   - El modelo predice correctamente los perfiles de temperatura obtenidos experimentalmente en el reactor de pared enfriada dcons-

truído en la Universidad de Valladolid.

- Se ha observado que la llama hidrotermal es influenciada por parámetros geométricos tales como diámetro y longitud del inyector, o la distancia hasta el techo del reactor.
- La aplicación del modelo CFD ha permitido realizar un análisis de distribución de tiempos de residencia de este sistema complejo, algo que sería difícil de realizar experimentalmente. El estudio de los RTD muestra un área de estancamiento en la parte superior del reactor cuando se usan inyectores cortos.
- Al diseñar este tipo de reactores, se debe elegir la longitud del inyector teniendo en cuenta un compromiso entre evitar el estrés en las paredes debido a las altas temperaturas de las llamas y reducir el volumen muerto del reactor.
- El comportamiento de este reactor, en lo que se refiere a tiempos de residencia, puede ser descrito como una combinación de modelos de reactores de flujo ideal.

4. *Estudio energético de un nuevo diseño de reactor.* Un nuevo diseño de reactor de pared enfriada para oxidación en agua supercrítica ha sido presentado:

   - El reactor puede producir una corriente de productos con alta calidad de energía y muy baja cantidad de sales. Se consigue la eliminación total de compuestos orgánicos y nitrogenados sin la necesidad de pre-calentar la alimentación gracias a la llama hidrotermal formada dentro del reactor. La reacción y la precipitacióon de sales ocurren en un único equipo.
   - El modelo CFD predice de forma cuantitativa el perfil de temperatura dentro del reactor y como éste es afectado por la distribución de flujos entre las dos salidas.
   - Eficiencias de eliminación de TOC superiores al 99,9 % han sido obtenidas en ambos efluentes siempre que el porcentaje de productos sacados por la salida superior es menor que 70 %. Para flujos más altos por la salida superior, la remoción de TOC en el efluente inferior no es completa. Se puede obtener una corriente superior a 600°C con un contenido de sales inferior a 100 ppm, y la recuperación media de sales en el efluente inferior es de 17 %.
   - El proceso es energéticamente auto-suficiente y podría ser integrado en plantas convencionales de tratamiento de residuos y/o de generación de energía.

En esta tesis se ha buscado seleccionar las herramientas numéricas existentes, y desarrollar otras nuevas, para un mejor entendimiento de las lamas hidrotermales en reactores de oxidación en agua supercrítica. Sin embargo, los resultados de la investigación traen nuevos cuestionamientos que pueden servir como base para investigaciones futuras:

1. Sería interesante obtener datos experimentales de referencia de las propiedades de transporte para mezclas acuosas en estado sub y supercrítico, con el objetivo de validar los métodos de estimación existentes y para desarrollar otros nuevos.

2. Se han presentado herramientas para el modelado de la OASC admitiendo flujos monofásicos, lo cual es una aproximación aceptable a los reactores reales pero no considera las zonas a baja temperatura. Sería interesante acoplar modelos CFD multifásicos con los modelos correspondientes de transferencia de masa y de equilibrio de fases. Esto ayudaría a comprender los mecanismos de evaporación de las gotas de combustible y cómo se inicia la reacción.

3. Un modelo de llama turbulenta de premezcla se ha aplicado a las llamas hidrotermales. El modelo supone que las fluctuaciones turbulentas en la concentración del combustible obedecen a una distribución de probabilidades prescrita (β-pdf). Sería interesante estudiar el efecto de las fluctuaciones en otras variables, como la temperatura y la densidad, utilizando funciones de densidad de probabilidad conjuntas.

4. Las alternativas que se han presentado para el aprovechamiento energético y la generación de electricidad se basan en las tecnologías tradicionales de expansión de vapor a alta presión. Nuevas tecnologías para turbinas y sistemas de expansión deberían ser estudiadas para optimizar la utilización del alto contenido energético de los efluentes de los reactores OASC.

About the author

João Paulo Silva Queiroz was born in Caruaru, Pernambuco, Brazil on April 26, 1985. He graduated in Chemical Engineering in a Dual-Degree program by Universidade Federal de Pernambuco - Brazil (2008) and Universidad de Valladolid - Spain (2009). After obtaining a Master's Degree in Research into Fluid Thermodynamics Engineering by Universidad de Valladolid, Universidad de Burgos and Universidad Rovira i Virgili - Spain (2010), he started the PhD Thesis. During his PhD studies, the author has spent four months in a research internship at the *Institute for Combustion Technology* of Universität Stuttgart - Germany (2013).

List of publications

- Queiroz, J. P. S., Bermejo, M. D., and Cocero, M. J. Numerical study of the influence of geometrical and operational parameters in the behavior of a hydrothermal flame in vessel reactors. *Chemical Engineering Science 112* (June 2014), 47–55

- Cabeza, P., Queiroz, J. P. S., Arca, S., Jiménez, C., Gutiérrez, A., Bermejo, M. D., and Cocero, M. J. Sludge destruction by means of a hydrothermal flame. optimization of ammonia destruction conditions. *Chemical Engineering Journal 232* (Oct. 2013), 1–9

- Queiroz, J., Bermejo, M., and Cocero, M. Kinetic model for isopropanol oxidation in supercritical water in hydrothermal flame regime and analysis. *The Journal of Supercritical Fluids 76* (Apr. 2013), 41–47

- Martin, A., Rodriguez-Rojo, S., Navarrete, A., de Paz, E., Queiroz, J., and Cocero, M. J. CHAPTER 8 post-extraction processes: Improvement of functional characteristics of extracts. In *Natural Product Extraction: Principles and Applications*. The Royal Society of Chemistry, 2013, pp. 285–313

- Bermejo, M. D., Cabeza, P., Queiroz, J. P. S., Jimenez, C., and Cocero, M. J. Analysis of the scale up of a transpiring wall reactor with a hydrothermal flame as a heat source for the supercritical water oxidation. *Journal of Supercritical Fluids 56*, 1 (Apr. 2011), 21–32

- Bermejo, M. D., Martin, A., Queiroz, J. P. S., Bielsa, I., Rios, V., and Cocero, M. J. Computational fluid dynamics simulation of a transpiring wall reactor for supercritical water oxidation. *Chemical Engineering Journal 158*, 3 (Apr. 2010), 431–440

Submitted

- Cabeza, P., Queiroz, J. P. S., Bermejo, M. D., Martín, Á., Mato, F., and Cocero, M. J. Chapter 7 reactors for supercritical water oxidation processes. In *Near-critical and Supercritical Water and Their Applications for Biorefineries*, Z. Fang and C. C. Xu, Eds., no. 2 in Biofuels and Biorefineries. Springer Verlag, 2014

- Bermejo, M. D., Martín, Á., Queiroz, J. P. S., Cabeza, P., Mato, F., and Cocero, M. J. Chapter 15 supercritical water oxidation (SCWO) of solid, liquid and gaseous fuels for energy generation. In *Near-critical and Supercritical Water and Their Applications for Biorefineries*, Z. Fang and C. C. Xu, Eds., no. 2 in Biofuels and Biorefineries. Springer Verlag, 2014

Patent

- Bermejo, M. D., Cabeza, P., Queiroz, J. P. S., Jimenez, C., and Cocero, M. J. Aparato y pocedimiento para la generación de llamas hidrotermales autotérmicas, May 2012. ES2381345 A1

Contributions to conferences

Oral communications

- Queiroz, J., Bermejo, M., Cabeza, P., Jimenez, C., and Cocero, M. Behavior of SCWO vessel reactors with a hydrothermal flame: Modeling and experimental results. In *PROSCIBA 2010* (Natal, Brazil, Apr. 2010)

- Cabeza, P., Bermejo, M., Jimenez, C., Queiroz, J., and Cocero, M. Experimental study of the hydrothermal flame formation and

behavior in a vessel reactor for supercritical water oxidation. In *12th European Meeting on Supercritical Fluids* (Graz, Austria, May 2010)

- Carvalho, D. K. E., Silva, R. S., Queiroz, J. P. S., Willmersdorf, R. B., and Lyra, P. R. M. A control volume formulation for the simulation of flows in porous media with aid of high performance tools. In *International Conference on Computational Modeling and Simulation for the Petroleum Industry* (Recife, Brazil, Sept. 2007)

Poster presentations

- Queiroz, J. P. S., Bermejo, M. D., and Cocero, M. J. Modeling of supercritical water oxidation: Hydrothermal flames as heat source. In *Workshop on Supercritical Fluids and Energy* (Campinas, Brazil, Dec. 2013)

- Cabeza, P., Criado, M., Queiroz, J. P. S., Jiménez, C., Bermejo, M. D., and Cocero, M. J. Analysis of the behavior of a SCWO cooled wall reactor working with two outlets. experimental results and energetic study. In *PROSCIBA 2013* (Cartagena de Indias, Colombia, Apr. 2013)

- Cabeza, P., Criado, M., Queiroz, J. P. S., Jiménez, C., Bermejo, M. D., and Cocero, M. J. Analysis of the behavior of a SCWO cooled wall reactor working with two outlets. experimental results and energetic study. In *6th INTERNATIONAL SYMPOSIUM ON HIGH PRESSURE PROCESSES TECHNOLOGY* (Belgrade, Serbia, Sept. 2013)

- Cabeza, P., Jiménez, C., Queiroz, J. P. S., Criado, M., Bermejo, M. D., and Cocero, M. J. Nuevo diseño de reactor para mejorar el aprovechamiento energético del proceso de oxidación en agua supercrítica en presencia de llama hidrotermal. In *VI Reunión de FLUCOMP* (Madrid, June 2012), p. 60

- Queiroz, J. P. S., Bermejo, M. D., and Cocero, M. J. Plant for sludge oxidation in supercritical water with electricity generation: Study of viability. In *Water & Industry Specialist Conference Chemical Industries IWA 2011* (Valladolid, Spain, May 2011)

- Queiroz, J. P. S., Bermejo, M. D., Cabeza, P., Jiménez, C., and Cocero, M. J. Numerical study of the influence of geometrical and operational parameters in behavior of a hydrothermal flame in

vessel reactor. In *13th European Meeting on Supercritical Fluids* (The Hague, Netherlands, Oct. 2011), p. 167

- Cabeza, P., Bermejo, M. D., Jiménez, C., Queiroz, J. P. S., and Cocero, M. J. Experimental study of the viability of the destruction of different kind of waste by supercritical water oxidation at hydrothermal flame regime. In *13th European Meeting on Supercritical Fluids* (The Hague, Netherlands, Oct. 2011), p. 169

- Bermejo, M. D., Queiroz, J. P. S., Cabeza, P., Jiménez, C., Gutiérrez, A., and Cocero, M. J. Novel vessel reactor for energy production by means of a hydrothermal flame. In *8th European Conference in Chemical Engineering (ECCE)* (Berlin, Sept. 2011)

- Bermejo, M., Cabeza, P., Queiroz, J., Jimenez, C., Cocero, M., and Matias-Gago, A. Oxidación en agua supercrítica con reactores de tanque en régimen de llma hidrotermal. In *IV Reunión de FLUCOMP* (Ciudad Real, Spain, Feb. 2010)

- Bermejo, M., Cabeza, P., Queiroz, J., Jimenez, C., and Cocero, M. Water oxidation in vessel reactors with a hydrothermal flame inside. In *Supergreen 2009* (Sendai, Japan, Oct. 2009)

- Bermejo, M., Martín, A., Ríos, V., Cabeza, P., Queiroz, J., Jimenez, C., and Cocero, M. Desarrollo de reactores para la oxidación en agua supercrítica: resultados experimentales, modelado y escalado. In *III Reunión de Flucomp* (Madrid, Feb. 2009)

- Lyra, P. R. M., Carvalho, D. K. E., Luna, B. G. B., Queiroz, J. P. S., and Willmersdorf, R. B. A study of different mesh adaptive strategies for the simulation of two-phase flow in porous media. In *10th Pan American Congress of Applied Mechanics (PACAM X)* (Cancun, Mexico, 2008)

- Lyra, P. R. M., Carvalho, D. K. E., Luna, B. G. B., Queiroz, J. P. S., and Willmersdorf, R. B. A study of h-type mesh adaptive strategy for the simulation of two-phase flow in porous media. In *10th Pan American Congress of Applied Mechanics (PACAM X)* (Cancun, Mexico, 2008)

- Lyra, P. R. M., Carvalho, D. K. E., Luna, B. G. B., Queiroz, J. P. S., and Willmersdorf, R. B. Utilização de estratégias de adaptação de malhas na simulação computacional de escoamentos

bifásicos em meios porosos. In *8º Congreso Iberoamericano de Ingeniería Mecánica (8º CIBIM)* (Cusco, Peru, 2007)

- Carvalho, D. K. E., Luna, B. G. B., Willmersdorf, R. B., Lyra, P. R. M., and Queiroz, J. P. S. Numerical simulation of oil-water displacements in porous media using a mesh adaptive finite volume formulation. In *19th International Congress of Mechanical Engineering (COBEM)* (Brasilia, Brazil, Nov. 2007)